Mössbauer parameters of iron in sulfate minerals

M. Darby Dyar[1], Elly Breves[1], Erica Jawin[1,*], Gerard Marchand[1], Melissa Nelms[1], Vanessa O'Connor[2], Samantha Peel[1,†], Yarrow Rothstein[1], Elizabeth C. Sklute[1,‡], Melissa D. Lane[3], Janice L. Bishop[4], and Stanley A. Mertzman[5]

[1]Dept. of Astronomy, Mount Holyoke College, South Hadley, Massachusetts 01075, U.S.A.

[2]Dept. of Geosciences, Smith College, Northampton, Massachusetts 01063

[3]Planetary Science Institute, Tucson, Arizona 85719, U.S.A.

[4]SETI Institute/NASA-Ames Research Center, Mountain View, California, 94043, U.S.A.

[5]Dept. of Earth and Environment, Franklin and Marshall College, Lancaster, Pennsylvania 17603, U.S.A.

*Present address: Department of Geological Sciences, Brown University, Providence, Rhode Island 02912, U.S.A.

†Present address: Department of Earth and Planetary Science, University of Tennessee, Knoxville, Tennessee 37996, U.S.A.

‡Present address: department of Geosciences, Stony Brook University, Stony Brook, New York 11794, U.S.A.

Submitted to American Mineralogist

REVISION 1

Abstract

Although Fe-sulfate minerals occur only rarely on Earth as alteration products of sulfidic basalts or in hydrothermal systems, multiple lines of evidence point to the importance of Fe- (and other) sulfate minerals on the surface of Mars. One such Martian data set comes from the MIMOS II Mössbauer spectrometers on the Mars Exploration Rovers, which acquired hundreds of spectra from the martian surface at two locations. Interpretation of those spectra has been limited by the lack of a comprehensive set of laboratory analog spectra of the broad range of naturally-occurring sulfate minerals. Accordingly, this study reports Mössbauer data of 99 samples representing 47 different sulfate mineral species, all containing six- or higher-coordinated Fe. The resultant Mössbauer parameters are related to the local polyhedral environment around the Fe cation in each mineral to explain variations in spectral characteristics. Results show that the size of the coordination polyhedron is the best predictor of quadrupole splitting, which increases with both octahedral volume and mean bond length. Species within groups of structurally-similar minerals are shown to have comparable spectral peaks that generally fall within small ranges. Although coordination polyhedron geometry is not necessarily unique to any particular mineral species or group, Mössbauer data can be used to help constrain mineral identifications from martian spectra. However, the number of mineral species is large but the range of crystal structures and hyperfine parameters may be small, so that in many cases, individual minerals cannot be uniquely fingerprinted. Examples would include quenstedtite, coquimbite, kornelite, and lausenite, which have indistinguishable spectra, as do apjohnite, bilinite, dietrichite, and römerite. Overlap of Mössbauer parameters is a particular complication for identification of Fe^{3+}-rich phases because the range of Mössbauer parameters for Fe^{3+} in any coordination number is so small. Previous analyses of martian Mössbauer spectra reported the

presence of jarosite (Klingelhöfer et al. 2004; Morris et al., 2004) and an unspecific ferric sulfate (Morris et al. 2008). New data presented here indicate that botryogen, metasideronatrite, and slavikite exhibit Mössbauer spectra similar to those attributed to jarosite at Meridiani Planum. Fibroferrite and rhomboclase have parameters similar to those observed at Arad Samra, and copiapite and parabutlerite could be present at Tyrone Mount Darwin and Berkner Island. Unique mineral identifications are generally not possible from Mössbauer data alone, particularly for paramagnetic phases, although combining Mössbauer results with other datasets enables a greater level of confidence in constraining mineralogy. This study provides a new expansive dataset for future interpretation of iron sulfates on Mars.

I. INTRODUCTION

Iron sulfates, many of which form as alteration products of sulfides, are relatively rare on Earth, particularly as hydrous species. They may form as a result of chemical interaction of acidic groundwater with mafic rocks (basalts) under ambient (and cold) conditions or in hydrothermal systems (Tosca et al. 2004). However, elsewhere in our solar system, sulfur may be a more common and significant element in crustal rocks and thus conditions may be more favorable for the formation of sulfate minerals. This is especially true on Mars, where the low temperatures and pH found in the martian permafrost create ideal conditions for the formation of this group of minerals (Burns 1987), which includes such phases as coquimbite, $Fe^{3+}_2(SO_4)_3 \cdot 9H_2O$, and amarantite, $FeSO_4(OH) \cdot 3H_2O$. Viking, Mars Pathfinder, Mars Exploration Rover, and remotely sensed data (e.g., Clark et al. 1982, Blaney and McCord 1995, Rieder et al. 2004, Bonello et al. 2004, McAdam et al. 2013, and Yen et al. 2013) have all suggested that sulfur is a relatively abundant element on the surface of Mars, but the mineralogy

of the sulfur-rich phases is not well constrained. Lane et al. (2004) suggests that hydrous iron sulfates (HIS) might contribute to the Martian thermal emission, reflectance, and Mössbauer spectra.

Before the Mars Science Laboratory landed its CheMin instrument (Blake et al. 2012), the most pivotal tool for in-situ identification of sulfate mineralogy on Mars was the MIMOS II Mössbauer spectrometer, which was part of the payload of both the Spirit and Opportunity rovers. Klingelhöfer et al. (2004) identified jarosite at Meridiani Planum, Mars, based on an isomer shift of 0.37±0.02 mm/s and quadrupole splitting of 1.20±0.02 mm/s. These Mössbauer parameters are the best match with jarosite of all the samples in the Mössbauer Effect Data Center database of published spectra and at that time there were no "reasonable alternatives for jarosite" (Morris et al. 2006). They further noted that the "jarosite" doublet seen in the Mars spectra was a perfect match to those previously reported for jarosite by Leclerc (1980). Moreover, the existence of jarosite and other sulfates had been predicted by Roger Burns in several papers (1986, 1987, 1988, 1993; Burns and Fisher, 1990). For these reasons, the idea of jarosite on Mars became generally accepted, and has been commonly used to constrain phase equilibria and aqueous processes on Mars (Tosca et al. 2004).

The exciting discovery of iron sulfate on Mars (Klingelhöfer et al., 2004; Morris et al. 2006), along with subsequent discovery of an unspecific ferric sulfate (Morris et al., 2008) illuminated the need for further Mössbauer data on this important class of minerals. At that time, little was known about the Mössbauer parameters that are characteristic of related sulfate minerals. Only a handful of sulfate Mössbauer spectra had been reported in 2004 (mostly those of jarosite), and nearly all were acquired at room temperature, and thus not optimal for matching with ~220K spectra from Mars. In subsequent years, several new studies have sought to

105 characterize sulfate minerals (e.g., Majzlan et al. 2011, Van Alboom et al., 2009, Kovacs et al.
106 2008, Ertl et al. 2008, and Hyde et al., 2011), but most focused only on a few examples of a
107 single mineral group. There remained a need for a robust survey of iron sulfate minerals acquired
108 under consistent conditions, which is fulfilled by the current paper. These new data are expected
109 to lead to new discoveries about iron sulfate minerals on Mars.

110 To address this deficiency, this study reports Mössbauer data of 99 samples representing
111 45 different sulfate mineral species. To put the data in a crystal chemical context, this paper
112 seeks to relate the resultant Mössbauer parameters to both the local polyhedral environment
113 around the Fe cations in these minerals and the overall structural characteristics of each species.
114 The groundwork for these comparisons has been laid by the thorough discussion and
115 classification of sulfate minerals presented by Hawthorne et al. (2000). It seems logical to
116 assume that minerals of the same structure classes will have similar spectral features. Similarly,
117 mineral species that belong to the same hydration sequence might also be assumed to have
118 similar spectra. However, little work has been done to explore or test this hypothesis. This
119 project was designed to look at the big picture and examine general trends in Mössbauer
120 spectroscopy of sulfate minerals at 295K. Mars temperature measurements will be considered in
121 a future paper.
122

123 ## II. BACKGROUND

124 There are ~370 sulfate mineral species, and structures are known for about 80% of them
125 (Hawthorne et al. 2000). Sulfates are similar to silicates (and phosphates and arsenates) in that
126 the structures are based on a tetrahedral unit, SO_4, that is analogous to the familiar SiO_4 building
127 blocks of most silicates. However, the charge of the S^{6+} cation is greater than that of Si^{4+}, so the

oxygen atoms in the SO_4^{-2} tetrahedra must be linked to satisfy charge balance in a manner that is different from what is observed in SiO_4^{-4}-based silicates.

For example, framework silicates such as quartz and feldspar are the most common minerals in the Earth's crust. They are based upon corner-sharing tetrahedra in which charge balance is satisfied by sharing all four corners of SiO_4^{-4} tetrahedra (with substitution of Al for Si accommodated by Na, Ca, and K in the case of feldspars). In the sulfate minerals, the structures are fundamentally different because this type of complete polymerization among solely SO_4^{-2} tetrahedra (or in combination with other tetrahedral oxyanions such as PO_4, AsO_4, VO_4, SiO_4) is unstable (Hawthorne et al. 2000). Another distinction of sulfate minerals is that substitution of other cations for S^{6+} is not as common, though it does occur in gypsum and beudantite ($As^{5+} \leftrightarrow S^{6+}$; Lin et al. 2013, Szymanski 1988) vergasvaite ($Mo^{6+} \leftrightarrow S^{6+}$; Berlepsch et al. 1999), and hashemite ($Cr^{6+} \leftrightarrow S^{6+}$; Duesler and Foord 1986). It is questionable whether $Fe^{3+} \leftrightarrow S^{6+}$ substitution even occurs because there are (to date) no Mössbauer studies that report tetrahedral Fe^{3+} in a sulfate mineral species. It is thus expected that Fe^{3+} in sulfate minerals will be generally confined to six-coordinated sites, which may also be occupied by Fe^{2+}. However, this study will examine the validity of this assumption.

So sulfate structures are commonly composed of SO_4^{-2} tetrahedra bonded with cations in octahedral (the vast majority) or larger coordination polyhedra (Figure 1). Thus tetrahedral Fe^{3+} occupancy (i.e., in S-deficient structures) is highly unlikely. Interpretation of the Mössbauer spectra of these structures is greatly simplified, and is generally a matter of distinguishing between octahedral Fe^{3+} and Fe^{2+} (and rarely dodecahedra, as when Fe^{2+} might substitute into dodecahedral or larger sites in Ca sulfates such as anhydrite). These distinctions are described using the positions of the peaks in doublets of a Mössbauer spectrum using the terms isomer shift

(IS, δ, or sometimes center shift) and quadrupole splitting (QS, ΔE_Q, or Δ), expressed in velocity units by convention in this field. Isomer shift is caused by overlap between the nucleus and the *s*-electron charge distributions that causes a shift in the nuclear energy levels in the Fe atom. Isomer shift is most sensitive to oxidation state and less sensitive to distortions in the surrounding site geometry. Isomer shift is measured as the offset of the doublet's centroid from zero velocity, and its value in silicates is generally low (0.25-0.5 mm/s) for octahedral Fe^{3+} and much higher (>1.10 mm/s) for octahedral Fe^{2+}. Its error is usually given as ±0.02 mm/s (Dyar 1984, Dyar et al., 2008).

Quadrupole splitting results from interactions between the nuclear quadrupole moment and the gradient of the surrounding electric field, which cause the I = 3/2 level to split into two sublevels. QS is the separation between the two component peaks. QS is sensitive to both oxidation state and site geometry. As an example, consider Fe^{2+} in perfectly octahedral (6-fold) coordination. The electronic configuration of Fe^{2+}, $3d^6$, is in general high spin for minerals, i.e., $t_{2g}^4 e_g^2$. The sixth electron populates the three degenerate (all the same energy) t_{2g} levels equally, so spherical symmetry is maintained and, ignoring lattice terms, there is no quadrupole splitting. However, a distortion of the octahedral environment lifts the degeneracy of the t_{2g} levels, leading to unequal occupancy of the *d* orbitals and a large contribution to Δ from the electronic field. In high-spin Fe^{3+}, which has electronic configuration $t_{2g}^3 e_g^2$, the *d* orbitals remain equally populated even when the octahedral environment is distorted, and the electronic field remains spherical. Of course, in both cases, asymmetry in the lattice field causes $^{[6]}Fe^{2+}$ and $^{[6]}Fe^{3+}$ to split the I = 3/2 level, but in general, Δ for Fe^{2+} (>1.5 mm/s) >> Δ for Fe^{3+} (<1.3 mm/s). In general, the larger the Δ value, the more distorted the coordination polyhedron surrounding the Fe atom (Burns and

Solberg 1990, Dyar et al. 2006a). The error of Δ on fitted spectra is usually given as ±0.02 mm/s (Dyar 1984, Dyar et al., 2008).

Given that the parameters have wide ranges, it may be possible to assign certain ranges of parameters to particular types of bonding environments or coordination polyhedra. Thus this paper presents Mössbauer spectra of well-characterized sulfate minerals and determine characteristic parameters for minerals with different structure types. In many cases, these are the first Mössbauer measurements of Fe^{3+}/Fe^{2+} ratios for these mineral species. The results shed light on stoichiometry and charge-balancing substitutions in these phases as well as the parageneses and redox environments in which these mineral form.

III. Experimental and Analytical Procedures

Samples for this project (Table 1) were selected from the collections of the coauthors; others were purchased from collectors or came from E. Cloutis (U. Winnepeg), the National Museum of Natural History (Smithsonian) and the Harvard Mineralogical Museum. Diversity of samples from multiple localities was sought so that compositional variability within each group could be assessed. All samples were kept in dry air in a desiccator when not being analyzed. Samples were first hand-picked to purify them, a step that was critical because many of these phases occur as intergrowths with other minerals. This job was made more difficult by the fact that many sulfates are yellow in color, making it necessary to distinguish coexisting phases on the bases of morphology and subtle color variations. However, it is important to note that in some cases, individual species were mingled with other species at such a small scale that it is unrealistic to expect that pure separates could be created. In such cases, minor contributions in spectra from the impurities would be expected. One of the advantages of the current study is that more than one example of most species was analyzed, and so the diagnostic spectral

197 characteristics that various samples have in common can be identified in spite of the presence of
198 potential impurities.

199 A majority of the separates was then analyzed by XRD to confirm their purity and make
200 unequivocal phase identifications. This task was potentially complicated by the fact that several
201 of these minerals are extremely rare, and thus not represented in XRD databases (e.g., ilesite and
202 bilinite). For this reason, it was sometimes necessary in a few instances to make educated
203 guesses about the identity of some minerals, drawing on the fact that many of the samples
204 studied here came from their type localities. Each of these is detailed in the footnotes to Table 1.
205 During the drawn-out collection and culling phase of the samples, various XRD analyses were
206 conducted at Franklin and Marshall College, Smith College, Indiana University, and the
207 University of New Mexico.

208 Samples were then prepared by mixing the sulfates with sucrose, gently mixing them into
209 a homogeneous powder to fill the sample holder for Mössbauer spectroscopy. Then 295K
210 Mössbauer spectra were acquired using a source of 100-40 mCi ^{57}Co in Rh, which was used on a
211 WEB Research Co. (now See Co.) model W100 spectrometer. Run times ranged from 12-96
212 hours, and results were calibrated against α-Fe foil.

213 Spectra were fit with Lorentzian doublets using the MEX_FielDD program acquired from
214 the University of Ghent courtesy of E. De Grave. Isomer shifts (IS, or δ), and quadrupole
215 splittings (QS, or Δ) of the doublets were allowed to vary, and widths (full width at half
216 maximum) of all peaks were coupled to vary in pairs. All major Fe species were represented by

well-resolved quadrupole pairs so the fits were straightforward, though it was sometimes necessary to fit small doublets representing impurities (Table 2[1]).

IV. Results: Mössbauer Parameters

Mössbauer parameters for all samples studied at room temperature are given in full in Table 2 and for all doublets with areas greater than 5% of the total peak area in Tables 3-6, where minerals with similar parameters are grouped together to compare and contrast features. Because Fe^{3+} and Fe^{2+} have quite distinct parameters, it is convenient to discuss the results and spectral features separately, beginning with the Fe^{3+}-bearing sulfates, which are the most numerous.

One of the most striking things about the data set for Fe^{3+} parameters is the consistency of the isomer shift (δ), which ranges from 0.37-0.52 mm/s, but is most commonly in the range from 0.41-0.43 mm/s (Figure 2). Error bars associated with isomer shift are commonly quoted as ±0.01-0.05 mm/s, so many of the isomer shift values for Fe^{3+} sulfates are essentially the same. However, as noted at the onset, quadrupole splitting (Δ) varies considerably among the various sulfates studied here. It is thus convenient to group and discuss the Fe^{3+} doublets in sulfates according to quadrupole splitting.

A. Lowest Δ Sulfates

Some of the most unusual Mössbauer spectra found in the sulfates belong to members of the hydration series $Fe_2(SO_4)_3 \cdot nH_2O$, which includes quenstedtite, coquimbite, kornelite, and

[1]Deposit item AM-13-xxxx, Table 2 Deposit items are available two ways: For a paper copy contact the Business Office of the Mineralogical Society of America (see inside front cover of recent issue for price information). For an electronic copy visit the MSA web site at http://www.minsocam.org, go to The American Mineralogist Contents, find the table of contents for the specific volume/issue wanted, and then click on the deposit link there.

lausenite (Table 3). All these minerals have Mössbauer spectra (Figure 3) that closely resemble singlets because of their low quadrupole splitting, which in turn implies that there is only a negligible electric field gradient at the nucleus of the Fe^{3+} cation.

In quenstedtite, $Fe^{3+}_2(SO_4)_3 \cdot 11H_2O$, there are two types of clusters: *cis*-$[Fe^{3+}(SO_4)_2(H_2O)_4]$ and $[Fe^{3+}(SO_4)(H_2O)_5]$, along with H_2O groups (Thomas et al. 1974; Hawthorne et al. 2000). However, the coordination polyhedra occupied by Fe^{3+} cations in these clusters are still very similar despite the difference between five vs. four O^{2-} anions (Figure 3). Thus the Mössbauer spectrum of quenstedtite consists of two highly-overlapping doublets with very small Δ values, one of which is nearly a singlet. Its parameters are $\delta = 0.47$ and 0.40 mm/s and $\Delta = 0.13$ and 0.24 mm/s.

Perhaps the most commonly occurring (on Earth) sulfate species in this group is coquimbite ($Fe^{3+}_2(SO_4)_3 \cdot 9H_2O$). The major feature in four of the samples studied here is again nearly a singlet, with parameters of roughly $\delta = 0.46$ mm/s and $\Delta = 0.09$ mm/s. Its structure, along with its polytype paracoquimbite (Fang and Robinson 1970), is composed of isolated clusters of $[Fe^{3+}_3(SO_4)_6]$ along with $\{Fe^{3+}(H_2O)_6\}$ octahedra and (H_2O) groups. The Fe octahedra are slightly different in geometry. As seen in Figure 3, the Al1 and Fe2 sites are nearly identical, though the Fe1 site is distinct. This implies that there may be two different Fe^{3+} doublets in coquimbite, and this is indeed observed. The doublet with very low Δ just noted is most likely assigned to the $[Fe^{3+}_3(SO_4)_6]$ site because that site is most similar to that in quenstedtite. The other group of samples containing coquimbite (SPT131, SPT132, and S63) has spectra dominated by a doublet with larger Δ and will be discussed later. Note that the sample of paracoquimbite studied here is mostly Fe^{2+} but its Fe^{3+} doublet matches one of the doublets in coquimbite ML-S63.

When these clusters depolymerize, they form the same chains found in two closely-related hydration states of kornelite and lausenite. Kornelite ($Fe^{3+}_2(SO_4)_3 \cdot 7H_2O$) is composed of spiral chains of $\{Fe^{3+}(H_2O)_6\}$ octahedra and SO_4 tetrahedra, cross-linked by additional SO_4 tetrahedra. The structure also includes partially-occupied sites between the chains, making kornelite a heptahydrate. Early workers believed that lausenite ($Fe^{3+}_2(SO_4)_3 \cdot 5H_2O$) had the kornelite structure with none of these extra water molecules (Robinson and Fang, 1973), but more recent work by Majzlan et al. (2005) shows that a different arrangement is likely. In lausenite, the chains are tilted to free up one of the H_2O molecules, with bridging oxygens coordinating S^{6+} and Fe^{3+} (Majzlan et al. 2005). Two symmetrically distinct Fe^{3+} sites exist as seen in Figure 3; Fe^{3+} is coordinated either by four O and two H_2O (the Fe1 site) or three O and three H_2O (the Fe2 site). The Mössbauer spectra of kornelite and lausenite are quite similar. In three of the four samples, a doublet with $\delta = 0.48$ mm/s and $\Delta = 0.13$ mm/s dominates, quite like those found in coquimbite. The fourth sample, 104175, is mostly $Fe^{2+}$with a Fe^{3+} doublet with higher δ and Δ, probably due to an impurity. By way of comparison, Huggins and Huffman (1979) reported $\delta = 0.44$ mm/s and $\Delta = 0.15$ mm/s for kornelite.

Another related structure is that of ungemachite, $K_3Na_8[Fe^{3+}(SO_4)_6](NO_3)_2(H_2O)_6$, which is also based on clusters. Ungemachite belongs to the glaserite crystal structure type, in which an octahedron shares six corners with (SO_4) tetrahedra, forming pinwheels (Moore 1973). The pinwheels are then linked into tetrahedra to form layers. Many sulfate, phosphate, chromate, and silicate minerals are based on this structure, including millosevichite ($Al_2(SO_4)_3$), glaserite ($K_3Na(SO_4)_2$), and mikasaite ($Fe_2(SO_4)_3$). An early paper by DeBenedetti et al. (1961) gave parameters for mikasaite of $\delta = 0.46$ mm/s and $\Delta = 0.00$ mm/s, while Nomura et al. (2005) reported values of $\delta = 0.47$ mm/s and $\Delta = 0.34$ mm/s. Sgarlata (1985) reported only a singlet at

283 0.44 mm/s for millosevichite ($Al_2(SO_4)_3$). These data suggest that the glaserite structure-type
284 minerals will all also have low Δ values. Clearly, more work on a broader range of species would
285 be useful to confirm this trend in the Mössbauer parameters of this structure type, which is
286 largely unexplored.

287 Ferrinatrite, $Na_3(H_2O)_3[Fe^{3+}(SO_4)_3]$, is formally classified as a chain sulfate, but the
288 linkages between $[Fe^{3+}(SO_4)_3]$ octahedral-tetrahedral chains create octahedra that are very
289 similar to the clusters in coquimbite (Hawthorne et al. 2000), as can be seen in Figure 3.
290 Mössbauer parameters of ferrinatrite (Table 3) are also indistinguishable from those of the
291 $Fe(SO_4)_3 \cdot nH_2O$ hydration series.

292 Voltaite ($K_2[Fe^{2+}_5Fe^{3+}_3(H_2O)_{12}(SO_4)_{12}]\{Al(H_2O)_6\}$) and the related Mg-rich species
293 pertlikite (Ertl et al. 2008) have multiple Mössbauer doublets because there are two distinct
294 octahedral sites occupied by Fe^{3+} and Fe^{2+}: 32 M1 and 96 M2 sites per unit cell. Ideally, Fe^{3+}
295 occupies all of the M1 sites and the M2 sites are shared by both valence states of Fe. However,
296 this mineral shows a great deal of variation among the eight samples studied here. Voltaite has
297 one group of large doublets at δ = 0.44-0.54 mm/s and Δ = 0.35-0.40 mm/s, as well as a second
298 group of smaller doublets at δ = 0.10-0.16 mm/s and Δ = 0.47-0.69 mm/s. All the samples
299 studied here contained roughly equal distributions of Fe^{2+} and Fe^{3+}. Their spectra are similar in
300 appearance to those of Long et al. (1980), but they did not publish δ and Δ for their Fe^{3+}
301 doublets. Hermon et al. (1976) also had trouble resolving contributions from different Fe^{3+}
302 doublets, but concluded that multiple doublets must be present on the basis of increasing
303 linewidth at low temperatures. They suggested that the larger Δ Fe^{3+} doublet corresponds to the
304 M2 site, while the less distorted M1 doublet had a smaller Δ. They also suggest that there may be
305 some divalent cations in the smaller M1 site, even when there are trivalent cations in the larger

M2 site. Majzlan et al. (2011) measured three samples, and obtained consistent parameters for two doublets with δ = 0.59 and 1.42 mm/s and Δ = 0.26 and 2.52-2.68 mm/s respectively. These do not agree well with current results, but the reason for the discrepancy may lie in the fact that they only modeled two doublets. Majzlan et al. (2013) studied a large suite of synthetic voltaites and found parameters of δ = 0.45-0.47 mm/s and Δ = 1.29-1.31 mm/s that are closer to those from the current study and previous workers. Support for the fits used in the current study lies in the fact that doublets with the same parameters are also found in rhomboclase, where they are clearly resolved at >75% of the total spectral area.

Rhomboclase, $(H_5O_2)[Fe^{3+}(H_2O)_2(SO_4)_2]$, has a structure somewhat related to kornelite, in that it is also a sheet of SO_4 tetrahedra and $Fe^{3+}O_6$ octahedra. Two-dimensional linkages between adjacent clusters link them into sheets, with hydrogen bonding of interstitial $(H_5O_2)^+$ dimers (Hawthorne et al. 2000). Mössbauer parameters of δ = 0.54 and Δ = 0.59 mm/s were reported by Majzlan et al. (2011) and all five samples in the current study had those quite similar parameters: ca. δ = 0.44 mm/s and Δ = 0.51-0.54 mm/s. The Fe site in rhomboclase is apparently quite similar to the Fe1 site in voltaite, as is apparent in Figure 3.

B. Minerals with Δ = 0.31-0.81 mm/s

The Mössbauer spectrum of yavapaiite ($K[Fe^{3+}(SO_4)_2]$) is a single doublet with δ = 0.48 mm/s and Δ = 0.31 mm/s (Table 4 and Figure 4a). Those parameters match those reported for three samples by Nomura et al. (2005) almost exactly. Its structure is based upon sheets of SO_4 tetrahedra and $Fe^{3+}O_6$ octahedra that are created by corner sharing of $[Fe^{3+}(SO_4)O_2]$ chains (Hawthorne et al. 2000). The same sheet geometry is also found in kröhnkite ($Na_2[Cu^{2+}(H_2O)_2(SO_4)_2$), merwinite ($Ca_3Mg(SiO_4)_2$), and brianite ($Na_2CaMg(PO_4)_2$), as well as members of the fairfieldite sub-group of hydrated phosphates, so Fe^{3+} substitution in those

329 structures should result in yavapaiite-like Mössbauer parameters. Krausite, $K[Fe^{3+}(H_2O)_2SO_4)_2]$,
330 has a related structure based on infinite double chains like those found in kröhnkite (Graeber et
331 al., 1965); its Mössbauer parameters of $\delta = 0.41$ mm/s and $\Delta = 0.41$ mm/s are similar to (though
332 slightly higher than) those of yavapaiite. The Fe octahedra from the crystal structure refinements
333 of these two minerals, as shown in Figure 4a, are slightly different. Note that the Fe site in
334 krausite is slightly more distorted than the Fe site in yavapaiite, which would cause the higher Δ.
335 Goldichite ($KFe^{3+}(SO_4)_2 \cdot 4H_2O$) is a slightly higher hydration state of potassium ferric
336 sulfate, such that the Fe^{3+} coordination polyhedron now has two *trans*-OH. Thus its Mössbauer
337 spectrum is not the same as those of yavapaiite and the other structures based on infinite double
338 chains. Rather, goldichite has two Fe^{3+} doublets with parameters, one with $\delta = 0.19$ mm/s and Δ
339 $= 0.61$ mm/s as seen in coquimbite, and one with $\delta = 0.48$ mm/s and $\Delta = 0.29$ mm/s comparable
340 to yavapaiite and krausite. The structure of kainite ($K_4[Mg_4(H_2O)_{10}(SO_4)_4](H_2O)Cl_4$) is also
341 based on kröhnkite-like chains, and probably has Mössbauer parameters like krausite. All these
342 minerals have quite similar Mössbauer spectra (Figure 4a).
343 Copiapite group minerals share the general formula
344 $[Fe^{3+}{}_2(OH)(H_2O)_4(SO_4)_3]_2\{A(H_2O_6\}(H_2O)_6$, where $A = Fe^{2+}$, Fe^{3+}, Al, Mg, Cu, Ca, and/or Zn
345 (Hawthorne et al., 2000). Their structures are composed of layers of the $\{A(H_2O_6\}$ octahedra that
346 are linked to layers of $[Fe^{3+}{}_2(OH)(H_2O)_4(SO_4)_3]$, forming $[M_2(SO_4)_2(O,H_2O)_7]$ clusters that
347 resemble those in phosphates (Hawthorne 1979). Only one sample studied here (168257) had an
348 Fe^{2+} doublet with 51% of the total area, defining it to be copiapite rather than ferricopiapite. All
349 the other copiapite samples in the data set studied here have only Fe^{3+}, and so are really
350 ferricopiapite despite the species names given to them, and the single zincocopiapite sample has
351 identical Mössbauer parameters to those of the ferricopiapites. The ferricopiapites have two

distinct distributions of Mössbauer parameters with the same δ = 0.42-0.43 mm/s but different quadrupole splittings: Δ = 0.35-0.40 mm/s for one group and 0.77-0.88 mm/s for the other. These probably correspond to sites in the two different layers mentioned above but it is unclear at this point which doublet represents which site. Two similar sites were observed in Mössbauer spectra of samples from the Río Tinto basin in Spain by Fernández-Remolar et al. (2005): δ = 0.37 and 0.39 mm/s and Δ = 0.34 mm/s and 0.74 mm/s, respectively. Majzlan et al. (2011) also reported copiapite data with parameters of δ = 0.53 mm/s and Δ = 0.30-0.38 and 0.79-0.80 mm/s.

Halotrichite group minerals share a structure with $[M(SO_4)_2(H_2O)_4]$ clusters of M^{2+} and M^{3+} octahedral cations. The two $\{M^{3+}(H_2O)_6\}$ octahedra are charge-balanced by the presence of $[M^{2+}(SO_4)(H_2O)_5]$ octahedra, with an additional five H_2O molecules held in place by hydrogen bonding (Hawthorne 1985). Three Fe^{3+}-rich halotrichite group minerals were studied here, apjohnite, bilinite, and dietrichite, and their Mössbauer spectra (Figure 4b) are somewhat similar. The main feature in the apjohnite spectrum is a large doublet with δ = 0.43 mm/s and Δ = 0.58 mm/s, similar to that of rhomboclase. The bilinite spectrum has a broad doublet at δ = 0.49 mm/s and Δ = 0.37 mm/s, identical to one of the doublets in copiapite. Dietrichite has two doublets with δ = 0.42 and 0.43 mm/s and Δ = 0.35 and 0.79 mm/s.

In the very-similar römerite structure, Fe occupies octahedral sites that are parts of an analogous $Fe(SO_4)_2(H_2O)_4$ cluster (Figure 1). As in the halotrichite group, the clusters have a *cis* arrangement of polyhedra (Figure 4b). In addition to the cluster, Fe in römerite is also found in isolated $\{Fe^{2+}(H_2O)_6\}$ octahedra. Several different examples of römerite were obtained, and nearly all the samples contain both Fe^{2+} and Fe^{3+}. These minerals should have Fe^{3+} parameters similar to those for the halotrichite minerals, and this is indeed what is observed: δ_{Bil} = 0.49 mm/s and Δ_{Bil} = 0.37 mm/s, while $\delta_{Röm}$ = 0.43-0.47 mm/s and $\Delta_{Röm}$ = 0.23-0.55 mm/s. Huggins

and Huffman (1979) found similar parameters for two doublets in römerite of δ = 0.38 and 0.53 mm/s and Δ = 0.37 and 0.25 mm/s, respectively, while Majzlan et al. (2011) reported δ = 0.52 and 0.59 mm/s, with Δ = 0.38 and 0.17 mm/s (note again that their δ values are slightly high). They also observed the Fe^{2+} doublet with δ = 1.38 and Δ = 3.49 mm/s.

Metavoltine ($K_2Na_6[Fe^{3+}_3O(SO_4)_6(H_2O)_3]_2\{Fe^{2+}(H_2O)_6\}(H_2O)_6$) is related to römerite because it is also based on isolated clusters, in this case with composition $[Fe^{3+}_3(SO_4)_6O(H_2O)_3]$, and the clusters are linked by hydrogen bonding (Hawthorne 1985). There are three Fe sites: two for Fe^{3+} that occur within the clusters (Fe(1) and Fe(2)), and those in isolated Fe(3) octahedra that the formula suggests should be strictly Fe^{2+} (Giacovazzo et al. 1976). As would be appropriate for the formula given above, the spectra have predominantly Fe^{3+} features. One doublet has δ = 0.33-0.44 mm/s and Δ = 0.24-0.46 mm/s, a second has parameters of δ = 0.38-0.42 mm/s and Δ = 0.37-0.53 mm/s, and a third has δ = 0.43 mm/s and Δ = 0.74-0.76 mm/s. All have comparable areas, suggesting that some Fe^{3+} is occupying the Fe sites in the structure equally. Sgarlata (1985) reported parameters of δ = 0.43 mm/s and Δ = 0.36 mm/s for Fe^{3+} in metavoltine, similar to those observed for the first doublet.

As noted above, there are two different types of sites in coquimbite: isolated clusters of $[Fe^{3+}_3(SO_4)_3]$ and $\{Fe^{3+}(H_2O)_6\}$ octahedra. In some samples, only a doublet with very small quadrupole splitting (~0.10 mm/s) is observed, and stoichiometry suggests that this must represent Fe^{3+} in both sites. However, several of the samples studied here instead have a doublet with higher Δ that is very similar to the Fe^{3+} doublet in römerite (which also has two distinct octahedral sites), with parameters of δ = 0.42 mm/s and Δ = 0.44-0.47 mm/s. This higher Δ doublet is found in multiple samples from different parageneses that have been positively identified by XRD, so the existence of an impurity is unlikely. It was also reported by Pankhurst

et al. (1986), who gave δ = 0.35-0.36 mm/s and Δ = 0.56-0.60 mm/s. It is likely that substitution of other cations (such as Mg and Al) may be lowering the symmetry of the site, thus increasing its quadrupole splitting. Both XRD and reflectance spectroscopy (Lane et al. 2013) confirm that all the samples studied contain coquimbite, so the observed variations in site occupancy must be due to formation conditions or other unknown crystal chemical constraints.

Taken together with the very low Δ doublets observed in all coquimbite samples studied here, the coquimbite data corroborate the work of Huggins and Huffman (1979), who found doublets with δ= 0.51 and 0.43 mm/s and Δ = 0.00 and 0.26 mm/s, respectively. Fernández-Remolar et al. (2005) could not easily distinguish a doublet assigned to coquimbite and reported slightly high parameters of δ= 0.44 mm/s and Δ = 0.22 mm/s. The higher values of Δ from these workers may represent unresolved contributions from a doublet with higher Δ, or they may represent variations in Mössbauer parameters as a function of some unrecognized compositional effect.

The isostructural rozenite group minerals (rozenite, $FeSO_4 \cdot 4H_2O$, starkeyite, ilesite, aplowite, and boyleite) are based on clusters, which might suggest that their Mössbauer parameters should be similar to those of halotrichite, metavoltine, and coquimbite. Each cluster is composed of two tetrahedra each sharing two corners with two octahedra; the resultant formula is $M_2(SO_4)_2O_8$, where M = Fe, Mg, Mn, Co, and/or Zn. In the sample suite studied here, minerals in this group are dominantly Fe^{2+}-rich and will thus be discussed below in section G; only a few tiny doublets (<2% of the total spectral area) with very scattered parameters are observed for Fe^{3+} in rozenite. However, the Mössbauer spectrum of a low-Fe starkeyite gave parameters like those of römerite, with δ = 0.16 and 0.06 mm/s and Δ = 0.64 and 0.49 mm/s.

Ilesite (the Mn equivalent of rozenite) contains only Fe^{3+}, with parameters of $\delta = 0.31$ mm/s and $\Delta = 0.62$ mm/s.

Within this group of sulfates based on linked clusters (Figures 3, 4a, 4b), it should be apparent that no mineral species has a diagnostic or truly characteristic Mössbauer spectrum. Due to the similarities in their crystal structures and the resultant effect on the geometries of the Fe coordination polyhedra, none of these mineral species could be uniquely identified on the basis of their Mössbauer spectra alone.

C. Octahedral Corner-Sharing Chain Structures

A large group of sulfates with related structures is represented by a continuum of Mössbauer parameters with Δ ranging from ~0.80-1.2 mm/s. Their spectra are all quite similar, as seen in Figures 5a and b. This group includes butlerite and parabutlerite, slavikite, fibroferrite, botryogen, sideronatrite, metasideronatrite, metahohmannite, and the alunite group. What do all these minerals have in common?

All but alunite have structures composed of infinite chains of SO_4 tetrahedra and $M(O,H_2O)_6$ octahedra, as noted by and described in Moore (1970). The chains have a repeat distance of ~7 Å (see butlerite in Figure 1). In butlerite and parabutlerite, the tetrahedra alternate along the chain, linking to vertices of the octahedra (Hawthorne et al. 2000). The structure of slavikite is based on open sheets of corner-sharing octahedra and tetrahedra that are similar to fragments of the chains found in butlerite (Hawthorne et al. 2000); the Mössbauer spectra could thus be indistinguishable.

Sakai et al. (1981) reported the 300K spectrum of butlerite to have $\delta = 0.42$ mm/s and $\Delta = 0.94$ mm/s, and parameters for three samples from this study are an excellent match: $\delta = 0.41$ mm/s and $\Delta = 0.95$-0.98 mm/s. One of the parabutlerite samples in this study is consistent, with δ

443 = 0.41 mm/s and Δ = 0.98 mm/s, but sample 157716 is not. The latter has three distributions with
444 parameters of δ = 0.22, 0.58, and 0.34 mm/s and Δ = 0.55, 0.54, and 1.14 mm/s. X-ray
445 diffraction confirms that this sample is indeed parabutlerite, so these three doublets must
446 represent a different cation ordering than is found in the other samples.
447 Moore (1970) notes the structural similarity of the chains in butlerite to those in the
448 phosphate mineral laueite ($Mn^{2+}Fe^{3+}_2(OH)_2(H_2O)_6(PO_4)_2 \cdot 2H_2O$) and its isotypes. Coincidentally,
449 data on laueite from Monmouth County, New Jersey (Segeler et al., 2012) have a broad doublet
450 corresponding to Fe^{3+} parameters of δ = 0.41 and Δ = 0.66 mm/s for the unresolved contributions
451 of Fe in the M1 ($M^{2+}(H_2O)_4(PO_4)_2$) and M3 ($Fe^{3+}(H_2O)_2(OH)_2(PO_4)_2$) sites and δ = 0.40 and Δ =
452 1.29 mm/s for the M2 site ($Fe^{3+}(OH_2)(PO_4)_4$). Several other phosphate minerals such as tancoite,
453 paravauxite, wavellite, eosphorite, and strunzite share this same chain structure, and should also
454 have the same Mössbauer parameters.
455 The slavikite structure (Parafiniuk et al. 2010) is composed of open sheets of corner-
456 sharing octahedra and tetrahedra (Hawthorne et al. 2000) but the fragments are similar to those in
457 the butlerite 7 Å chain (compare in Figure 5a). Both Mössbauer spectra of slavikites have a
458 doublet at δ = 0.36 mm/s and Δ = 1.14 mm/s like those in butlerite. Sample 140229 also contains
459 Fe^{3+} in copiapite-like sites, with δ = 0.22 and 0.58 mm/s and Δ = 0.55 and 0.54 mm/s, while the
460 second slavikite, VZO122/123, is dominated by a doublet with δ = 0.37 and Δ = 0.57 mm/s.
461 Similar chains are found in fibroferrite, though the linkages are with the *cis*-corners
462 (compare parabutlerite and fibroferrite in Figure 5a) rather than the *trans*-corners of the
463 octahedra in butlerite. This difference must not affect the geometry of the Fe coordination
464 polyhedra very much, because the fibroferrite samples in this study have parameters quite similar
465 to those of slavikite and parabutlerite.

The structures of the botryogen group minerals and sideronatrite are also based on 7 Å chains (Hawthorne et al. 2000). It is thus no surprise that Fe^{3+} in these octahedra all give rise to similar Mössbauer parameters, even though they are noticeably different than those from butlerite and related phases just discussed. All the botryogen, sideronatrite, and metasideronatrite spectra are dominated by the same doublet with $\delta = 0.41$ mm/s and $\Delta = 1.14$-1.21 mm/s. Botryogen is also related to and in the same Strunz classification group as copiapite; recall from discussion above that copiapite also has a doublet with parameters of $\delta = 0.42$-0.43 mm/s and $\Delta = 0.77$-0.80 mm/s. In addition to the doublets with $\Delta \approx 1.15$ mm/s, other samples of botryogen also have a second doublet in their Mössbauer spectra with an unusually high $\Delta = 1.63$ mm/s. This probably represents Fe^{3+} occupancy in the "branching" octahedra that link to the sides of the 7 Å chains. The botryogen and sideronatrite structures are again based on 7 Å chains, and the Fe coordination polyhedra are nearly identical (compare Figures 5a and 5b).

Metahohmannite, hohmannite, and amarantite are all members of the amarantite group, and are intimately related by dehydration (hohmannite in particular is not stable under ambient conditions). Metahohmannite has Mössbauer parameters of $\delta = 0.43$ mm/s and $\Delta = 0.94$ mm/s exactly like those found in butlerite, parabutlerite, and fibroferrite. Amarantite, on the other hand, most closely matches botryogen ($\delta = 0.40$ mm/s and $\Delta = 1.19$ mm/s). The difference is that metahohmannite and amarantite include an OH^- group substituting for O^{2-} in the structure (Scordari et al., 2004), but both are still based on the aforementioned 7 Å chains.

D. Alunite Group

The alunite group minerals, which include both alunite and jarosite, are composed of $[M^{3+}(OH)_6(SO_4)_2]$ sheets, where M is most commonly Fe^{3+} and/or Al^{3+}; monovalent and divalent cations such as K, Na, or H_3O^+ lie between the sheets. The Fe atoms occupy octahedra arranged

in six-membered, corner-sharing rings as well as three-membered rings (Hawthorne et al. 2000). Mössbauer spectra of alunite group minerals have been studied extensively by numerous workers (Grinkevich et al.1963, Hrynkiewicz et al. 1965, Herzenberg et al. 1966, Takano et al. 1968, Afanasev et al. 1974, Johnston 1973; Leclerc 1980, Huggins et al. 1983, Taneja et al. 1984, van der Kraan et al. 1984, Audley et al. 1986, Pax et al. 1988, Gracia et al. 1990, Gancedo et al. 1992, Music et al. 1994, Morris et al. 1996, Herbert 1997, Ahmed et al. 1999, 2003, Fajardo et al. 1999, Ristić et al. 2005, Verma et al. 2000, Waanders et al. 2003, Reyes et al. 2003, Ribiero et al., 2003, Eneroth et al. 2004, Rodriguez et al. 2005). Reported parameters range from δ = 0.30-0.45 mm/s and Δ = 1.00-1.22 mm/s, with most Δ values between 1.18 and 1.21 mm/s. The work of Rothstein (2006) and Dyar et al. (2006b) suggests that synthetic compositions across the compositional range of K-Na-H_3O^+ for jarosite have indistinguishable Mössbauer parameters, although there may be a relationship between isomer shift and Fe^{3+}/Al, with δ = 0.39 mm/s for Fe^{3+} end-members and δ = 0.37 mm/s for Al-rich ones. The jarosite spectra are nearly indistinguishable from sideronatrite and match those of botryogen and metasideronatrite very closely even though the structures are not specifically related.

E. Other Ferric-Bearing Sulfates

This study also included two samples of anhydrite and one of celestine. As Ca- and Ba-dominated sulfates, respectively, they do not fall in the same hierarchy as those previously discussed here. The relatively large size of the Ca and Ba cations requires large sites in the structures, which are usually 8-12-coordinated. Anhydrite is based on chains of alternating edge-sharing SO_4 tetrahedra and CaO_6 dodecahedra (Hawthorne et al. 2000) linked by edge and corner sharing between chains (Figure 1). Celestine consists of isolated SO_4 tetrahedra cross-linked by 12-coordinated Sr and Ba atoms (Brigatti et al. 1997). Thus these structures would seem unlikely

to incorporate Fe^{3+} in their structures, although Fe^{2+} might substitute. However, their Mössbauer spectra are both dominated by Fe^{3+}. For sample SPT132, the identification of the impurity as coquimbite by XRD is consistent with the Mössbauer parameters of the largest doublet. XRD of the celestine ML-S13 and anhydrite 159132 showed no impurities, but given the crystal structural constraints, it is unlikely that this Fe^{3+} is not actually in the anhydrite or celestine; rather, it is reasonable to assume that it arises from an impurity of another Fe^{3+} phase. The anhydrite localities studied both include phosphates, so it is also possible that the impurity could be some Fe^{3+} phosphate. The phase assemblage of the Michigan locality of the celestine is unreported. However, celestine from the Moldanubian Zone of the Bohemian Massif in the Czech Republic has been reported with anhydrite, pyrite, pyrrhotite, and chalcopyrite, and parameters in this study are consistent with those possibilities.

F. Ferrous Iron

It is again convenient to group and discuss the Fe^{2+} doublets in sulfates according to quadrupole splitting, which arises from a distribution of surrounding charges with less than cubic symmetry. Some samples in which Fe^{3+} features dominate merit revisiting because of their significant Fe^{2+} contents. The lowest values of Fe^{2+} quadrupole splitting in this study belong to voltaite (Table 3), with doublets at δ = 1.15-1.35 mm/s and Δ = 1.58-1.82 mm/s. Multiple doublets are found due to the presence of two M sites in the structure (both octahedral), as noted above in the section on Fe^{3+} in voltaite. The M1 site is coordinated to six O atoms from adjacent SO_4 tetrahedra, and has a slight trigonal distortion. It is the smaller of the two sites, with an average Fe-O distance of 2.004 Å (Mereiter 1972). This site may contain either Fe^{2+} or Fe^{3+}, according to the work of Long et al. (1980). The larger of the sites is designated the M2 site (with a multiplicity of three relative to one M1). It is coordinated to $FeO_4(H_2O)_2$, with Fe-O

distances of 2.097 Å and Fe-H_2O distances of 2.075 Å (Mereiter 1972). Because of its size, only Fe^{2+} and larger cations occupy this site. Mössbauer results from this study agree very well with work by Long et al. (1980), who report values of δ_{M2} = 1.17-1.27 mm/s and Δ_{M2} = 1.59-1.80 mm/s. They also identified a second peak assigned to the $^{[M1]}Fe^{2+}$ site as well as a $^{[M2]}Fe^{3+}$ peak, but neither one was sufficiently resolved to determine parameters.

There is no other closely-related structure to voltaite among the sulfate minerals studied to date, so no similar Mössbauer parameters would be expected except as coincidence. Perhaps other species with frameworks of SO_4 tetrahedra and $Fe(H_2O)_6$ octahedra, as listed in Table 12 of Hawthorne et al. (2000), might have similar spectra. Small doublets with similar Mössbauer parameters were found in some of other spectra in this work. However, it is likely that these may represent small amounts of voltaite impurities – especially because the impurities occur in mineral species known to coexist with voltaite.

As noted in the earlier discussion of Fe^{3+} species, the structure of metavoltine contains isolated $\{Fe^{2+}(H_2O)_6\}$ octahedra in the Fe(3) site; there should be one Fe^{2+} for every ~six Fe^{3+} (Giacovazzo et al., 1976). Wet chemical analyses reported by Scordari (1975) suggest that Fe^{2+} in three different occurrences of metavoltine are only ~10% of the total Fe, with the balance made up by Cu, Ni, Co, and Zn. Sample G2677 has 81% of the total Fe as Fe^{2+}, with doublet parameters of δ = 1.27 mm/s and Δ = 3.23 mm/s. These parameters are consistent with those observed by Sgarlata (1985).

None of the sulfates measured to date has *significant* Mössbauer doublets with quadrupole splittings between ~1.9 and 2.7 mm/s (Figure 2). Above 2.70 mm/s, szomolnokite ($FeSO_4 \cdot H_2O$) is the Fe end-member of the six kieserite group minerals, which have butlerite-like chains cross-linked by sharing of corners between adjacent tetrahedra and octahedra. The Fe (and

Mg, Mn, Cu, etc.) cations occupy octahedra with four corners shared with SO_4 and two with H_2O. Because they are isostructural, Fe^{2+} in all kieserite group phases (Figure 1) would have the same or similar Mössbauer parameters. The main doublet in szomolnokite (Table 6 and Figure 6a) occurs at δ = 1.26-1.31 mm/s and Δ = 2.73-2.89 mm/s. Szmikite and gunningite spectra are similar to their szomolnokite relative, with a doublet with δ =1.24-1.25 mm/s and Δ = 2.59-2.74 mm/s. These compare well with results of the many workers who have studied szomolnokite, including Van Alboom et al. (2009), Huggins and Huffman (1979), Montano (1981), Stiller et al. (1978), Russell and Montano (1978) and Giester et al. (1994). In general, these studies report Mössbauer parameters of δ = 1.18-1.26 mm/s and Δ = 2.67-2.71 mm/s for szomolnokite.

Of particular note is the work of Giester et al. (1994), who studied synthetic compositions along $FeSO_4 \cdot H_2O$ – $CuSO_4 \cdot H_2O$ solid-solution series. They found values for δ = 1.24-1.26 mm/s for $^{[M1]}Fe^{2+}$ and 1.35-1.25 mm/s for $^{[M2]}Fe^{2+}$, with Δ = 2.60-2.71 mm/s for $^{[M1]}Fe^{2+}$ and 2.89-2.90 mm/s for $^{[M2]}Fe^{2+}$. Their work predicted a site preference of Cu^{2+} for the more distorted M1 octahedra, due to the Jahn-Teller effect. Their assignment of the lower Δ doublet to M1 and the higher Δ doublet to M2 was necessary to allow consistent interpretation of their cation ordering results and x-ray results. Although this trend is counter to what would be predicted by theory, it might represent a difference between sulfates and silicates. An alternate interpretation might be that differential recoil-free fractions on the two sites are giving anomalous doublet areas, complicating interpretation of their results.

However, those same parameters are also shared by other types of sulfate structures. The four chalcanthite group minerals, chalcanthite, siderotil, pentahydrite, and jokokuite, have solid solution between the species, and are closely related to their dehydration product, rozenite. They have formulas of $(Cu,Fe,Mg,Mn) \cdot 5H_2O$. Mössbauer spectra of chalcanthite (δ = 1.30 mm/s and Δ

581 = 2.88 mm/s), pentahydrite (δ = 1.26 mm/s and Δ = 3.00 mm/s), and jokokuite (δ = 1.26 mm/s
582 and Δ = 3.00 mm/s) as seen in Figure 6b are similar as expected, and reflect Fe^{2+} occupancy of
583 octahedra linked to two SO_4 and four H_2O in corner-sharing chains.

584 Because halotrichite group minerals and römerite share very similar structures, the
585 Mössbauer parameters of their Fe^{2+} doublets should be as similar as they were for Fe^{3+}, and this
586 is again observed: δ_{Hal} = 1.28 mm/s and Δ_{Hal} = 2.76 mm/s, while $\delta_{Röm}$ = 1.26-1.34 mm/s and
587 $\Delta_{Röm}$ = 2.59-2.78 mm/s. The Fe^{2+} doublets in the related species apjohnite and bilinite are
588 slightly higher: δ_{Apj} = 1.27 mm/s and Δ_{Apj} = 3.31 mm/s, while δ_{Bil} = 1.06 mm/s and Δ_{Bil} = 3.69
589 mm/s (but note that the latter doublet is only 5% of the area in a dominantly-Fe^{3+} sample, so the
590 Fe^{2+} peaks are poorly resolved because they are so small).

591 Römerite also has a small doublet at δ = 1.24 mm/s and Δ = 2.38 mm/s which probably
592 represents Fe^{2+} in the isolated $\{Fe^{2+}(H_2O)_6\}$ octahedra (Figure 1). Work by Huggins and
593 Huffman (1979) found one Fe^{2+} doublet in römerite at δ = 1.27 and Δ = 3.27 mm/s (along with
594 two Fe^{3+} doublets as mentioned in the preceding section), while Sgarlata (1985) observed δ =
595 1.31 mm/s and Δ = 3.25 mm/s for halotrichite.

596 The next higher hydration state above chalcanthite is the hexahydrite group of minerals
597 $(Mg,Zn,Fe,Co,Ni,Mn)\cdot 6H_2O$, which is not represented in the currently-studied suite of spectra.
598 Their structures are composed of $M(H_2O)_6$ octahedra linked by weak hydrogen bonds to SO_4
599 tetrahedra. Their Mössbauer parameters would be predicted to be intermediate between those of
600 chalcanthite and the melanterite group minerals, $(Fe,Cu,Zn,Co,Mn)\cdot 7H_2O$, because melanterite
601 has a somewhat similar structure with only slightly higher Δ = 3.20 mm/s (and δ = 1.27 mm/s).

602 The probably-isostructural melanterite group minerals melanterite ($Fe^{2+}{}_2SO_4\cdot 7H_2O$) ,
603 boothite, zinc-melanterite, bieberite, and mallardite are composed of isolated $M(H_2O)_6$ octahedra

and SO_4 tetrahedra, again linked by hydrogen bonding (Figure 1). This group is also structurally related to the epsomite group, which would be expected to have similar Mössbauer parameters. Melanterite 2070 in this study has parameters of δ = 1.27 mm/s and Δ = 3.21 mm/s, similar to those reported by Cheetham et al. (1981), Grant et al. (1966), Sakai et al. (1981), Montano (1981), Eissa et al. (1994a,b), and Sallam et al. (1994) with a collective range of δ = 1.16-1.31 mm/s and Δ = 3.17-3.24 mm/s.

The isostructural rozenite group minerals (rozenite, $FeSO_4 \cdot 4H_2O$, starkeyite, ilesite, aplowite, and boyleite) are based on clusters (cf. Anderson et al. 2012), which might suggest that their Mössbauer parameters should be similar to those of the halotrichite group. Each cluster is composed of two tetrahedra each sharing two corners with two octahedra; the resultant formula is $M_2(SO_4)_2O_8$, where M = Fe, Mg, Mn, Co, and/or Zn. Rozenite SPT130 has prameters of δ = 1.27 mm/s and Δ = 3.21 mm/s, comparable to those of the halotrichite group. Because they are isostructural, Fe^{2+} in all species within the rozenite group should have similar Mössbauer parameters. Parameters given in the literature for rozenite are δ = 1.23-1.32 mm/s and Δ = 3.17 mm/s (Montano 1981).

VI. Relationships Among Coordination Polyhedra Geometries and Mössbauer Parameters

As noted earlier, Mössbauer parameters are related to the geometries of the individual coordination polyhedra surrounding the Fe cations in each site. In particular, distortion of the octahedral environment may lead to unequal occupancy of the *d* orbitals and a large contribution to Δ from the electronic field. Thus, it should be possible to directly correlate Δ values with the characteristics of the octahedral sites in each mineral studied.

626 For this comparison, single crystal structure refinements (SREF) of sulfate species were
627 collected from the American Mineralogist Crystal Structure Database using data from the same
628 species (though not the exact same samples) studied here. References to the SREF studies
629 employed are given in captions to Figures 3-6. Using those crystal structure data and the
630 CrystalMaker® software package, parameters describing the six-coordinated sites in each of the
631 sulfates studied (except bilinite, for which no refinement has been published) were evaluated. On
632 the basis of the atomic coordinates, calculated mean bond length, mean octahedral quadratic
633 elongation (λ), and angular variance (σ) of each cation site where Fe may reside in these
634 minerals were calculated. The latter two parameters were devised by Robinson et al. (1971) to
635 summarize variations in bond length and bond angle. The quadratic elongation parameter (λ)
636 provides a quantitative measurement of polyhedral distortion that is independent of polyhedral
637 size:

638 $$\lambda = \sum_{i=1}^{n} \left(\frac{l_i}{l_0}\right)^2 / n, \qquad (1)$$

639 where l_i is the measured bond distance (where $n = 6$ for 6-coordination) and l_0 is the bond
640 distance in a perfect (undistorted, equal volume) octahedron. Angular variance (σ) is calculated
641 using the expression:

642 $$\sigma = \sum_{i=1}^{n} (\theta_i - \theta_{avg.})^2 / (n-1), \qquad (2)$$

643 where θ_i is the measured angle in the crystal structure (there are n = 12 angles in a six-
644 coordinated site) and θ_{avg} is the bond angle for a perfect octahedron (all angles are 90º). These
645 structural data were compared with Δ values for the samples studied. In cases where there are
646 multiple sites possible for Fe atoms, Mössbauer doublets were assigned on the basis of
647 consistency with related structures and relative distortion. Refinements where the composition

was low in Fe were not used, because those site characteristics are more reflective of the other cation than of Fe occupancy. The refinement of apjohnite by Mechetti and Sabelli (1976) was not used because its parameters lay far off the trends of all other samples, suggesting a possible problem with the Crystallographic Interchange File format.

Results of these comparisons are shown for Fe^{3+} in Figure 7. The plot of angular variance shows no systematics with Δ, but the other polyhedral parameters show some interesting trends despite the varying quality and sophistication of the structure refinements. There is an increase in quadrupole splitting with octahedral volume and mean bond length. Quadratic elongation decreases slightly with increasing Δ. This observation may seem counter to the assumption that Δ generally increases with distortion, but λ is just one of the possible formulations that could be used to describe that distortion and λ is also insensitive to polyhedral size. No trend is seen for angular variance. Thus it appears that for sulfate minerals, the best predictor of quadrupole splitting (and thus peak location) is the size of the coordination polyhedron in any given mineral species. Comparable plots for Fe^{2+} are not shown because there are only a few data points and they all fall within two small groups of quadrupole splitting.

V. Implications: Uniqueness of Sulfate Mössbauer Parameters

As noted at the onset, the MIMOS II Mössbauer spectrometers on the Mars Exploration Rovers identified jarosite at the Meridiani Planum landing site based on the presence of a peak with Δ = 1.22 mm/s at T = 240±40K. Errors on the Mars fit parameters are quoted as ±0.02 mm/s. The same Mars spectra were also fit using the software from the current study (Dyar et al., 2006c), resulting in more variability in peak positions, with δ = 0.28-0.41 and Δ = 1.19-1.27 mm/s. The extrapolation of the low and variable temperature to 295K was estimated by

671 Klingelhöfer et al. (2004) to be -0.07 mm/s, though Rothstein (2006) found only a -0.02 mm/s
672 offset in laboratory spectra. In any case, based on the data available to them in 2004, the team
673 assigned that doublet to jarosite, later suggested to be hydronium jarosite (Morris et al. 2007).
674 Results from the current study (blue squares and green circles) are plotted with the Mars data
675 (orange and red circles) in Figure 8, and support the assignment to jarosite but show that many
676 sulfate minerals have parameters close to those of jarosites, as measured under optimal
677 laboratory conditions with state of the art equipment, including botryogen, metasideronatrite,
678 slavikite, etc. A small deviation in peak position of the Mars data could easily result in overlap
679 with many different possible sulfate mineral species. As seen in Figure 9, the Fe polyhedra in
680 these sulfates are strikingly similar, so it is not surprising that the Mössbauer peaks should be so
681 similar as well.

682 At the Gusev Crater site, there are two different features that might be assigned to Fe^{3+}
683 sulfate. The first is a doublet designated Fe3D1, which is assigned by Morris et al. (2008) to a
684 generic Fe^{3+} alteration product nanophase Fe oxide, though Morris et al. (2007) suggest that the
685 higher Δ doublets in that range might be attributed to hydronium jarosite. The parameters of the
686 Fe3D1 doublet do not overlap with those from any of the Fe^{3+} sulfates from this paper, in support
687 of the assignment to nanophase Fe oxides. The second feature noted by Morris et al. (2008) is
688 assigned to an Fe^{3+} sulfate designated as Fe3D2 (Figure 10) that is not specified. On the basis of
689 the current study, optimal candidates for the feature at Arad Samra would be fibroferrite and
690 rhomboclase and likely copiapite or parabutlerite at Tyrone Mount Darwin and Berkner Island
691 (Figure 10). It must be stressed, however, that such assignments presume that the phase in
692 question is one of those studied here, and that it is indeed a sulfate.

693 In making these conclusions, it is important to note the importance of independent
694 corroboration from other techniques, without which Mössbauer results cannot be used to
695 distinguish sulfates from other common Fe^{3+}-bearing phases (even sulfides). The current study
696 was focused on hydrous sulfates, and sample selection was biased in that direction. However,
697 there are other sulfate, sulfide, and S-containing minerals that should be considered as candidates
698 for Mars. For example, the related phase schwertmannite ($Fe^{3+}_{16}O_{16}(OH)_{12}(SO_4)_2$) is formally
699 considered to be a hydroxide containing hydroxyl (Dana class 6). Mössbauer spectra of
700 schwertmannite have been extensively studied by many workers, including Bigham et al. (1994),
701 Schwertmann et al. (1995), Bishop and Murad (1996), and Bigham and Murad (1997). Typical
702 parameters are δ = 0.37 mm/s and Δ = 0.61-0.81 mm/s, which overlap with those of other
703 hydrous Fe^{3+} sulfates discussed above. Mössbauer spectra of sulfide minerals also overlap with
704 several species in this study, including pyrite (Silva et al. 2011: δ = 0.27-0.30 and Δ = 0.55-0.62
705 mm/s) and sphalerite (unpublished data: δ = 0.30 mm/s and Δ = 0.46 mm/s).
706 For Fe^{2+} sulfates, identification on the basis of Mössbauer spectra is complicated by the
707 potential for overlap with olivine peaks (Lane et al. 2004). The range of measured Mössbauer
708 parameters for Fe^{2+} in synthetic olivines has been well-studied (Sklute et al. 2005; Sklute 2006):
709 δ = 1.13-1.17 mm/s and Δ = 2.80-3.05 mm/s. Fe^{2+} sulfates (Table 6) have comparable Δ but
710 higher δ values (ca. 1.25-1.33 mm/s), allowing olivine to be distinguished from Fe^{2+} sulfates
711 under optimal experimental conditions. When these parameters are converted to peak positions,
712 it is apparent that an error of 0.1 mm/s in velocity would be enough to make sulfates and olivines
713 indistinguishable.
714 This discussion highlights both the strengths and weaknesses of Mössbauer spectroscopy.
715 Highly reproducible spectra can be acquired under a range of conditions and instrument

716 geometries from transmission to backscatter mode, in the laboratory or on the surface of Mars.
717 Species within groups of naturally-occurring minerals have spectral peaks that generally fall
718 within small velocity ranges. Spectral parameters can be qualitatively related to the geometries of
719 the individual Fe coordination polyhedra. In cases where independent constraints on phase
720 identity are available, this capability allows Mössbauer spectroscopy to assist in understanding
721 the distribution of Fe and its valence states among different coexisting phases. On Mars, the
722 MIMOS spectrometers were pressed into service for mineral identification in conjunction with
723 bulk chemical results from the alpha particle x-ray spectrometer instrument and deductions based
724 on phase equilibria of likely martian assemblages. The success of the MER missions owes much
725 to constraints placed on mineral identification by the Mössbauer spectrometers based on
726 comparisons to contemporary databases of spectra.

727 However, for paramagnetic minerals, it must be acknowledged that the range of
728 Mössbauer parameters is small (particularly for Fe^{3+}), and many phases have overlapping
729 parameters (Figure 11). For example, Fe^{2+} doublets in orthopyroxene will be unrecognizable
730 from Fe^{2+} in clinopyroxene (Dyar et al. 2013) and analogous to several different Fe^{3+} sulfates
731 (among many other possibilities). Pyroxene, amphibole, and mica (including clay mineral)
732 spectra will be generally indistinguishable because the structures are all so similar. In other
733 words, the number of mineral species is large and the range of hyperfine parameters is small, so
734 that in many cases, phases cannot be uniquely identified. This is particularly true for Fe^{3+}-rich
735 phases, because the absolute range of Mössbauer parameters for Fe^{3+} in any coordination number
736 is so small.

737 Evaluating the crystal structures of these minerals provides explanations for the
738 similarities in Mössbauer parameters. Because mineral structures based on varying linkages

739 among tetrahedra are universal (cf. Figure 1), silicate and sulfate (and phosphate, perchlorate,
740 etc.) structures will have much in common. The resultant octahedral sites between those
741 tetrahedra will occur in a variety of geometries, but crystal chemistry shows that many groups
742 will be similar because their structural frameworks are the same. In turn, Fe cations in those
743 similar crystallographic sites will give rise to Mössbauer doublets with comparable parameters,
744 and thus the range of observed Mössbauer parameters is relatively small for most minerals. For
745 this reason, Mössbauer spectroscopy is rarely used in terrestrial labs for mineral identification
746 because so many other more appropriate techniques are widely available (e.g. x-ray diffraction).
747 The true strength of the Mössbauer technique lies in its ability to measure valence states and site
748 occupancies of Fe and identify magnetic phases. This study shows that Mössbauer data can also
749 inform our understanding of the local environment around the Fe polyhedra, and thus provide
750 distinctions among different phases that, when combined with other types of information, can
751 assist with mineral identification even in paramagnetic materials.
752
753 **Acknowledgments:** We are grateful to Ed Cloutis, the Harvard Mineralogical Museum, and the
754 NMNH for the loan of samples, and for support from NSF grants EAR-043907 and EAR-
755 0439161 and NASA grants NNG04GG12G, NAG5-12687, and NNX11AF11G. Student support
756 for this project was provided by the Massachusetts Space Grant Consortium. Thoughtful
757 suggestions from two anonymous reviewers and Juraj Majzlan were greatly appreciated. We
758 thank David Palmer for help with the CrystalMaker® models. This is PSI Contribution Number
759 605.

760 **REFERENCES**

761 Afanasev, A.M., Gorobchenko, V.D., Kulgawczuk, D.S., and Lukashevich, I.I. (1974). Nuclear
762 γ-Resonance in Tron Sulphates of the Jarosite Group. Physica Status Solidi, 26,697- 701.
763 Ahmed, M. A., Blesa, M.J., Juan, R., and Vandeberghe, R.E. (2003) Characterization of an
764 Egyptian coal by Mössbauer and FT-IR spectroscopy. Fuel, 82, 1825-1829.
765 Ahmed, M. A., Vandenberghe, R.E., De Grave, E., Eissa, N.A., and Ibarra, J.V. (1999)
766 Characterisation of Spanish coal by means of Mössbauer spectroscopy. Fuel, 78, 453-
767 457.
768 Anderson, J.L., Peterson, R.C., and Swainson, I. (2012) The atomic structure of deuterated
769 boyleite $ZnSO_4 \cdot 4D_2O$, ilesite $MnSO_4 \cdot 4D_2O$, and bianchite $ZnSO_4 \cdot 6D_2O$. American
770 Mineralogist, 97, 1905-1914.
771 Audley, G. J., Pyne, G.S., Tricker, M.J., Cranshaw, T.E., and Laundy, B.J. (1986) A New
772 Approach to the Determination of Pyrite in Coals by Mössbauer Spectroscopy. Fuel, 65,
773 1103-1107.
774 Bacon, G.E., and Titterton, D.H. (1975) Neutron-diffraction studies of $CuSO_4 \cdot 5(H_2O)$ and
775 $CuSO_4 \cdot 5(D_2O)$. Zeitschrift fur Kristallographie, 141, 330-341.
776 Ballirano P, Bellatreccia F, Grubessi O (2003) New crystal-chemical and structural data of
777 dietrichite, ideally $ZnAl_2(SO_4)_4 \cdot 22H_2O$, a member of the halotrichite group. European
778 Journal of Mineralogy, 15, 1043-1049.
779 Basciano, L.C., and Peterson, R.C. (2007) Jarosite - hydronium jarosite solid solution series with
780 full iron occupancy: Mineralogy and crystal chemistry. American Mineralogist, 92, 1464-
781 1473.
782 Baur, W.H. (1962) Zur kristallchemie der salzhydrate. Die kristallstrukturen von $MgSO_4 \cdot 4H_2O$
783 (leonhardtit) und $FeSO_4 \cdot 4H_2O$ (rozenit). Acta Crystallographica, 15, 815-826.

784 Berlepsch, P., Armbruster, T., Brugger, J., Bykova, E.Y., and Kartashov, P.M. (1999) The
785 crystal structure of vergasovaite $Cu_3O[(Mo,S)O_4SO_4]$ and its relation to synthetic
786 $Cu_3O[MoO_4]_2$. European Journal of Mineralogy, 11, 101-110.
787 Bigham, J.M., and Murad, E. (1997) Mineralogy of ocher deposits formed by the oxidation of
788 iron sulfide minerals. In Advances in GeoEcology, K. Auerswald, H. Stanjek, and J.M.
789 Bigham, eds., Catena Verlag, Reiskirchen, 35447, Germany, pp. 193-225.
790 Bigham, J.M., Carlson, L., and Murad, E. (1994) Schwertmannite: A new iron
791 oxyhydroxysulphate from Pyhasalmi, Finland, and other localities. Mineralogical
792 Magazine, 58, 641-648.
793 Bishop, J.L., and Murad, E. (1996) Schwertmannite on Mars? Spectroscopic analyses of
794 schwertmannite, its relationship to other ferric minerals, and its possible presence in the
795 surface material on Mars. In Mineral Spectroscopy: A Tribute to Roger G. Burns,
796 Geochemical Society Special Publication, 5, 337-358.
797 Blake, D., Vaniman, D., Achilles, C., Anderson, R., Bish, D., Bristow, T., Chen, C., Chipera, S.,
798 Crisp, J., Des Marais, D., Downs, R.T., Farmer, J., Feldman, S., Fonda, M., Gailhanou,
799 M., Ma, H., Ming, D.W., Morris, R.V., Sarrazin, P., Stolper, E., Treiman, A., and Yen, A.
800 (2012) Characterization and calibration of the CheMin mineralogical instrument on Mars
801 Science Laboratory. Space Science Reviews, 170, 341-399.
802 Blaney, D L. and McCord, T.B. (1995) Indications of sulfate minerals in the Martian soil from
803 Earth-based spectroscopy. Journal of Geophysical Research, 100, 14433-14441.
804 Bonello, G., Bibring, J.P., Poulet, F., Gendrin, A., Gondet, B., Langevin, Y., and Fonti, S.
805 (2004) Visible and infrared spectroscopy of minerals and mixtures with the OMEGA-
806 Mars-EXPRESS instrument. Planetary and Space Sciences, 52, 133-140.

Borene, J. (1970) Structure cristalline de la parabutlerite. Bulletin de la Societe Francaise de Mineralogie et de Cristallographie, 93, 185-189.

Bregeault, J., Herpin, P., Manoli, J., and Pannetier, G. (1970) Affinement de la structure de la kieserite $Mg(SO_4)$ (H_2O). Bulletin de la Societe Chimique de France, 1970, 4243-4248.

Brigatti, M.F., Gali, E., and Medici, L. (1997) Ba-rich celestine: new data and crystal structure refinement. Mineralogical Magazine, 61, 447-451.

Burns, R.G. (1986) Terrestrial analogues of the surface rocks of Mars?, Nature, 320, 55– 56.

Burns, R.G. (1987) Ferric sulfates on Mars, Proc. Lunar Planet. Sci. Conf.17th, Part 2, Journal of Geophysical Research, 92, suppl., E570– E574.

Burns, R.G. (1988) Gossans on Mars. Proceedings of the Lunar and Planetary Science Conference, 18, 713–721.

Burns, R.G. (1993) Rates and mechanisms of chemical weathering of ferromagnesian silicate minerals on Mars. Geochimica et Cosmochimica Acta, 57, 4555–4574.

Burns, R.G., and Fisher, D.S. (1990) Evolution of sulfide mineralization on Mars. Journal of Geophysical Research, 95, 14,169–14,173.

Burns, R.G., and Solberg, T.C. (1990) ^{57}Fe-bearing oxide, silicate, and aluminosilicate minerals, crystal structure trends in Mossbauer spectra, in Spectroscopic Characterization of Minerals and Their Surfaces, pp. 262–283, American Chemical Society, Washington, D.C.

Caminiti, R., Marongiu, G., and Paschina, G. (1982) A comparative X-ray diffraction study of aqueous MnSO4 and crystals of $MnSO_4 \cdot 5H_2O$. Zeitschrift fur Naturforschung, A37, 581-586.

Cheetham, A.K., Cole, A.J., and Long, G.J. (1981) Investigation of the mixed-metal sulfide (Mn,Fe)S_2 by analytical electron microscopy and Mössbauer spectroscopy. Inorganic Chemistry, 20, 2747-2750.

Clark, B.C., Baird, A.K., Welcon, R.J., Tsusaki, D.M., Schnabel, L., and Candelaria, M.P. (1982) Chemical composition of Martian fines. Journal of Geophysical Research, 87, 10059-10067.

DeBenedetti, S., Lang, G., and Ingalls, R. (1961) Electric quadrupole splitting and the nuclear volume effect in the ions of Fe^{57}. Physical Review Letters, 6, 60-62.

Duesler, E.N., and Foord, E.E. (1986) Crystal structure of hashemite, $BaCrO_4$, a barite structure type. American Mineralogist, 71, 1217-1220.

Dyar, M.D. (1984) Precision and interlaboratory reproducibility of measurements of the Mössbauer effect in minerals. American Mineralogist, 69, 1127-1144.

Dyar, M.D. Agresti, D.G., Schaefer, M., Grant, C.A., and Sklute, E.C. (2006a) Mössbauer spectroscopy of earth and planetary materials. Annual Reviews of Earth and Planetary Science, 34, 83-125.

Dyar, M.D., Podratz, L., Sklute, E.C., Rusu, C., Rothstein, Y., Tosca, N., Bishop, J.L., and Lane, M.D. (2006b). Mössbauer spectroscopy of synthetic alunite group minerals. Workshop on Martian Sulfates as Recorders of Atmospheric-Fluid-Rock Interactions, #7053.

Dyar, M.D., Rothstein, Y., Schaefer, M.W., and Agresti, D. (2006c) Mössbauer spectroscopy of outcrop at the Merdiani Planum site. Lunar and Planetary Science XXXVII, Abstract #2382.

Dyar, M.D., Schaefer, M.W., Sklute, E.C., and Bishop, J.L. (2008) Mössbauer spectroscopy of phyllosilicates: Effects of fitting models on recoil-free fractions and redox ratios. Clay Minerals, 43, 3-33.

Dyar, M.D., Klima, R.L., Fleagle, A., and Peel, S.E. (2013) Fundamental Mössbauer parameters of synthetic Ca-Mg-Fe pyroxenes. American Mineralogist, 98, 1172-1186.

Eissa, N.A., Sallam, H.A., Sheta, N.H., Radwan, Sh.N., and Soliman, M.A. (1994b) Mössbauer study of the role of Fe^{2+}/Fe^{3+} ratio and water of hydration on the optical and electrical properties of gamma-irradiated melanterite. Arab Journal of Nuclear Sciences and Applications, 27, 143-154.

Eissa, N.A., Sheta, N.H., El-Mossallamy, S.M., Soliman, M.A., and El-Fouly, M.H. (1994a) Study of the dehydration process of melanterite under heat treatment and gamma irradiation effects using Mössbauer spectroscopy and thermal analysis measurements. Arab Journal of Nuclear Sciences and Applications, 27, 33-45.

Eneroth, E., and Koch, C.B. (2004) Fe-Hydroxysulphates from bacterial Fe^{2+} oxidation. Hyperfine Interactions, 156, 423-429.

Ertl, A., Dyar, M.D., Hughes, J.M., Brandstätter, F., Gunter, M., Prem, M., and Peterson, R.C. (2008) Pertlikite, a new netragonal Mg-rich member of the voltaite group from Madeni Zakh, Iran. Canadian Mineralogist, 46, 661-669.

Fajardo, M., Mojica, J., Barraza, J., Perez Alcazar, G.A., and Tabares, J.A. (1999) Mineral identification in Colombian coals using Mössbauer spectroscopy and X-ray diffraction. Hyperfine Interactions, 122, 129-138.

Fanfani, L., Nunzi, A., and Zanazzi, P.F. (1970) The crystal structure of römerite. American Mineralogist, 55, 78-89.

873 Fanfani, L., Nunzi, A., and Zanazzi, P.F. (1971) The crystal structure of butlerite. American
874 Mineralogist, 56, 751-757.
875 Fanfani, L., Nunzi, A., Zanazzi, P.F., and Zanzari, A.R. (1973) The copiapite problem: The
876 crystal structure of a ferrian copiapite. American Mineralogist, 58, 314-322.
877 Fang, J.H., and Robinson, P.D. (1970) Crystal structures and mineral chemistry of hydrated
878 ferric sulfates. I. The crystal structure of coquimbite. American Mineralogist, 55, 1534-
879 1540.
880 Fernández-Remolar, D.C., Morris, R.V., Gruener, J.E., Amils, R., and Knoll, A.H. (2005) The
881 Río Tinto Basin, Spain: Mineralogy, sedimentary geobiology, and implications or
882 interpretation of outcrop rocks at Meridiani Planum, Mars. Earth and Planetary Science
883 Letters, 240, 149-167.
884 Foley, C.N., Economou, T., and Clayton, R.N. (2004) Final chemical results from the Mars
885 Pathfinder alpha proton X-ray spectrometer. Journal of Geophysical Research, 108,
886 doi:10.1029/2002JE002019.
887 Gancedo, J. R., Gracia, M., Martinez-Alonso, A., Miranda, J.L., and Tascon, J.M.D. (1992)
888 Mössbauer study of the effect of acidic treatment on iron minerals during the
889 demineralization of coals. Hyperfine Interactions, 71, 1403-1406.
890 Giacovazzo, C., Scordari, F., Todisco, A., and Menchetti, S. (1976) Crystal structure model for
891 metavoltine from Sierra Gorda. Tschermaks Mineralogische und Petrographische
892 Mitteilungen, 23, 155-166.
893 Giester, G., Lengauer, C.I., and Redhammer, G. (1994) Characterization of the $FeSO_4 \cdot H_2O$-
894 $CuSO_4 \cdot H_2O$ solid solution series and the nature of poitevinite, $(Cu,Fe)SO_4 \cdot H_2O$. The
895 Canadian Mineralogist, 32, 873-884.

Gracia, M., Gancedo, J.R., Martinez-Alonso, A., and Tascon, J.M.D. (1990) Comparative Mössbauer study of the oxidation of pyrite under different conditions. Hyperfine Interactions, 58, 2581-2588.

Graeber, E.J., and Rosenzweig, A. (1971) The crystal structures of yavapaiite, $KFe(SO_4)_2$, and goldichite, $KFe(SO_4)_2.4H_2O$. American Mineralogist, 56, 1917-1933.

Graeber, E.J., Morosin, B., and Rosenzweig, A. (1965) The crystal structure of krausite, $KFe(SO_4)_2.H_2O$. American Mineralogist, 50, 1929-1936.

Grant, R.W., Wiedersich, H., Muir, A.H. Jr., Gonser, U., and Delgass, W.N. (1966) Sign of the nuclear quadrupole coupling constants in some ionic ferrous compounds. The Journal of Chemical Physics, 45, 1015-1019.

Grinkevich, A. Z. and Kul'gavchik., D.S. (1963) The fine structure of Mössbauer spectra in mineral compounds of iron. Proceedings of the Dubna Conference on the Mössbauer Effect, 18-EOA.

Hawthorne, F.A. (1985) Toward a structural classification of minerals: the $^{VI}M^{IV}T_2\Phi_n$ minerals. American Mineralogist, 70, 455-473.

Hawthorne, F.C. (1979) The crystal structure of morinite. Canadian Mineralogist, 17, 93-102.

Hawthorne, F.C., and Ferguson, R.B. (1975) Anhydrous sulphates. II. Refinement of the crystal structure of anhydrite. The Canadian Mineralogist, 13, 289-292.

Hawthorne, F.C., Krivovichev, S.V., and Burns, P.C. (2000) The crystal chemistry of sulfate minerals. Reviews in Mineralogy, 40, 1-112.

Held, P., and Bohaty, L. (2002) Manganese(II) sulfate tetrahydrate (ilesite). Acta Crystallographica, E58, i121-i123.

Herbert, R.B.J. (1997) Properties of goethite and jarosite precipitated from acidic groundwater, Dalarana, Sweden. Clays and Clay Minerals, 45, 261-273.

Hermon, E., Haddad, R., Simkin, D., Brandão, and Muir, W.B. (1976) Magnetic properties and the distribution of iron ions in voltaites. Canadian Journal of Physics, 54, 1149-1156.

Herzenberg, C. L., and Toms, D. (1966). Mössbauer Absorption Measurements in Iron-containing Minerals. Journal Of Geophysical Research, 71, 2661-2677.

Hrynkiewicz, A.Z., Kubisz, J., and Kulgawczuk, D.S. (1965). Quadrupole splitting of the 14.4 keV gamma line of ^{57}Fe in iron sulphates of the jarosite group. Journal of Inorganic Nuclear Chemistry, 27, 2513- 2517.

Huggins, F.E., Huffman, G.P., and Lin, M.C. (1983) Observations on low-temperature oxidation of minerals in bituminous coals. International Journal of Coal Geology, 3, 157-182.

Huggins, G.P. and Huffman, F.E. (1979) Mössbauer analysis of iron-bearing phases in coal, coke, and ash. Analytical Methods for Coal and Coal Products, 3, 371-423.

Hyde, B.C., King, P.L., Dyar, M.D., Spilde, M.N., Ali, A.-M.S., and Kinkel, T. (2011) Methods to analyze metastable and microparticulate hydrated and hydrous iron sulfate minerals. American Mineralogist, 96, 1856-1869.

Johnston, J.H. (1977). Jarosite and akagenite from White Island Volcano, New Zealand- an x-ray and Mossbauer study. Geochimica et Cosmochimicia Acta, 41, 539-544.

Klingelhöfer, G., R.V. Morris, B. Bernhardt, C. Schröder, D.S. Rodionov, P.A. deSouza, A. Yen, R. Gellert, E.N. Evlanov, B. Zubkov, J. Foh, U. Bonnes, E. Kankeleit, P. Gutlich, D.W. Ming, F. Renz, T. Wdowiak, S.W. Squyres, and R.E. Arvidson (2004), Jarosite and hematite at Meridiani Planum from Opportunities Mossbauer spectrometer, Science, 306, 1740-1745.

941 Kovács, K., Kuzmann, E., Homonnay, Z., Vértes, A., Gunneriusson, L.and Sandstron, A. (2008)
942 Mössbauer study of synthetic jarosites. Hyperfine Interactions, 186, 69-73.
943 Lane, M.D. Bishop, J.L., Hiroi, T., Dyar, M.D., Bish, D.L., Mertzman, S.A.(submitted) Mid-
944 infrared emission spectroscopy and visible-near infrared reflectance spectroscopy of iron
945 sulfate minerals. American Mineralogist, submitted.
946 Lane, M.D., M.D. Dyar, and J.L. Bishop (2004), Spectroscopic evidence for hydrous iron sulfate
947 in the martian soil, Geophy. Res. Lett., 31, L19702, doi: 10.1029/2004GL021231.
948 Leclerc, A. (1980) Room temperature Mössbauer analysis of jarosite-type compounds. Physics
949 and Chemistry of Minerals**,** 6, 327-334.
950 Lin, J., Chen, N., Nilges, M.J., and Pan, Y. (2013) Arsenic speciation in synthetic gypsum
951 ($CaSO_4 \cdot 2H_2O$): A synchrotron XAS, single-crystal EPR, and pulsed ENDOR study.
952 Geochimica et Cosmochimica Acta, 106, 524-540.
953 Long, G.J., Longworth, G., Day, P., and Beveridge, D. (1980) A Mössbauer effect study of the
954 electronic and magnetic properties of voltaite, a mixed-valence mineral. Inorganic
955 Chemistry, 19, 821-829.
956 Lovas, G.A. (1986) Structural study of halotrichite from Recsk (Matra Mts., N. Hungary). Acta
957 Geologica Hungarica, 29, 389-398.
958 Majzlan, .J, Alpers, C.N., Bender Koch, C., McCleskey, R.B., Myneni, S.C.B., and Neil, J.M.
959 (2011) Vibrational, X-ray absorption, and Mössbauer spectra of sulfate minerals from the
960 weathered massive sulfide deposit at Iron Mountain, California. Chemical Geology, 284,
961 296-305.

962 Majzlan, J., Botez, C., and Stephens, P W. (2005) The crystal structures of synthetic
963 $Fe_2(SO_4)_3(H_2O)_5$ and the type specimen of lausenite. American Mineralogist, 90, 411-
964 416.
965 Majzlan, J., Schlicht, H., Wierzbicka-Wieczorek, M., Giester, G., Pollman, H., Brömme, B.,
966 Doyle, S., Buth, S., and Bender Koch, C. (2013) A contribution to the crystal chemistry
967 of the voltaite group: solid solutions, Mössbauer and infrared spectra, and anomalous
968 anisotropy. Mineralogy and Petrology, 107, 221-233.
969 McAdam, A.C., Franz, H., Archer, P., Jr., freissiner, C., Sutter, B., Glavin, D., Eigenbrode, J.,
970 Bower, H., Stern, J., Mahaffy, P.R., Morris, R., Ming, D., Rampe, E., Brunner, A., Steele,
971 A., Navarro-Gonzolez, R., Bish, D., Blake, D., Wray, J., Grotzinger, J., and the MSL
972 Science Team (2013) Insights into the sulfur mineralogy of martian soil at Rocknest,
973 Gale Crater, enabled by evolved gas analysis. Lunar and Planetary Science, 44, Abstract
974 44, 1751.
975 Menchetti, S., and Sabelli, C. (1976) The halotrichite group: The crystal structure of apjohnite.
976 Mineralogical Magazine, 40, 599-608.
977 Mereiter, K. (1972) Die kristallstruktur des voltaits, $K_2Fe^{2+}{}_5Fe^{3+}{}_3Al[SO_4]_{12}\cdot 18H_2O$. Tschermaks
978 Mineralogische und Petrographische Mitteilungen, 18, 185-202.
979 Mereiter, K. (1974) Die kristallstruktur von rhomboklas, $H_5O_2^+\{Fe[SO_4]_2\cdot 2H_2O\}$. Tschermaks
980 Mineralogische und Petrographische Mitteilungen, 21, 216-232.
981 Miyake, M., Minato, I., Morikawa, H., and Iwai, S.I. (1978) Crystal structure and sulphate force
982 constants of barite, celestite, and anglesite. American Mineralogist, 63, 506-510.
983 Montano, P.A. (1981) Transformations and role of iron sulfides in coal liquefaction. Bulletin of
984 the American Physical Society, 26, 201-201.

985 Moore, P.B. (1970) Structural hierarchies among minerals containing octahedrally coordinating
986 oxygen. Neues Jahrbuch für Mineralogie Monatshefte, 1970, 163-173.
987 Moore, P.B. (1973) Bracelets and pinwheels – Topological geometrical approach to calcium
988 orthosilicate and alkali sulfate structures. American Mineralogist, 58, 32-42.
989 Morris, R.V., Ming, D.W., Golden, DC., and Bell, J.F. (1996) An occurrence of jarositic tephra
990 on Mauna Kea, Hawaii; implications for the ferric mineralogy of the Martian surface.
991 Mineral spectroscopy; a tribute to Roger G. Burns Special Publication - Geochemical
992 Society, 5, 327-336.
993 Morris, R.V., Klingelhöfer, G., Bernhardt, B., Schröder, C., Rodionov, D.S., deSouza, P.A., Yen,
994 A., Gellert, R., Evlanov, E.N., Foh, J., Kankeleit, E., Gütlich, P., Ming, D.W., Renz, F.,
995 Wdowiak, T., Squyres, S.W., and Arvidson, R.E. (2004) Mineralogy at Gusev Crater
996 from the Mossbauer spectrometer on the Spirit rover. Science, 305, 833-836.
997 Morris, R.V., Klingelhöfer, G., Schröder, C., Fleischer, I., Ming, D.W., Yen, A.S., Gellert, R.,
998 Arvidson, R.E., Rodionov, D.S., Crumpler, L.S., Clark, B.C., Cohen, B.A., McCoy, T.J.,
999 Mittlefehldt, D.W., Schmidt, M.E., de Souza, P.A. Jr., and Squyres, S.W. (2008) Iron
1000 mineralogy and aqueous alteration from Husband Hill through Home Plate at Gusev
1001 Crater, Mars: Results from the Mössbauer instrument on the Spirit Mars Exploration
1002 Rover. Journal of Geophysical Research, 113, E12S42, doi:10.1029/2008JE003201.
1003 Morris, R.V., Klingelhöfer, G., Schröder, C., Rodionov, D.S., Yen, A., Ming, D.W., de Souza,
1004 P.A. Jr., Wdowiak, T., Fleischer, I., Gllert, R., Bernhardt, B., Bonnes, U., Cohen, B.A.,
1005 Evlanov, E.N., Foh, J., Gütlich, P., Kankeleit, E., McCoy, T., Mittlefehldt, D.W., Renz,
1006 F., Schmidt, M.E., Zubkov, B., Squyres, S.W., and Arvidson, R.E. (2006) Mössbauer
1007 mineralogy of rock, soil, and dust at Meridiani Planum, Mars: Opportunity's journey

across sulfate-rich outcrop, basaltic sand and dust, and hematite lag deposits. Journal of Geophysical Research, 111, E12S15, doi:10.1029/2006JE002791.

Morris, R.V., Ming, D.W,m Yen, A., Arvidson, R.E., Gruener, J., Humm, D., Klingelhöfer, G.,. Murchie, S., Schroder, C., Seelos, F. IV, Squyres, S., Wiseman, S., Wolff, M., and the MER and CRISM Science Teams (2007) Possible evidence for iron sulfate, iron sulfides, andelemental sulfur at Gusev Crater, Mars, from MER, CRISM, and analog data. 7th International Conference on Mars, Abstract 3393.

Musíc, S., Orehovec, Z., Popovic, S., and Czako-Nagy, I. (1994) Structural properties of precipitates formed by hydrolysis of Fe^{3+} ions in $Fe_2(SO_4)_3$ solutions. Journal of Materials Science**,** 29, 1991-1998.

Nomura, K., Takeda, M., Iiyama, T., and Sakai, H. (2005) Mössbauer studies of jarosite, mikasaite, and yavapaiite, and implication to their martian counterparts. Hyperfine Interactions, 166, 657-664.

Pankhurst, Q.A., McCann, V.H., and Newman, N.A. (1986) Identification of the iron-bearing minerals in some bituminous coals using Mössbauer spectroscopy. Fuel, 65, 880-883.

Parafiniuk, J., Bobrzycki, L., and Wozniak, K. (2010) Slavikite - revision of chemical composition and crystal structure. American Mineralogist, 95, 11-18.

Pax, R.A., and Clark, P.E. (1988) Application of Mössbauer spectroscopy to the coals of central Queensland. Hyperfine Interactions, 41, 839-842.

Peterson, R.C. (2003) The relationship between Cu content and distortion in the atomic structure of melanterite from the Richmond mine, Iron Mountain, California. The Canadian Mineralogist, 41, 937-949.

Peterson, R.C., Hammarstrom, J.M., and Seal, R.R. (2006) Alpersite (Mg,Cu)SO_4·7H2O, a new mineral of the melanterite group, and cuprian pentahydrite: Their occurrence within mine waste. American Mineralogist, 91, 261-269.

Reyes, F. A.G., Barraza, J.M., Bohorquez, A., Tabares, J.A., Speziali, N.L. (2003) Mössbauer and XRD characterization of the mineral matter of coal from the Guachinte mine in Colombia. Hyperfine Interactions, 148, 39-46.

Ribeiro, F.R., Mussel, W.N., Fabris, J.D., Novais, R.F., and Garg, V.K. (2003) Identification of iron-beraing minerals in solid residues from industrial kaolin processing. Hyperfine Interactions, 148/149, 47-52.

Rieder, R., R. Gellert, R.C. Anderson, J. Brückner, B.C. Clark, G. Dreibus, E. Economou, G. Klingelhöfer, G.W. Lugmair, D.W. Ming, S.W. Squyres, C. d'Uston, H. Wänke, A. Yen, and J. Zipfel (2004) Chemistry of rocks and soil at Meridiani Planus from the alpha particle X-ray spectrometer. Science, 306, 1746-1768.

Ristić, M., Musić, S., and Orehovec, Z. (2005) Thermal decomposition of synthetic ammonium jarosite. Journal of Molecular Structure, 744-747, 295-300.

Robinson, K., Gibbs, G.V., and Ribbe, P.H. (1971) Quadratic elongation: A quantitative measure of distortion in coordination polyhedra. Science, 172, 567-570.

Robinson, P.D., and Fang, J.H. (1971) Crystal structures and mineral chemistry of hydrated ferric sulphates: II. The crystal structure of paracoquimbite. American Mineralogist, 56, 1567-1572.

Robinson, P.D., and Fang, J.H. (1973) Crystal structures and mineral chemistry of hydrated ferric sulphates. III. The crystal structure of kornelite. American Mineralogist, 58, 535-539.

1053 Rodríguez, N., Menéndez, N., Tornero, J., Amils, R., and de la Fuente, V. (2005) Internal iron
1054 biomineralization in Imperata cylindrical, a perennial grass: chemical composition,
1055 speciation and plant localization. New Phytologist, 165, 781-789.
1056 Rothstein, Y. (2006) Spectroscopy of jarosite and implications for the mineralogy of Mars. B.A.
1057 thesis, Mount Holyoke College.
1058 Russell, P.E., and Montano, P.A. (1978) Erratum: Magnetic hyperfine parameters of iron
1059 containing minerals in coals. Journal of Applied Physics, 49, 4615-4617.
1060 Sakai, N., Sekizawa, H., and Ono, K. (1981) Mössbauer spectroscopic identification of the
1061 gamma-ray radiolytic product of $FeSO_4 \cdot 7H_2O$ as $FeSO_4OH \cdot 2H_2O$. Journal of Inorganic
1062 and Nuclear Chemistry, 43, 1731-1734.
1063 Sallam, H.A., Eissa, N.A., Sheta, N.H., Soliman, M.A., and El-Fouly M.H. (1994) Mössbauer
1064 effect, x-ray diffraction, and infrared studies of the effect of gamma irradiation on the
1065 molecular bonding of melanterite. Physics and Chemistry of Solids, 55, 1175-1180.
1066 Schwertmann, U., Bigham, J.M., and Murad, E. (1995) The first occurrence of schwertmannite
1067 in a natural stream environment. European Journal of Mineralogy, 7, 547-552.
1068 Scordari, F. (1975) The metavoltine problem: metavoltine from Madeni Zakh and Chuquicamata,
1069 and a related artificial compound. Minrralogical Magazine, 41, 371-374.
1070 Scordari, F. (1977) The crystal structure of ferrinatrite, $Na_3(H_2O)_3[Fe(SO4)_3]$ and its
1071 relationship to Maus's salt, $(H_3O)_2K_2\{K_{0.5}(H_2O)_{0.5}\}_6[Fe_3O(H_2O)_3(SO_4)_6](OH)_2$.
1072 Mineralogical Magazine, 41, 375-383.
1073 Scordari, F. (1981) Fibroferrite: A mineral with a $\{Fe(OH)(H_2O)_2SO_4\}$ spiral chain and its
1074 relationship to $Fe(OH)SO_4$, butlerite and parabutlerite. Tschermaks Mineralogische und
1075 Petrographische Mitteilungen, 28, 17-29.

Scordari, F. and Ventruti, G. (2009) Sideronatrite, $Na_2Fe(SO_4)_2(OH)\cdot 3H_2O$: Crystal structure of the orthorombic polytype and OD character analysis. American Mineralogist, 94, 1679-1686.

Scordari, F., Ventruti, G., and Gualtieri, A.F. (2004) The structure of metahohmannite, $Fe_2[O(SO_4)_2].4H_2O$, by in situ synchrotron powder diffraction. American Mineralogist 89, 365-370.

Segeler, C.G., Moore, P.B., Dyar, M.D., Leans, F., and Ferraiolo, J.A. (2012) Ferrolaueite, a new mineral from Monmouth County, New Jersey, USA. Australian Journal of Mineralogy 16, 69-76.

Sgarlata, F. (1985) The role of iron in halotrichite and in an osumilite. In Applications of the Mossbauer Effect, vol. 5, Yu.M. Kagan and I.S. Lyubutin, eds., 1775-1778.

Silva, L.F.O., Izquierdo, M., Querol, X., Finkelman, R.B., Oliveira, M.L.S., Wollenschlager, M., Towler, M., Pérez-López, R., Macias, F. (2011) Leaching of potential hazardous elements of coal cleaning rejects. Environmental Monitoring Assessment, 175, 109-26.

Sklute, E.C. (2006) Mössbauer spectroscopy of synthetic olivine across the Fe-Mg solid solution. B.A. Thesis, Mount Holyoke College.

Sklute, E.C., Y. Rothstein, M.W. Schaefer, O.N. Menzies, P.A. Bland, and F.J. Berry (2005), Temperature dependence and recoil-free fraction effects in olivines across the Mg-Fe solid solution, Lunar and Planetary Science Conference, 36, Abstract #1888.

Stiller, A.H., Renton, J.J., Montano, P.A., and Russell, P.E. (1978) Application of Mössbauer spectroscopy to monitor acidmine drainage potentials of coal seams. Fuel, 57, 447-448.

Süsse, P. (1967) Die kristallstruktur des botryogens. Naturwissenschaften, 54, 139-139.

Süsse, P. (1968a) Die kristallstruktur des botryogens. Acta Crystallographica, B24, 760-767.

1099 Süsse, P. (1968b) The crystal structure of amarantite, $Fe_2(SO_4)_2O{\cdot}7H_2O$. Zeitschrift fur
1100 Kristallographie, 127, 261-275.
1101 Szymanski, J.T. (1988) The crystal structure of plumbojarosite $Pb(Fe,Al)_3((As,S)O_4)_2(OH)_2$.
1102 Canadian Mineralogist, 23, 659-668.
1103 Takano, M., Shinio, T., Kiyama, M., and Takada, T. (1968). Magnetic Properties of Jarosites,
1104 $RFe_3(OH)_6(SO_4)_2$(R=NH_4, Na or K). Journal of Physical Science of Japan, 25, 902.
1105 Taneja, S. P., and Jones, C.H.W. (1984) Magnetic hyperfine parameters of iron containing
1106 phases in coal and coal ash. Nuclear Physics and Solid State Physics Symposium, 26,
1107 288-289.
1108 Thomas, J.N., Robinson, P.D., and Fang, J.H. (1974) Crystal structures and mineral chemistry of
1109 hydrated ferric sulfates. IV. The crystal structure of quenstedtite. American Mineralogist,
1110 59, 582-586.
1111 Tosca, N.J., S.M. McLennan, D.H. Lindsley, and M.A.A. Schoonen (2004) Acid-sulfate
1112 weathering of synthetic martian basalt: The acid fog model revisited, Journal of
1113 Geophysical Research, 109, E05003, doi: 10.1029/2003JE002218.
1114 Van Alboom, A., De Resende, V.G., De Grave, E., and Gomez, J.A.M. (2009) Hyperfine
1115 interactions in szomolnokite ($FeSO_4{\cdot}H_2O$). Journal of Molecular Structure, 924-926, 448-
1116 456.
1117 van der Kraan, A. M., Niemantsverdriet, J.W., and Gerkema, E. (1984) Mössbauer spectroscopy
1118 used in energy studies. Energiespectrum, 84, 104-111.
1119 Ventruti, G., Stasi, F., and Scordari, F. (2010) Metasideronatrite: crystal structure and its relation
1120 with sideronatrite. American Mineralogist, 85, 329-334.

Verma, H.C., and Tripathi, R.P. (2000) Characterization of iron-bearing minerals in Giril lignite from Rajasthan and study of their decomposition during combustion using Fe-57 Mössbauer spectroscopy. Fuel, 79, 599-606.

Waanders, F. B., Vinken, E., Mans, A., and Mulaba-Bafubiandi, A.F. (2003) Iron minerals in coal, weathered coal and coal ash - SEM and Mössbauer results. Hyperfine Interactions, 148, 21-29.

Wildner, M., and Giester, G. (1991) The crystal structures of kieserite-type compounds. I. Crystal structures of $Me(II)SO_4 \cdot H_2O$ (Me = Mn,Fe,Co,Ni,Zn). Neues Jahrbuch fur Mineralogie, Monatshefte, 1991, 296-306.

Yen, A.A., Gellert, R., Clark, B.C., Ming, D.W., King, P.L., Schmidt, M.E., Leshin, L., Morris, R.V., Squyres, S.W.,Spray, J., Campbell, J.L., and the MSL Science Team. (2013) Evidence for a global martian soil composition extends to Gale Crater. Lunar and Planetary Science Conference, 44, Abstract #2495.

FIGURE CAPTIONS

Figure 1. Contrasting structures within the sulfate minerals that combine SO_4 tetrahedra and $M(O,OH,OH_2)_6$ octahedra in various ways (Hawthorne et al. 2000): melanterite (structure from Peterson et al. 2003) has unconnected groups of SO_4 tetrahedra, römerite (Fanfani et al., 1970) has SO_4 tetrahedra linked to Fe2 octahedra in a *cis* arrangement on adjacent corners, butlerite (Fanfani et al. 1971) has infinite chains, rhomboclase (Mereiter 1974) has infinite sheets, and kieserite (Bregault et al. 1970) has an infinite framework. Anhydrite (Hawthorne and Ferguson 1975) has a structure with SO_4 tetrahedra linked to larger cation sites that can accommodate Ca.

Figure 2. Mössbauer parameters of sulfates measured in this study. The top panel shows peak positions plotted in terms of isomer shift and quadrupole splitting. The bottom panel shows the actual positions of the peaks, which follow a continuum across velocity space.

Figure 3. Mössbauer spectra and Fe coordination polyhedra in sulfates with very small Δ values less than ~0.35 mm/s. Data points are plotted are ±standard deviations but are cropped at the baseline, which is defined to be 100% absorption. Polyhedra were created using CrystalMaker® software and data from the American Mineralogist Crystal Structure Database: quenstedtite (Thomas et al. 1974), coquimbite (Fang and Robinson 1970), kornelite (Robinson and Fang 1973), lausenite (Majzlan et al. 2005), ferrinatrite (Scordari 1977), voltaite (Mereiter 1972), and rhomboclase (Mereiter 1974). Oxygen atoms are shown in red, OH in gray, Al in blue, and Fe in orange. Note that XRD suggests that the R6214 ferrinatrite contains minor amounts of coquimbite that cannot be distinguished because the spectra are so similar.

Figure 4a. Mössbauer spectra and Fe coordination polyhedra in sulfates with Δ values between ~0.31 and 0.74 mm/s. Polyhedra were created using CrystalMaker® software and data from the American Mineralogist Crystal Structure Database: yavapaiite (Graeber and Rosenzweig 1971), krausite (Graeber et al. 1965), goldichite (Graeber and Rosenzweig 1971), copiapite, ferricopiapite, and zincocopiapite (Fanfani et al., 1973). Oxygen atoms are shown in red, OH in gray, and Fe in orange.

Figure 4b. Mössbauer spectra and Fe coordination polyhedra in sulfates with Δ values between 0.58 and 0.79 mm/s. Polyhedra were created using CrystalMaker® software and data from the American Mineralogist Crystal Structure Database: apjohnite (Menchetti and Sabelli 1976), dietrichite (Ballirano et al. 2003), metavoltine (Giacovazzo et al. 1976), starkeyite (Baur 1962) and ilesite (Held and Bohaty 2002). No crystal structure is available for bilinite. Oxygen atoms are shown in red, OH in gray, H in pink, Mg in yellow, Al in blue, and Fe in orange. Metavoltine G2677 has a römerite impurity (large QS doublet); its Fe^{3+} feature is nearly a singlet, as also seen in bilinite.

Figure 5a. Mössbauer spectra and Fe coordination polyhedra in sulfates with Δ values between ~0.80 and 1.12 mm/s. Polyhedra were created using CrystalMaker® software and data from the American Mineralogist Crystal Structure Database: butlerite (Fanfani et al. 1971), parabutlerite (Borene 1970a), slavikite (Parafiniuk et al. 2010), fibroferrite (Scordari 1981), botryogen (Süsse 1967), and zincobotryogen (Süsse 1968a). Oxygen atoms are shown in red, OH in gray, H in pink, Mg in yellow, and Fe in orange.

Figure 5b. Mössbauer spectra and Fe coordination polyhedra in sulfates with Δ values between 0.94 and 1.22 mm/s. Polyhedra were created using CrystalMaker® software and data from the American Mineralogist Crystal Structure Database: sideronatrite and metasideronatrite (Ventruti et al. 2010; metasideronatrite has the same structural unit topology as sideronatrite; Scordari and Ventruti 2009), metahohmannite (Scordari et al., 2004), amarantite (Süsse 1968b), jarosite (Basciano and Peterson 2007), and plumbojarosite (Szymanski 1988). Note the presence of a magnetic phase impurity in plumbojarosite. Oxygen atoms are shown in red, H in pink, Mg in yellow, and Fe in orange.

Figure 5c. Mössbauer spectra and Fe coordination polyhedra in sulfates without nominal Fe in their structures. Polyhedra were created using CrystalMaker® software and data from the American Mineralogist Crystal Structure Database: anhydrite (Hawthorne and Ferguson 1975) and celestine (Miyake et al. 1978). Oxygen atoms are shown in red, Ca in blue, and Sr in green. Neither of these minerals is likely to contain much Fe because of the large size of the coordination polyhedra as seen here; these are configured to accommodate the Ca^{2+} cation, which is significantly larger than Fe^{3+}. Thus although the hand sample of SPT132 is mostly anhydrite, XRD reveals a significant component of coquimbite, which dominates the spectrum of the mixture because it is so much more Fe-rich. Celestine ML-S13 is pure by XRD, but some Fe-rich phase is present there, too, at low concentrations. These data cannot discriminate between Fe in the celestine structure and Fe in an impurity.

Figure 6a. Mössbauer spectra and Fe^{2+} coordination polyhedra in sulfates with Δ values larger than 2.70 mm/s. Polyhedra were created using CrystalMaker® software and data from the American Mineralogist Crystal Structure Database: szomolnokite, szmikite, gunningite (Wildner and Giester 1991), chalcanthite (Bacon and Titterton 1975), and pentahydrite (Peterson et al. 2006). Oxygen atoms are shown in red, H in pink, Mg in yellow, Cu in purple, and Fe and Zn in orange.

Figure 6b. Mössbauer spectra and Fe^{2+} coordination polyhedra in sulfates with highest Δ values. Polyhedra were created using CrystalMaker® software and data from the American Mineralogist Crystal Structure Database: halotrichite (Lovas 1986), jokokuite (Carminiti et al. 1982), römerite (Farfani et al. 1970), melanterite (Peterson 2003), rozenite (Baur 1962), and starkeyite (Baur 1962). Oxygen atoms are shown in red, OH in gray, H in pink, Mg in yellow, Al in blue, and Fe in orange.

Figure 7. Quadrupole splitting plotted against various characteristics of the geometry of the Fe^{3+} coordination polyhedra: octahedral volume, mean octahedral bond length, mean quadratic elongation, and angular variance. See text for definitions. Purple circles represent parameters of structures with only one possible Fe cation site. Orange squares are mineral species in which Fe occupies more than one site; Mössbauer parameters were matched with sites by inspection. Error bars are ±0.03-0.05 mm/s for quadrupole splitting and highly variable for the structure refinements, depending on the accuracy of the original measurements. The few labeled outliers are so far out of range from the majority of the measurements that they may likely be attributed to problems with the original refinements or their transcription into CIF files.

The parameters for Fe^{2+} sites are not shown because there are too few data points and the parameters group together in two clumps.

Figure 8. Mössbauer parameters of several sulfates with very similar peak positions (close-up of Figure 2). Blue squares represent Fe^{3+}-bearing sulfates from this study, not including jarosites. Green circles are jarosite data from this study. Circles display parameters and locations for Mars data from Morris et al. (2006) offset by -0.07 mm/s or -0.02 mm/s to correct Mars data to room temperature. The error bar for both plots is shown at lower right in upper panel.

Figure 9. Comparison of the crystal structures surrounding the Fe^{3+} cations in several sulfates that have similar Mössbauer spectra (see Figure 8). Red spheres represent O^{2-}, gray are OH^{-}, pink are H^{+}, and the central gold cations are Fe^{3+}. Note that both slavikite (Fe1 at upper left, and Fe2 at top center) and metavoltine (Fe^{3+}1,2 at lower left and Fe^{2+}3 at bottom center) have multiple different Fe sites with slightly differing geometries.

Figure 10. Mössbauer parameters of several sulfates with very similar peak positions (close-up of Figure 2). Blue squares represent Fe^{3+}-bearing sulfates from this study. Red triangles are data from Mars (Morris et al. 2008) using a temperature-correcting offset of -0.07 mm/s. The error bar shown for apjohnite applies to all samples.

Figure 11. Mössbauer data from this study (blue circles) with data for silicates and oxides from Burns and Solberg (1990) superimposed. These results highlight the small range of

1249 Mössbauer parameters that occur in minerals, and underscore the non-uniqueness of the
1250 parameters to specific mineral groups.

Table 1. Samples Studied

Dana Number	Mineral species	Locality	Sample Number
28.3.1.2	Celestine	Maybee, Michigan	ML-S13
28.3.2.1	Anhydrite	Lavender Pit, Bisbee, Cochise Co., AZ	159266
28.3.2.1	Anhydrite	Borate, San Bernardino Co., CA	SPT132[1]
28.4.3.1	Yavapaiite	synthetic sample, courtesy Ferren Forray	ML-S79
29.1.1.1	Rhomboclase	Cerre de Pasco, Peru	81268
29.1.1.1	Rhomboclase	Alcaparra, Chile	ML-S85
29.1.1.1	Rhomboclase	Alcaparra, Chile	ML-S89
29.1.1.1	Rhomboclase	Near Cerritos Bay, Alcaparrosa, Chile	ML-S84
29.4.4.1	Ferrinatrite	Sierra Gorda, Cahacoles, Chile	R6214
29.4.4.1	Ferrinatrite	Sierra Gorda, Antofagaste, Chile	VZO105/106
29.4.6.1	Metavoltine	Mina Alcaparrosa, Calama, Atacama Desert, Chile	G2677
29.4.6.1	Metavoltine	Cetine Mine, Siena, Tuscany, Italy	VZO114[2]
29.5.1.1	Krausite	Sulfur Hole, Mule Canyon, San Bernard, CA	156916[3]
29.5.2.1	Goldichite	Pozzuoli, Solfatara (1969), Italy	123922
29.5.3.2	Amarantite	Los Pintados, Chile	G3775[4]
29.6.10.1	Melanterite	Locality unknown; Mount Holyoke College collection; sample labeled as boothite (Cu-melanterite)	2070[4]
29.6.2.2	Szomolnokite	Island Mountain, Trinity Co., CA	92942
29.6.2.2	Szomolnokite	Tintic Standard Mine, Dividend, UT	104276
29.6.2.2	Szomolnokite	Cuprian sample, Alma Pyrite mine, Alameda Co., CA	156925
29.6.2.2	Szomolnokite	Lavender Pit, Bisbee, Cochise Co., AZ	159266[5]
29.6.2.2	Szomolnokite	Rio Tinto Mine, Hvelva, Spain	136685-2
29.6.2.2	Szomolnokite	Joe Bishop Mine, San Juan Co., UT	ML-S103
29.6.2.2	Szomolnokite	Markey Mine, Red Canyon, San Juan Co., UT	ML-S60
29.6.2.2	Szomolnokite	Orovile, Washington	ML-S77
29.6.2.3	Szmikite	Toyoha Mine, Sapporo, Ishikari, Hokkaido, Japan	159189[6]
29.6.2.5	Gunningite	Alma Pyrite Mine, Alameda Co., CA	156925
29.6.6.1	Rozenite	Island Mountain, Trinity Co., CA	JB626B
29.6.6.1	Rozenite	Oage Mine, Ominato, Aomori-ken, Honshu, Japan	SPT130
29.6.6.2	Starkeyite	Habachtal, Pinzgau, Salzburg, Austria	137725
29.6.6.2	Starkeyite	Veneables Valley, Basque, British Columbia, Canada	ML-S65
29.6.6.3	Ilesite	McDonnell Mine, Park Co., CO	123277[7]
29.6.7.1	Chalcanthite	Smolnik, Eastern Slovakia, Slovak Republic	DD100 green
29.6.7.3	Pentahydrite	2700 Level, Cambell Shaft, Bisbee, AZ	VZO121[8]
29.6.7.4	Jokokuite	Locality unknown; Mount Holyoke College collection	G3536[4]
29.7.2.1	Römerite	Island Mountain, Trinity Co., CA	93825
29.7.2.1	Römerite	Cerre de Pusco, Peru	113733
29.7.2.1	Römerite	Alcaparrosa, Chile	159098-2[9]
29.7.2.1	Römerite	near Skauriatissa, Island of Cyprus, Greece	R8415
29.7.2.1	Römerite	Sulphur Hole, near Borate, San Bernardino Co., CA	SPT110
29.7.2.1	Römerite	Alcaparrosa, Chile	SPT122/126
29.7.3.2	Halotrichite	The Geysers, Sonoma Co., CA	104135[10]
29.7.3.2	Halotrichite	Golden Queen Mine, Soledad Mountain, Kern Co., CA	G1616[4]
29.7.3.2	Halotrichite	Sulfur Hole Prospect, near Yermo, CA	VZO128
29.7.3.3	Apjohnite	Alum Cave, Sevier Co., TN	121356[4]
29.7.3.4	Dietrichite	unknown	G-2429[4]
29.7.3.5	Bilinite	Arco, ID	169017[11]
29.8.1.1	Lausenite	United Verde Mine, Jerome, AZ	102923

[1]Sample has minor coquimbite impurity. [2]Sample has a known Fe^{2+} römerite impurity. [3]XRD reports that this sample is geigerite but the locality is consistent with metavoltine. [4]No XRD; sample too small. [5]XRD of this sample suggests it is anhydrite but its parameters are an exact match to those of szomolnokite, which may be an impurity in the sample. [6]XRD suggests this sample is a complex solid solution between kieserite and szimikite. [7]XRD identification on this sample was spangolite, but ilesite is not correctly represented in the XRD database. Note that this sample comes from the Smithsonian and is from the ilesite type locality. [8]Minor impurities from pickeringite, starkeyite, botryogen, and boussingaultite, [9]No XRD on this sample but NMNH identification was römerite. [10]XRD found small copiapite contaminant. [11]XRD suggests alunogen and wupatkiite in this sample but bilinite is not represented in XRD database, and so NMNH ID is used here.

Table 1. Samples Studied, continued

Dana Number	Mineral species	Locality	Sample Number
29.8.2.1	Kornelite	Smolnik, Slovenko, Czechoslavakia	95830[1]
29.8.3.1	Coquimbite	Borate, Calton Hills, San Bernardino, CA	R7661
29.8.3.1	Coquimbite	Atacama, Chile	ML-S63
29.8.3.1	Coquimbite	Dexter #7 Mine, San Rafael Swell, UT	SPT119
29.8.3.1	Coquimbite	Alcaparrosa, Chile	SPT126
29.8.3.1	Coquimbite	Borate, San Bernardino Co., CA	SPT131
29.8.3.1	Coquimbite	Borate, San Bernardino County, CA	SPT132
29.8.3.1	Coquimbite	Helper, Carbon Co., UT	VZO101/102
29.8.5.1	Quensdedtite	Tierra Amarilla, Copiapo, Chile	B8255[2]
29.9.1.1	Voltaite	Jerome District, AZ	85679
29.9.1.1	Voltaite	Smolnik, eastern Slovakia, Slovak Republic	95830
29.9.1.1	Voltaite	United Verde Mine, Jerome, AZ	115035
29.9.1.1	Voltaite	Boron Kern Country, CA	129313
29.9.1.1	Voltaite	Boron Kern Country, CA	137958
29.9.1.1	Voltaite	Minas Rio Tinto, Hvelva, Andalucia, Spain	158795
29.9.1.1	Voltaite	Mina Alcaparrosa, Cerritos Bayos, Calama, Chile	DD104
29.9.1.3	Pertlikite	Madeni, Iran	Mg-Voltaite
30.2.5.1	Jarosite	Sierra Pena Blanca Aldina, Chihuahua, Mexico	132060
30.2.5.1	Jarosite	Sierra Gorda, Chile	SPT113
30.2.5.1	Jarosite	Arabia District, Pershing Co., NV	SPT115
30.2.5.1	Jarosite	Copiapa Jarosite Mine, Dona Ana Co., NM	SPT116
30.2.5.1	Jarosite	Rustler Mine, Tooele Co., UT	SPT120
30.2.5.6	Plumbojarosite	Lomo de Toro Mine, Zimapan, Hidalgo, Mexico	ML-S15
31.8.3.1	Sideronatrite	Chuquicamata, Chile	115164
31.8.3.2	Sideronatrite	Crescent Valley, CA	SPT123[3]
31.8.4.1	Metasideronatrite	Chuqulcamata, Antofagasta, Chile	VZO112[4]
31.8.4.1	Metasideronatrite	Chuqulcamata, Antofagasta, Chile	105774-2[5]
31.9.1.1	Butlerite	Locality unknown; Mount Holyoke College collection	639[2]
31.9.1.1	Butlerite	Mina Quetena, Calama, Chile	C5534
31.9.1.1	Butlerite	Borate, Calico Hills, San Bernardino, CA	R7653
31.9.1.1	Butlerite	Riotorto, Tuscany, Italy-Ralph Dietz Collection	ML-S88
31.9.2.1	Parabutlerite	Chuquicamata, Antofagasta, Chile	157716[2]
31.9.2.1	Parabutlerite	Saghand Yazd, Iran	VZO115/116[2]
31.9.5.1	Metahohmannite	Quetena, Antofagasta, Chile	R12495[6]
31.9.6.1	Botryogen	Mina Santa Elena, La Alcaparrosa, Argentina	DD112[2]
31.9.6.1	Botryogen	unknown	G3775[2]
31.9.6.1	Botryogen	Redington Mine, Knoxville, Napa Co., CA	SPT124
31.9.6.2	Zincobotryogen	Mina Quetana, Calama, Chile	C5525-3
31.9.12.1	Slavikite	Valachov, Czech Republic	140229
31.9.12.1	Fibroferrite	Skouriatissa, Cyprus	SPT121
31.9.12.1	Fibroferrite	Borate, Calico Hills, San Bernardino, CA	VZO107/108[3]
31.9.12.1	Slavikite/gypsum	unknown	VZO122/123
31.10.5.1	Copiapite	Alma Pyrite Mine, Oakland, Alameda Co., CA	ML-S86
31.10.5.1	Copiapite	Alma Pyrite Mine, Oakland, Alameda Co., CA	SPT117
31.10.5.4	Ferricopiapite	Sulfur Mine, Contrary Creek, Mineral, Louisa Co., VA	168257[7]
31.10.5.4	Ferricopiapite	Sierra Gorda, Chile	ML-S35
31.10.5.4	Ferricopiapite	Borate, San Bernardino Co., CA	SPT 109[8]
31.10.5.4	Ferricopiapite	Sierra Gorda, Chile	SPT125
31.10.5.4	Ferricopiapite	Alcaparrosa, Chile	SPT133
30.10.5.6	Zincocopiapite	unknown	G-3637[8]

[1]XRD not available on this sample, so NMNH identification was used. [2]XRD not available on this sample. [3]Sample has small unidentified impurity. [4]XRD identified this sample as serpierite + metasideonatrite. [5]XRD found this sample to be 50% metasideronatrite and ~50% kanemite; the latter is nominally Fe-free. Metasideronatrite is not in the XRD database. [6]XRD of very small sample showed mixture of unspecified phases. [7]XRD not available on this sample. [8]XRD suggests presence of minor metavoltine impurity.

Mineral	Sample ID	Sample #	δ (ISO)	Δ(QUADR)	Γ (WID)	Area (%)	X^2	Normalized X^2
Amarantite	G3775	8102901	0.43	0.35	0.33	8	2744.11	5.36
Amarantite	G3775	8102901	0.44	0.98	0.30	8		
Amarantite	G3775	8102901	0.40	1.19	0.30	54		
Amarantite	G3775	8102901	0.39	1.60	0.30	30		
Anhydrite	159266	05030801	0.14	0.58	0.26	24	364.50	0.71
Anhydrite	159266	05030801	0.44	0.41	0.60	76		
Anhydrite	SPT132	02062101	0.40	0.46	0.47	93	211.03	0.41
Anhydrite	SPT132	02062101	0.38	1.02	0.23	7		
Apjohnite	121356	7012901	0.43	0.58	0.60	70	723.97	1.41
Apjohnite	121356	7012901	0.19	0.75	0.23	12		
Apjohnite	121356	7012901	1.27	3.31	0.27	18		
Bilinite	169017	06100302	0.49	0.37	0.74	71	1400.06	2.73
Bilinite	169017	06100302	0.09	0.79	0.40	17		
Bilinite	169017	06100303	1.37	1.78	0.40	7		
Bilinite	169017	06100304	1.06	3.69	0.23	5		
Botryogen	SPT124	02061601	0.08	0.52	0.24	3	242.15	0.47
Botryogen	SPT124	02061601	0.42	1.18	0.24	49		
Botryogen	SPT124	02061601	0.40	1.63	0.24	43		
Botryogen	SPT124	02061601	1.30	1.74	0.30	4		
Botryogen	G3775	9012001	0.41	0.35	0.29	30	510.40	1.00
Botryogen	G3775	9012001	0.41	0.80	0.30	31		
Botryogen	G3775	9012001	0.37	1.25	0.31	34		
Botryogen	G3775	9012001	1.34	2.58	0.45	5		
Botryogen	DD112	06091501	0.41	1.16	0.30	63	711.48	1.39
Botryogen	DD112	06091501	0.40	1.60	0.23	33		
Botryogen	DD112	06091501	1.28	1.68	0.30	3		
Botryogen	C5525-3	06091201	0.41	1.21	0.25	62	1094.70	2.13
Botryogen	C5525-3	06091201	0.39	1.65	0.23	38		
Butlerite	C5534	06090703	0.41	0.96	0.26	100	931.37	1.79
Butlerite	R7653	06091302	0.41	0.95	0.33	100	2978.78	5.62
Butlerite	639	8101401	0.41	0.98	0.25	100	13411.21	24.92
Fibroferrite	ML-S88	12020303a	0.42	0.99	0.24	19	566.90	1.10
Fibroferrite	ML-S88	12020303a	0.41	0.80	0.51	81		
Celestine	S13	06091801	0.15	0.54	0.23	65	668.30	1.31
Celestine	S13	06091801	0.24	0.87	0.22	35		
Chalcanthite	DD100 green	05031101a	0.10	0.51	0.24	29	335.55	0.66
Chalcanthite	DD100 green	05031101a	0.26	0.76	0.40	30		
Chalcanthite	DD100 green	05031101a	1.26	2.32	0.35	22		
Chalcanthite	DD100 green	05031101a	1.30	2.88	0.35	19		
Chalcopyrite	CHA101	06092302	0.25	-0.01	0.24	68	1205.17	2.35
Chalcopyrite	CHA101	06092302	0.70	0.03	0.23	4		
Chalcopyrite	CHA101	06092302	0.31	0.63	0.33	28		
Copiapite	SPT117	02060701	0.43	0.79	0.23	41	220.06	0.43
Copiapite	SPT117	02060701	0.42	0.35	0.24	43		
Copiapite	SPT117	02060701	0.21	0.34	0.30	6		
Copiapite	SPT117	02060701	0.34	1.00	0.42	10		
Copiapite	G596-1	8101501	0.37	1.18	0.26	100	1007.32	1.93
Copiapite	HSC-128 JB-834	8121001	0.41	0.36	0.38	45	493.05	0.96
Copiapite	HSC-128 JB-834	8121001	0.41	0.73	0.30	44		
Copiapite	HSC-128 JB-834	8121001	1.29	2.13	0.30	39		
Copiapite	HSC-128 JB-834	8121001	1.26	3.00	0.30	8		
Copiapite	MAC-2 JB-835	8120901	0.40	0.38	0.38	60	538.44	1.05
Copiapite	MAC-2 JB-835	8120901	0.40	0.81	0.30	40		
Copiapite	MAC-5 JB-836	8121601	0.42	0.37	0.42	56	498.67	0.97

Copiapite	MAC-5 JB-836	8121601	0.43	0.68	0.26	44		
Copiapite	MAC-7 JB-837	8121201	0.41	0.36	0.35	54	625.65	1.22
Copiapite	MAC-7 JB-837	8121201	0.42	0.80	0.30	46		
Copiapite	MAC-11 JB-838	8121301	0.40	0.36	0.43	51	603.82	1.18
Copiapite	MAC-11 JB-838	8121301	0.42	0.88	0.30	49		
Copiapite	FAC-1 JB-839	8121501	0.41	0.36	0.40	42	832.73	1.62
Copiapite	FAC-1 JB-839	8121501	0.42	0.65	0.30	58		
Copiapite	FAC-3 JB-840	8120801	0.40	0.36	0.32	43	631.70	1.23
Copiapite	FAC-3 JB-840	8120801	0.41	0.70	0.30	57		
Copiapite	FAC-5 JB-841	8121801	0.42	0.37	0.37	44	749.95	1.46
Copiapite	FAC-5 JB-841	8121801	0.43	0.66	0.30	56		
Copiapite	FAC-7 JB842	9011301	0.07	0.45	0.30	7	422.92	0.83
Copiapite	FAC-7 JB842	9011301	0.42	0.37	0.30	98		
Copiapite	FAC-7 JB842	9011301	0.42	0.76	0.30	55		
Copiapite	FAC-10 JB-843	8121701	0.42	0.37	0.41	50	665.77	1.30
Copiapite	FAC-10 JB-843	8121701	0.43	0.65	0.30	50		
Copiapite	ML-S86	12020201c	0.42	0.44	0.37	91	885.65	1.70
Copiapite	ML-S86	12020201c	0.42	0.81	0.03	9		
Coquimbite	VZO101/102	05030501	0.18	0.58	0.24	7	543.98	1.06
Coquimbite	VZO101/102	05030501	0.46	0.10	0.91	93		
Coquimbite	SPT132	02062101	0.18	0.71	0.24	6	214.89	0.42
Coquimbite	SPT132	02062101	0.42	0.47	0.46	94		
Coquimbite	SPT131	02062001	0.19	0.72	0.24	9	218.67	0.43
Coquimbite	SPT131	02062001	0.43	0.44	0.38	91		
Coquimbite	SPT126/127	02061801	0.16	0.66	0.24	5	267.71	0.52
Coquimbite	SPT126/127	02061801	0.45	0.08	0.64	95		
Coquimbite	SPT119	02061101	0.16	0.77	0.24	5	311.17	0.61
Coquimbite	SPT119	02061101	0.47	0.09	0.82	95		
Coquimbite	S63	05030401	0.44	0.25	0.63	86	398.08	0.78
Coquimbite	S63	05030401	0.31	0.58	0.24	7		
Coquimbite	S63	05030401	0.35	1.09	0.24	7		
Coquimbite	R7661	05030601	0.19	0.52	0.24	7	451.29	0.88
Coquimbite	R7661	05030601	0.46	0.11	0.82	93		
Dietrichite	G-2429	7011903	0.43	0.79	0.32	52	562.98	1.10
Dietrichite	G-2429	7011903	0.42	0.35	0.29	44		
Dietrichite	G-2429	7011903	1.28	3.28	0.26	4		
Ferricopiapite	SPT125	02061701	0.42	0.40	0.27	38	257.67	0.50
Ferricopiapite	SPT125	02061701	0.43	0.77	0.23	38		
Ferricopiapite	SPT125	02061701	0.38	1.18	0.24	25		
Ferricopiapite	S35	04030301a	0.43	0.39	0.23	35	388.54	0.76
Ferricopiapite	S35	04030301a	0.43	0.78	0.23	48		
Ferricopiapite	S35	04030301a	0.37	0.52	0.86	16		
Ferricopiapite	168257	08102201	0.42	0.37	0.37	26	1770.19	3.45
Ferricopiapite	168257	08102201	1.25	2.71	0.30	51		
Ferricopiapite	168257	08102201	0.43	0.78	0.30	17		
Ferricopiapite	168257	08102201	1.25	1.78	0.50	6		
Ferricopiapite	SPT 109	2052501	0.42	0.36	0.25	38	250.98	0.49
Ferricopiapite	SPT 109	2052501	0.42	0.74	0.33	62		
Ferricopiapite	SPT133	02062201	0.43	0.76	0.23	33	193.75	0.38
Ferricopiapite	SPT133	02062201	0.42	0.40	0.28	40		
Ferricopiapite	SPT133	02062201	0.38	0.53	0.55	27		
Ferrinatrite	VZO105/106	06090801	0.44	0.40	0.42	88	1387.87	2.69
Ferrinatrite	VZO105/106	06090801	0.40	1.13	0.24	12		
Ferrinatrite	R6214	06090802	0.47	0.05	0.57	100	1998.28	3.78
Fibroferrite	SPT121	02061301	0.41	0.52	0.23	37	218.07	0.42

Fibroferrite	SPT121	02061301	0.42	0.96	0.23	63		
Fibroferrite	VZO107/108	06091301	0.41	0.50	0.25	100	1098.34	2.12
Fibroferrite	R7653	6091302	0.41	0.96	0.30	100	2514.68	4.73
Goldichite	123922	7011901	0.19	0.61	0.42	29	547.98	1.07
Goldichite	123922	7011901	0.48	0.29	0.37	71		
Gunningite	156925	7012401	0.26	0.40	0.50	32	577.10	1.13
Gunningite	156925	7012401	0.37	1.26	0.23	10		
Gunningite	156925	7012401	1.25	2.74	0.29	58		
Halotrichite	VZO128	05032101a	0.13	0.49	0.24	10	322.99	0.63
Halotrichite	VZO128	05032101a	0.36	0.31	0.43	14		
Halotrichite	VZO128	05032101a	1.45	1.56	0.56	13		
Halotrichite	VZO128	05032101a	1.28	2.76	0.26	43		
Halotrichite	VZO128	05032101a	1.30	3.29	0.24	20		
Halotrichite	104135 30mg	06090902	0.42	0.37	0.34	44	703.36	1.37
Halotrichite	104135 30mg	06090902	0.42	0.81	0.30	31		
Halotrichite	104135 30mg	06090902	1.25	2.69	0.48	16		
Halotrichite	104135 30mg	06090902	1.26	3.29	0.23	9		
Halotrichite	104135 28mg	06091603	0.42	0.40	0.35	46	510.11	1.00
Halotrichite	104135 28mg	06091603	0.43	0.80	0.25	28		
Halotrichite	104135 28mg	06091603	1.36	1.68	0.54	4		
Halotrichite	104135 28mg	06091603	1.24	2.66	0.30	8		
Halotrichite	104135 28mg	06091603	1.27	3.27	0.30	13		
Halotrichite	G1616	08081201	1.27	3.29	0.24	92	648.53	1.27
Halotrichite	G1616	08081201	0.30	0.35	0.30	3		
Halotrichite	G1616	08081201	0.36	1.25	0.29	5		
Ilesite	123277	06091601a	0.31	0.62	0.27	97	666.89	1.30
Ilesite	123277	06091601a	0.55	0.94	0.30	32		
Jarosite	132060	03010802	0.38	1.30	0.29	100	414.88	0.77
Jarosite	SPT113	02060101	0.38	1.18	0.23	100	299.97	0.58
Jarosite	SPT116	02060501	0.38	1.23	0.23	100	834.35	1.54
Jarosite	SPT115	02060301	0.38	1.29	0.23	100	659.61	1.24
Jarosite	SPT120	02061201	0.38	1.14	0.23	44	198.89	0.39
Jarosite	SPT120	02061201	0.37	0.70	0.28	56		
Jokokuite	G3536	8090801	1.13	2.63	0.30	6	1260.00	2.46
Jokokuite	G3536	8090801	1.26	2.51	0.30	65		
Jokokuite	G3536	8090801	0.15	0.56	0.39	26		
Jokokuite	G3536	8090801	0.40	0.74	0.30	4		
Kornelite	95830	05022401a	0.51	0.15	0.27	44	437.13	0.85
Kornelite	95830	05022401a	0.40	1.13	0.30	7		
Kornelite	95830	05022401a	1.20	1.60	0.39	34		
Kornelite	95830	05022401a	1.14	2.08	0.24	15		
Kornelite	140175	06082501	0.39	0.71	0.57	16	634.58	1.24
Kornelite	140175	06082501	1.27	3.26	0.24	84		
Kornelite	R16185	06082404	0.44	0.11	0.47	100	1555.82	2.98
Krausite	156916	06090901	0.41	0.41	0.30	100	1398.18	2.73
Lausenite	102923	06091602	0.47	0.12	0.71	89	828.08	1.60
Lausenite	102923	06091602	1.03	2.53	0.30	2		
Lausenite	102923	06091602	1.25	2.63	0.30	6		
Lausenite	102923	06091602	1.31	3.23	0.30	3		
Melanterite	2070	06092901	1.27	3.21	0.27	100	1797.71	3.50
Melanterite	136727	5030101	0.50	0.63	0.45	5	330.00	0.65
Melanterite	136727	5030101	1.25	2.83	0.40	50		
Melanterite	136727	5030101	1.28	3.28	0.26	21		
Melanterite	136727	5030101	1.27	3.66	0.32	19		
Melanterite	136727	5030101	0.18	0.43	0.24	5		

Metahohmannite	R12495	06100701	0.43	0.94	0.33	100	2349.52	4.44
Metasideronatrite	105774-2	12020301a	0.35	1.20	0.30	43	1325.87	2.45
Metasideronatrite	105774-2	12020301a	0.44	1.18	0.30	57		
Metasideronatrite	VZO112	12020302e	0.42	1.17	0.31	48	633.48	1.23
Metasideronatrite	VZO112	12020302e	0.38	1.18	0.28	52		
Metavoltine	VZO114	06100101a	0.43	0.35	0.42	53	727.15	1.42
Metavoltine	VZO114	06100101a	0.40	1.04	0.29	36		
Metavoltine	VZO114	06100101a	1.16	2.01	0.64	11		
Metavoltine	G2677	8081202	1.27	3.23	0.26	81	853.09	1.67
Metavoltine	G2677	8081202	0.44	0.24	0.61	19		
Metavoltine	SPT109	02052501	0.43	0.74	0.23	43	223.57	0.44
Metavoltine	SPT109	02052501	0.42	0.37	0.24	38		
Metavoltine	SPT109	02052501	0.33	0.46	0.68	19		
Parabutlerite	VZO115/116	06090903	0.41	0.98	0.27	100	926.09	1.77
Parabutlerite	157716	06091102	0.37	1.20	0.22	12	861.13	1.69
Parabutlerite	157716	06091102	0.42	0.40	0.27	38		
Parabutlerite	157716	06091102	0.42	0.75	0.33	50		
Pentahydrite	VZO121	06090803	0.58	0.41	0.50	6	1038.91	2.03
Pentahydrite	VZO121	06090803	1.26	3.00	0.28	54		
Pentahydrite	VZO121	06090803	1.27	3.68	0.25	39		
Plumbojarosite	S15	06100401	0.29	0.70	0.30	12	31575.98	62.20
Plumbojarosite	S15	06100401	0.76	1.22	0.30	9		
Plumbojarosite	S15	06100401	0.37	1.22	0.36	79		
Quensdedtite	B8255	06112104	0.40	0.24	0.92	65	770.95	1.51
Quensdedtite	B8255	06112104	0.47	0.13	0.25	35		
Rhomboclase	ML-S84	07011702	0.54	0.43	0.37	23	685.24	1.33
Rhomboclase	ML-S84	07011702	0.43	0.53	0.24	77		
Rhomboclase	ML-S85	12020304h	0.44	0.52	0.24	97	558.71	1.08
Rhomboclase	ML-S85	12020304h	0.34	1.14	0.24	3		
Rhomboclase	ML-S89	12020602h	0.44	0.51	0.25	97	592.44	1.15
Rhomboclase	ML-S89	12020602h	0.29	0.80	0.24	3		
Rhomboclase	81268	12020603n	0.44	0.54	0.28	95	671.46	1.31
Rhomboclase	81268	12020603n	1.68	1.91	0.23	5		
Romerite	SPT110	02052901a	0.44	0.48	0.30	14	263.58	0.51
Romerite	SPT110	02052901a	0.31	0.61	0.24	36		
Romerite	SPT110	02052901a	1.27	2.72	0.24	50		
Romerite	SPT110	04070902a	0.43	0.55	0.37	23	494.66	0.96
Romerite	SPT110	04070902a	0.29	0.61	0.24	30		
Romerite	SPT110	04070902a	1.23	2.87	0.24	12		
Romerite	SPT110	04070902a	1.28	3.01	0.27	35		
Romerite	SPT122/126	02061401a	1.39	2.09	0.64	23	176.06	0.34
Romerite	SPT122/126	02061401a	1.27	2.74	0.24	44		
Romerite	SPT122/126	02061401a	1.27	3.27	0.24	7		
Romerite	SPT122/126	02061401a	0.32	0.45	0.64	26		
Romerite	113733	05022701	0.39	0.39	0.24	2	419.22	0.82
Romerite	113733	05022701	0.17	0.61	0.24	6		
Romerite	113733	05022701	0.44	0.37	0.62	69		
Romerite	113733	05022701	1.27	3.28	0.27	23		
Romerite	159098-2	05022801	0.15	0.64	0.24	7	721.89	1.40
Romerite	159098-2	05022801	0.46	0.36	0.59	49		
Romerite	159098-2	05022801	1.26	2.73	0.27	27		
Romerite	159098-2	05022801	1.26	3.30	0.27	18		
Romerite	C5602-1	05031801	0.15	0.58	0.24	7	10972.30	20.69
Romerite	C5602-1	05031801	0.45	0.33	0.55	50		
Romerite	C5602-1	05031801	1.27	3.30	0.27	11		

Romerite	C5602-1	05031801	1.28	2.76	0.29	32		
Romerite	93825	05031901	0.16	0.60	0.24	5	561.76	1.09
Romerite	93825	05031901	0.44	0.33	0.60	55		
Romerite	93825	05031901	1.29	3.31	0.24	15		
Romerite	93825	05031901	1.29	2.78	0.32	25		
Romerite	R8415	05032001	0.36	0.37	0.30	7	1120.00	2.18
Romerite	R8415	05032001	0.17	0.56	0.26	12		
Romerite	R8415	05032001	0.47	0.36	0.63	56		
Romerite	R8415	05032001	1.34	2.59	0.24	2		
Romerite	R8415	05032001	1.29	3.29	0.27	23		
Romerite	G2677	8081101	1.27	3.26	0.30	43	2687.16	5.22
Romerite	G2677	8081101	0.33	0.44	0.30	6		
Romerite	G2677	8081101	0.46	0.23	0.61	50		
Rozenite	JB626B	04061901a	0.13	0.56	0.24	2	1319.01	2.49
Rozenite	JB626B	04061901a	0.45	0.47	0.24	2		
Rozenite	JB626B	04061901a	0.38	1.06	0.24	2		
Rozenite	JB626B	04061901a	1.33	2.97	0.34	59		
Rozenite	JB626B	04061901a	1.33	3.39	0.25	34		
Rozenite	SPT130	02061901	0.39	0.95	0.35	8	298.06	0.58
Rozenite	SPT130	02061901	1.27	3.21	0.25	92		
Rozenite	SPT130	04040603	1.27	3.33	0.25	91	316.01	0.62
Rozenite	SPT130	04040603	0.20	0.48	0.31	4		
Rozenite	SPT130	04040603	0.37	1.15	0.30	5		
Sideronatrite	SPT123	02061501	0.42	1.15	0.23	100	1212.65	2.31
Sideronatrite	115164	8092201	0.41	1.15	0.25	100	3357.48	6.41
Sideronatrite	SPT126	8091701	0.41	1.14	0.25	100	3789.26	7.03
Slavikite	VZO122/123	06091303	0.38	1.15	0.36	24	782.22	1.53
Slavikite	VZO122/123	06091303	0.37	0.57	0.28	76		
Slavikite	140229	06091401	0.27	0.63	0.25	34	687.85	1.35
Slavikite	140229	06091401	0.38	1.23	0.27	27		
Slavikite	140229	06091401	0.55	0.52	0.24	39		
Sphalerite	R164122-1	06092402	0.30	0.46	0.28	90	1308.95	2.55
Sphalerite	R164122-1	06092402	1.29	2.66	0.24	10		
Stock Ferric Sulfate	MHC2046	06092802	0.45	0.26	0.34	96	702.11	1.37
Stock Ferric Sulfate	MHC2046	06092802	1.57	2.68	0.46	4		
Starkeyite	S65	06091101	0.06	0.49	0.25	39	593.69	1.16
Starkeyite	S65	06091101	0.16	0.64	0.27	61		
Starkeyite	137725	08081501	0.00	0.57	0.54	9	1791.84	3.45
Starkeyite	137725	08081502	1.14	2.65	0.23	91		
Szmikite	159189	7012201	0.52	0.93	0.48	18	7249.38	14.18
Szmikite	159189	7012201	1.24	2.59	0.39	82		
Szomolnokite	156925	05022101	0.11	0.62	0.24	70	882.71	1.72
Szomolnokite	156925	05022101	0.23	0.84	0.24	16		
Szomolnokite	156925	05022101	0.40	1.11	0.24	14		
Szomolnokite	S77	9011401	1.26	2.73	0.27	94	1164.17	2.23
Szomolnokite	S77	9011401	0.42	0.44	0.30	2		
Szomolnokite	S77	9011401	0.39	1.02	0.30	4		
Szomolnokite	92942	05030201a	0.60	0.61	0.45	4	2172.27	4.11
Szomolnokite	92942	05030201a	1.26	2.73	0.34	96		
Szomolnokite	136685-2	05030901a	0.23	0.69	0.24	12	1153.53	2.22
Szomolnokite	136685-2	05030901a	0.55	0.38	0.44	6		
Szomolnokite	136685-2	05030901a	1.29	2.74	0.26	82		
Szomolnokite	104276	05031401a	1.28	2.76	0.27	100	7785.66	14.58
Szomolnokite	S60	04041902a	1.31	2.89	0.24	57	1475.92	2.83
Szomolnokite	S60	04041902a	1.31	3.42	0.45	31		

Szomolnokite	S60	04041902a	0.23	0.76	0.24	5		
Szomolnokite	S60	04041902a	0.50	0.36	0.47	4		
Szomolnokite	S60	04041902a	0.55	0.85	0.24	2		
Szomolnokite	159098	05030701	0.49	0.18	0.51	12	400.56	0.78
Szomolnokite	159098	05030701	1.24	2.78	0.24	43		
Szomolnokite	159098	05030701	1.31	2.69	0.30	42		
Szomolnokite	159098	05030701	1.12	3.12	0.54	3		
Szomolnokite	159266	5030801	0.46	0.36	0.64	72	343.36	0.67
Szomolnokite	159266	5030801	0.14	0.56	0.30	28		
Szomolnokite	ML-S103	12020604g	0.43	0.42	0.48	7	741.82	1.44
Szomolnokite	ML-S103	12020604g	1.27	2.74	0.26	93		
Voltaite	DD104	05031501	1.35	1.82	0.30	43	726.16	1.41
Voltaite	DD104	05031501	1.42	2.28	0.30	8		
Voltaite	DD104	05031501	0.46	0.40	0.43	36		
Voltaite	DD104	05031501	0.13	0.47	0.25	13		
Voltaite	158795	05022201	1.20	1.58	0.36	24	381.48	0.75
Voltaite	158795	05022201	1.34	1.62	0.23	23		
Voltaite	158795	05022201	0.47	0.37	0.46	45		
Voltaite	158795	05022201	0.14	0.61	0.30	7		
Voltaite	137958	05022301	1.22	1.60	0.30	17	817.41	1.58
Voltaite	137958	05022301	1.33	1.77	0.24	29		
Voltaite	137958	05022301	1.26	2.83	0.24	21		
Voltaite	137958	05022301	0.46	0.37	0.44	34		
Voltaite	129313	04071501	1.26	1.79	0.29	58	706.18	1.37
Voltaite	129313	04071501	0.43	0.35	0.38	35		
Voltaite	129313	04071501	0.10	0.54	0.24	7		
Voltaite	115035	05022601	1.34	1.62	0.33	26	369.00	0.72
Voltaite	115035	05022601	1.20	1.63	0.29	16		
Voltaite	115035	05022601	0.47	0.38	0.51	48		
Voltaite	115035	05022601	0.11	0.59	0.30	10		
Voltaite	85679	04071601	1.30	1.79	0.33	32	713.05	1.39
Voltaite	85679	04071601	1.19	1.75	0.24	19		
Voltaite	85679	04071601	0.43	0.36	0.44	40		
Voltaite	85679	04071601	0.16	0.69	0.30	9		
Voltaite	95830	05022401	1.09	2.46	0.24	7	648.43	1.26
Voltaite	95830	05022401	1.15	1.69	0.34	23		
Voltaite	95830	05022401	1.31	1.63	0.25	15		
Voltaite	95830	05022401	0.54	0.38	0.46	43		
Voltaite	95830	05022401	0.34	0.37	0.24	12		
Yavapaiite	MDL-579	05010801	0.48	0.31	0.29	100	3041.68	5.82
Zincobotryogen	C5525-3	06091201	0.41	1.21	0.25	57	1121.79	2.18
Zincobotryogen	C5525-3	06091201	0.39	1.65	0.25	43		
Zincocopiapite	G-3637	07012902	0.07	0.45	0.25	7	519.39	1.02
Zincocopiapite	G-3637	07012902	0.43	0.38	0.29	42		
Zincocopiapite	G-3637	07012902	0.43	0.88	0.28	50		

Table 3. Mössbauer Parameters of Low Δ Sulfates Containing Dominantly Fe^{3+}

Mineral	Fig.	Sample	δ	Δ	area	δ	Δ	area	δ	Δ	area	δ	Δ	area	δ	Δ	area	δ	Δ	area	δ	Δ	area
Quenstedtite	3	B8255				0.47	0.13	35	0.40	0.24	65												
Coquimbite		VZO101/102	0.18	0.58	7	0.46	0.10	93															
		SPT132	0.18	0.71	6				0.42	0.47	94												
		SPT131	0.19	0.72	9				0.43	0.44	91												
	3	SPT126/127	0.16	0.66	5	0.45	0.08	95															
		SPT119	0.16	0.77	5	0.47	0.09	95															
		ML-S63				0.44	0.25	86	0.35	1.09	7	0.31	0.58	7									
		R7661	0.19	0.52	7	0.46	0.11	93															
Kornelite	3	R16185				0.44	0.11	100															
Lausenite	3	102923				0.47	0.12	89										1.25	2.63	6			
Ferrinatrite		VZO105/106[1]							0.44	0.40	88	0.40	1.13	12									
	3	R6214[2]				0.47	0.05	100															
Voltaite		DD104	0.13	0.47	13				0.46	0.40	36				1.35	1.82	43	1.42	2.28	8			
		137958							0.46	0.37	34				1.22	1.60	17	1.33	1.77	29	1.26	2.83	21
		158795	0.14	0.61	7				0.47	0.37	45				1.20	1.58	24	1.34	1.62	23			
	3	129313	0.10	0.54	7				0.43	0.35	35				1.26	1.79	58						
		115035	0.11	0.59	10				0.47	0.38	48				1.34	1.62	26	1.20	1.63	16			
		85679	0.16	0.69	9				0.43	0.36	40				1.30	1.79	32	1.19	1.75	19			
		95830†				0.34	0.37	12	0.54	0.38	43				1.15	1.69	23	1.31	1.63	15	1.09	2.46	7
Pertlikite	†	pertlikite							0.42	0.36	72				1.30	1.70	13	1.18	1.65	12			
Rhomboclase		ML-S84				0.54	0.43	23	0.43	0.53	77												
		ML-S85							0.44	0.52	97												
	3	ML-S89							0.44	0.51	97												
		81268							0.44	0.54	95												

Values for δ and Δ are given in mm/s and areas are given as percentage of the total spectra area. Errors bars are ±0.02 mm/s for δ and Δ and ±1-5% on doublet areas.
*Doublets with peak areas <5% of the total area are not included in this table. Their parameters, peak widths and goodness of fit parameters for all spectra are given in Table 2, in supplementary materials.
†Spectrum of this sample was published in Ertl et al. (2012).
[1] Sample also contains minor metavoltine. [2]Sample also contains a coquimbite impurity.

Table 4. Mössbauer Parameters of Predominantly Fe^{3+} Sulfate Minerals with Δ of 0.31-0.81 mm/s*

Mineral	Fig.	Sample	δ	Δ	area	δ	Δ	area	δ	Δ	area	δ	Δ	area	δ	Δ	area	δ	Δ	area	δ	Δ	area
Yavapaiite	4a	ML-579				0.48	0.31	100															
Krausite	4a	156916				0.41	0.41	100															
Goldichite	4a	123922	0.19	0.61	29	0.48	0.29	71															
Copiapite	4a	SPT117	0.21	0.34	6	0.42	0.35	43				0.43	0.79	41	0.34	1.00	10						
		G596-1													0.37	1.18	100						
Ferricopiapite		SPT125				0.42	0.40	38				0.43	0.77	38	0.38	1.18	25						
		ML-S35				0.43	0.39	35	0.37	0.52	16	0.43	0.78	48									
		168257				0.42	0.37	26				0.43	0.78	17				1.25	2.71	51			
	4a	SPT 109				0.42	0.36	38				0.42	0.74	62									
		SPT133				0.42	0.40	40	0.38	0.53	27	0.43	0.76	33									
Zincocopiapite	4a	G-3637	0.07	0.45	7	0.43	0.38	42				0.43	0.88	50									
Apjohnite	4b	121356	0.19	0.75	12	0.43	0.58	70													1.27	3.31	18
Bilinite	4b	169017	0.09	0.79	17	0.49	0.37	71										1.37	1.78	7	1.06	3.69	5
Dietrichite	4b	G-2429				0.42	0.35	44	0.43	0.79	52												
Römerite		SPT110				0.43	0.55	23	0.29	0.61	30							1.23	2.87	12	1.28	3.01	35
		SPT122/126													1.39	2.09	23**	1.27	2.74	44	1.27	3.27	7
	6b	113733	0.17	0.61	6	0.44	0.37	69	0.39	0.39	2										1.27	3.28	23
		159098-2	0.15	0.64	7	0.46	0.36	49										1.26	2.73	27	1.26	3.30	18
		C5602-1	0.15	0.58	7	0.45	0.33	50										1.28	2.76	32	1.27	3.30	11
		93825	0.16	0.60	5	0.44	0.33	55										1.29	2.78	25	1.29	3.31	15
		R8415	0.17	0.56	12	0.47	0.36	56	0.36	0.37	7							1.34	2.59	2	1.29	3.29	23
Metavoltine		VZO114				0.43	0.35	53							0.40	1.04	36						
															1.16	2.01	11						
		G2677				0.44	0.24	19													1.27	3.23	81
	4b	SPT109				0.33	0.46	19	0.42	0.37	38	0.43	0.74	43									
Starkeyite	4b	ML-S65	0.16	0.64	61																		
			0.06	0.49	39																		
Ilesite	3b	123277							0.31	0.62	97												

Values for δ and Δ are given in mm/s and areas are given as percentage of the total spectra area. Errors bars are ±0.02 mm/s for δ and Δ and ±1-5% on doublet areas.
*Doublets with peak areas <5% of the total area are not included in this table. Their parameters, peak widths and goodness of fit parameters for all spectra are given in Table 2, in supplementary materials.
**Likely an impurity.

Table 5. Mössbauer Parameters of Fe^{3+} Sulfate Minerals with Predominantly High Quadrupole Splitting*

Mineral	Fig.	Sample	δ	Δ	area	δ	Δ	area	δ	Δ	area	δ	Δ	area	δ	Δ	area	δ	Δ	area
Butlerite	5a	C5534										0.41	0.96	100						
		R7653										0.41	0.95	100						
		639										0.41	0.98	100						
		ML-S88							0.41	0.80	81	0.42	0.99	19						
Parabutlerite	5a	VZO115/116										0.41	0.98	100						
		157716				0.42	0.40	38	0.42	0.75	50	0.37	1.20	12						
Slavikite	5a	140229	0.27	0.63	34	0.55	0.52	39				0.38	1.23	39						
		VZO122/123[1]				0.37	0.57	76				0.38	1.15	24						
Fibroferrite		SPT121				0.41	0.52	37	0.42	0.96	63									
	5a	VZO107/108				0.41	0.50	100												
Botryogen		SPT124													0.42	1.18	49	0.40	1.63	43
		G3775				0.41	0.35	30	0.41	0.80	31				0.37	1.25	34			
	5a	DD112													0.41	1.16	63	0.40	1.60	33
Zincobotryogen	5a	C5525-3													0.41	1.21	57	0.39	1.65	43
Sideronatrite	5b	SPT123													0.42	1.15	100			
		115164													0.41	1.15	100			
Metasideronatrite	5b	105774-2										0.35	1.20	43	0.44	1.18	57			
		VZO112										0.42	1.17	48	0.38	1.18	52			
Metahohmannite	5b	R12495										0.43	0.94	100						
Amarantite	5b	G3775				0.43	0.35	8				0.44	0.98	8	0.40	1.19	54	0.39	1.60	30
Jarosite	5b	132060													0.38	1.30	100			
		SPT113													0.38	1.18	100			
		SPT116													0.38	1.23	100			
		SPT115													0.38	1.29	100			
		SPT120										0.37	0.70	56	0.38	1.14	44			
Plumbojarosite†	5b	ML-S15	0.29	0.70	12							0.37	1.22	79				0.76	1.22	9
Anhydrite		159266**				0.44	0.41	76	0.14	0.58	24									
	5c	SPT132**				0.40	0.46	93				0.38	1.02	7						
Celestine	5c**	ML-S13**				0.15	0.54	65				0.24	0.87	35						

Values for δ and Δ are given in mm/s and areas are given as percentage of the total spectra area. Errors bars are ±0.02 mm/s for δ and Δ and ±1-5% on doublet areas.
*Doublets with peak areas <5% of the total area are not included in this table. Their parameters, peak widths and goodness of fit parameters for all spectra are given in Table 2, in supplementary materials.
†This sample also contains a magnetic sextet from an unknown impurity.
**Mössbauer data cannot determine whether the Fe in these samples is actually part of the sulfate's structure, or if it is an impurity. SPT132 is known from XRD to be a mixture of anhydrite and coquimbite, but XRD of 159266 and ML-S13 show that they are "pure." However, it takes only a tiny amount of Fe-rich sulfate impurity to have a large influence on the spectrum of a low-Fe Ca sulfate.
[1]XRD suggests this sample is gypsum but there is apparently some slavikite impurity here, given the similarity of this spectrum to the known slavikite 140229.

Table 6. Mössbauer Parameters of Predominantly Fe^{2+} Sulfate Minerals*

Mineral	Fig.	Sample	δ	Δ	area	δ	Δ	area	δ	Δ	area	δ	Δ	area	δ	Δ	area	δ	Δ	area	δ	Δ	area
Szomolnokite		ML-S77																1.26	2.73	94			
		92942																1.26	2.73	96			
		136685-2				0.54	0.14	7	0.23	0.69	12							1.29	2.74	82			
	6a	104276																1.28	2.76	100			
	6a	ML-S60																1.31	2.89	57	1.31	3.42	31
		159098				0.49	0.18	12							1.31	2.69	42	1.24	2.78	43			
		159266				0.46	0.36	72	0.14	0.56	28												
		ML-S103				0.43	0.42	7										1.27	2.74	93			
Szmikite	6a	159189							0.52	0.93	18							1.24	2.59	82			
Gunningite	6a	156925				0.26	0.40	32				0.37	1.26	10				1.25	2.74	58			
Chalcanthite	6a	DD100	0.10	0.51	29				0.26	0.76	30							1.26	2.32	22	1.30	2.88	19
Pentahydrite[1]	6a	VZO121							0.50	0.83	8							1.26	3.00	53	1.27	3.68	38
Jokokuite	6b	G3536	0.15	0.56	26										1.13	2.63	6	1.26	2.51	65			
Halotrichite	6b	G1616																			1.27	3.29	92
		VZO128	0.13	0.49	10	0.36	0.31	14							1.45	1.56	13	1.28	2.76	43	1.30	3.29	20
Melanterite	6b	2070																			1.27	3.21	100
Rozenite		JB626B																1.33	2.97	59	1.33	3.39	34
	6b	SPT130										0.39	0.95	8							1.27	3.21	92
Starkeyite	6b	137725	0.00	0.57	9													1.14	2.65	91			

Values for δ and Δ are given in mm/s and areas are given as percentage of the total spectra area. Errors bars are ±0.02 mm/s for δ and Δ and ±1-5% on doublet areas.
*Doublets with peak areas <5% of the total area are not included in this table. Their parameters, peak widths and goodness of fit parameters for all spectra are given in Table 2, in supplementary materials.
[1]Sample known to include minor impurities from pickeringite, starkeyite, botryogen, and boussingaultite,

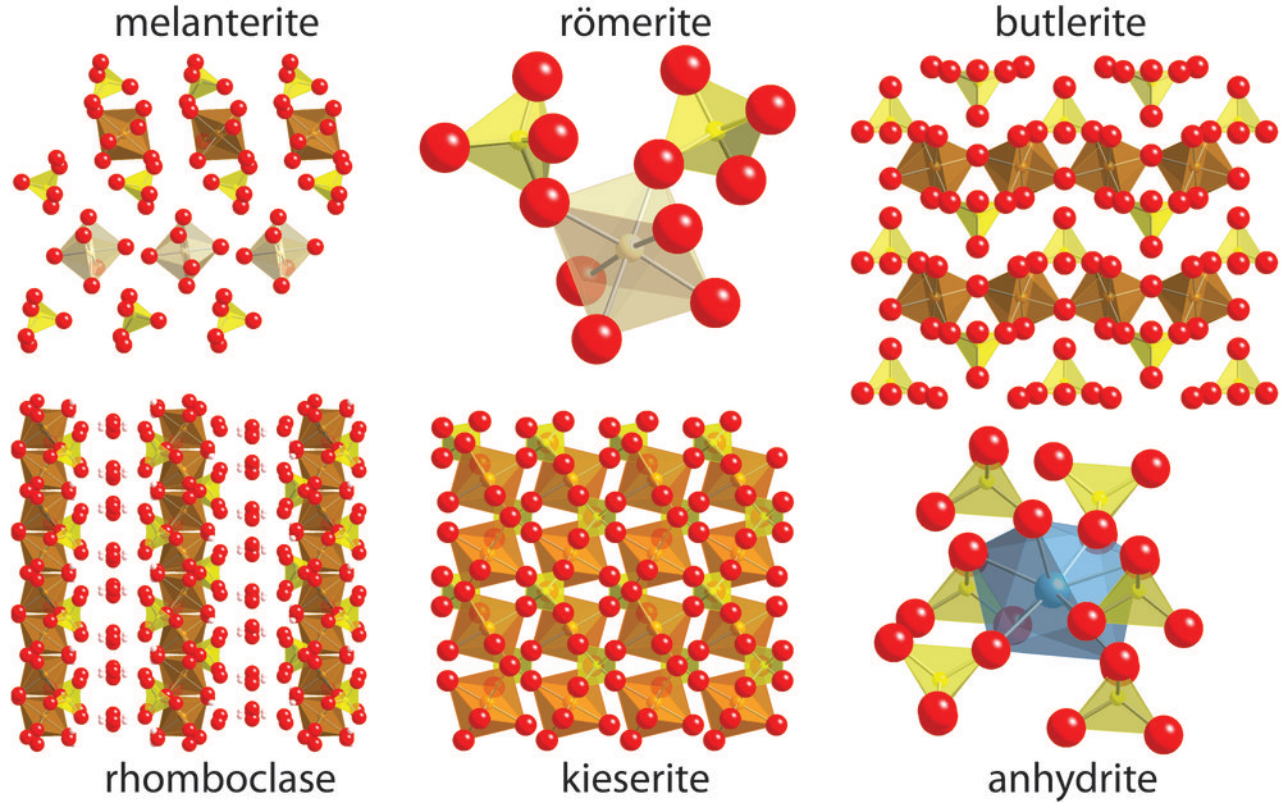
melanterite
römerite
butlerite
rhomboclase
kieserite
anhydrite

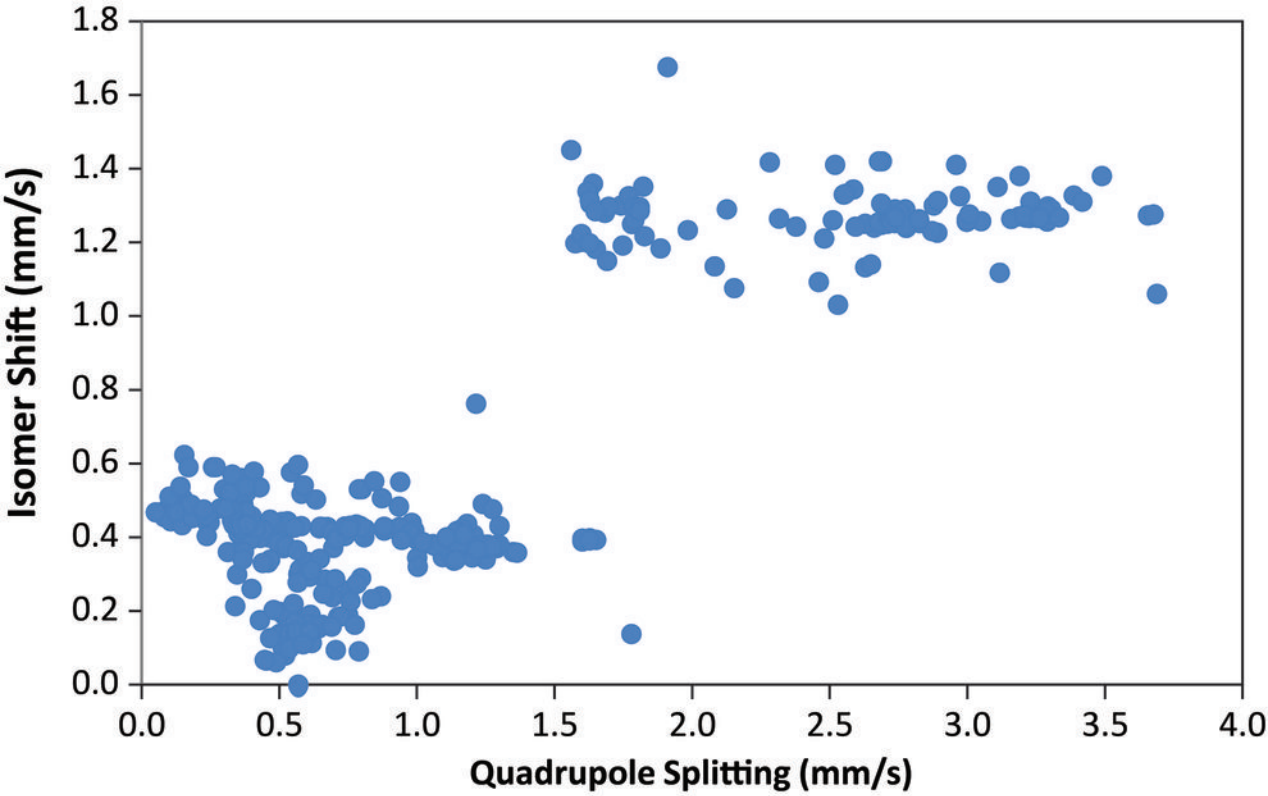
Isomer Shift (mm/s)
1.8
1.6
1.4
1.2
1.0
0.8
0.6
0.4
0.2
0.0
0.0
0.5
1.0
1.5
2.0
2.5
3.0
3.5
4.0
Quadrupole Splitting (mm/s)

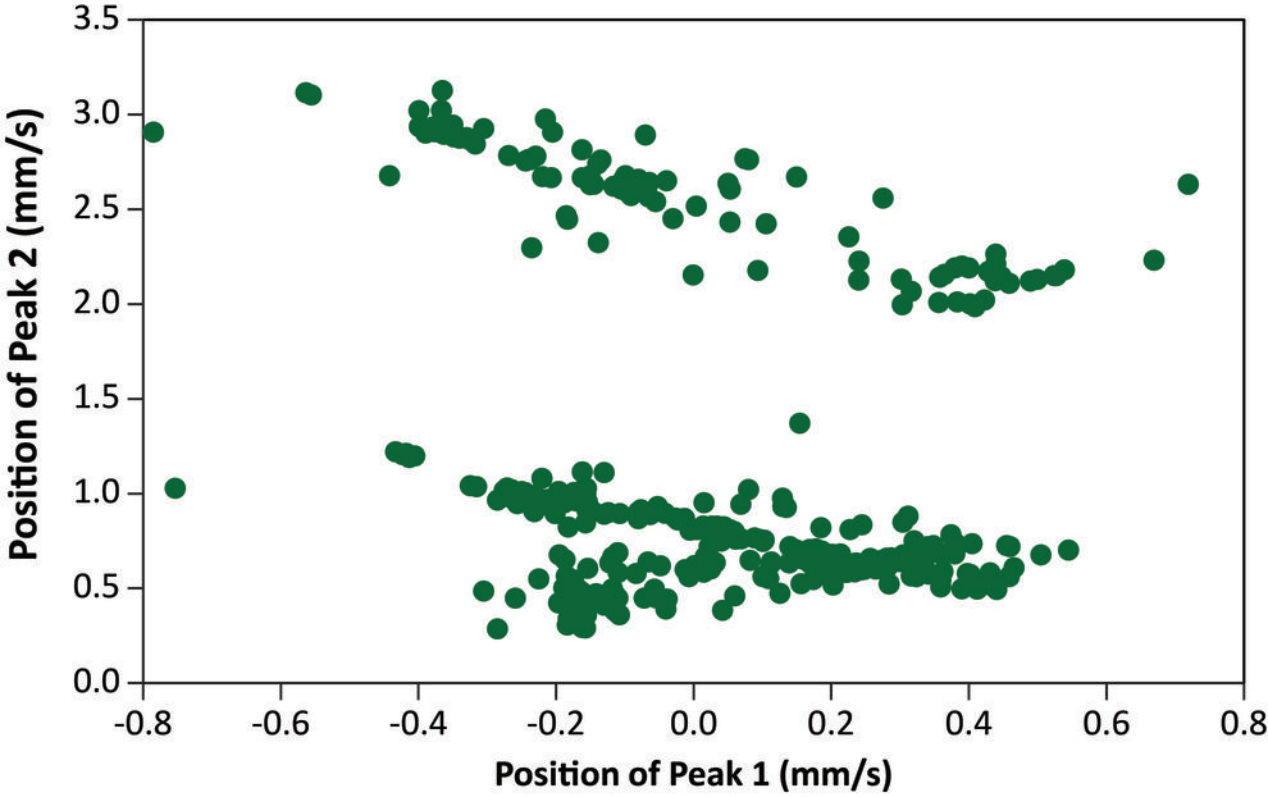
Position of Peak 2 (mm/s)
3.5
3.0
2.5
2.0
1.5
1.0
0.5
0.0
-0.8
-0.6
-0.4
-0.2
0.0
0.2
0.4
0.6
0.8
Position of Peak 1 (mm/s)

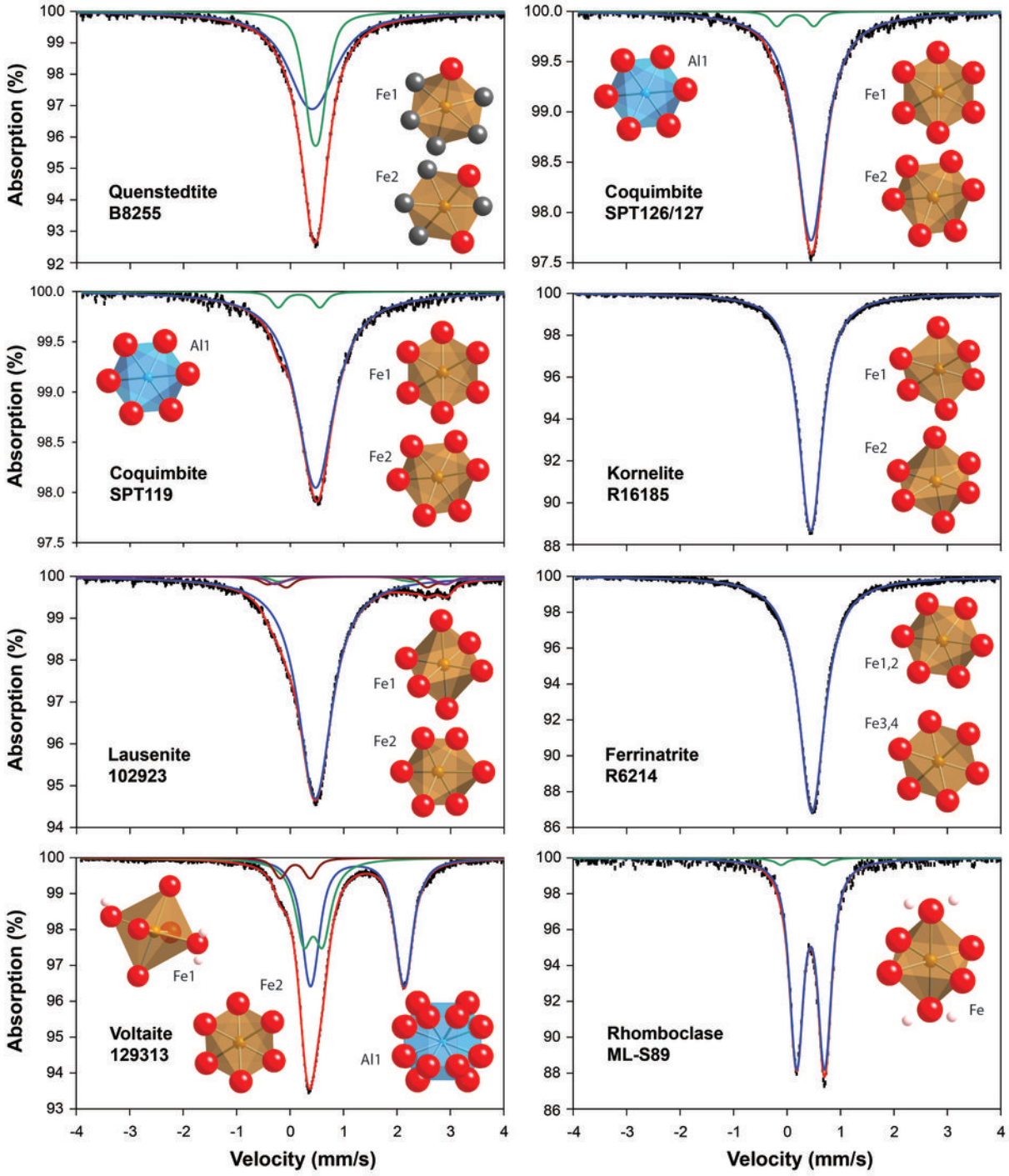
Absorption (%)
Quenstedtite
B8255
Fe1
Fe2
Coquimbite
SPT126/127
Al1
Coquimbite
SPT119
Kornelite
R16185
Lausenite
102923
Ferrinatrite
R6214
Fe1,2
Fe3,4
Voltaite
129313
Rhomboclase
ML-S89
Fe
Velocity (mm/s)

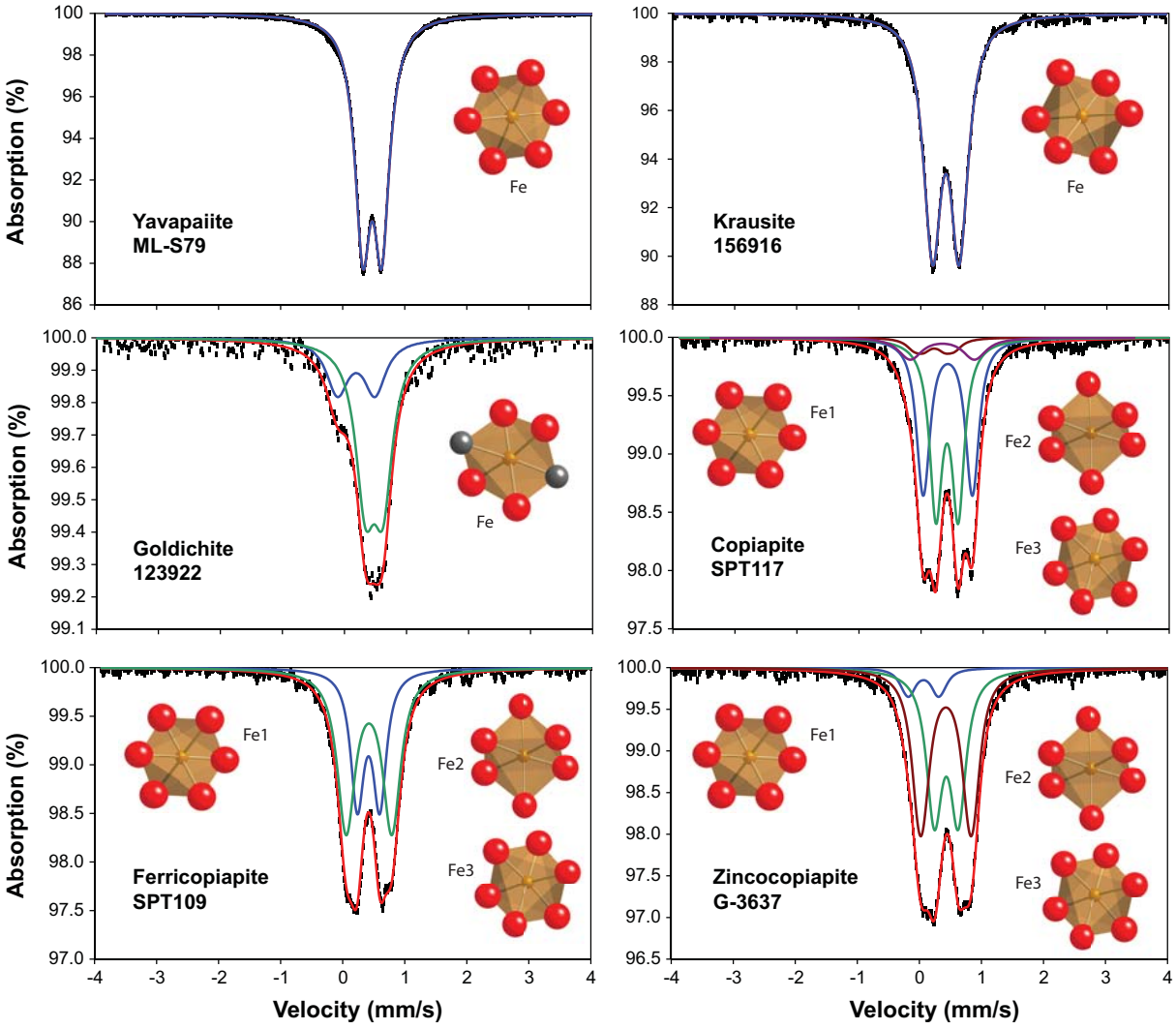
Absorption (%)
Yavapaiite
ML-S79
Fe
Krausite
156916
Fe
Goldichite
123922
Fe
Copiapite
SPT117
Fe1
Fe2
Fe3
Ferricopiapite
SPT109
Fe1
Fe2
Fe3
Zincocopiapite
G-3637
Fe1
Fe2
Fe3
Velocity (mm/s)
Velocity (mm/s)

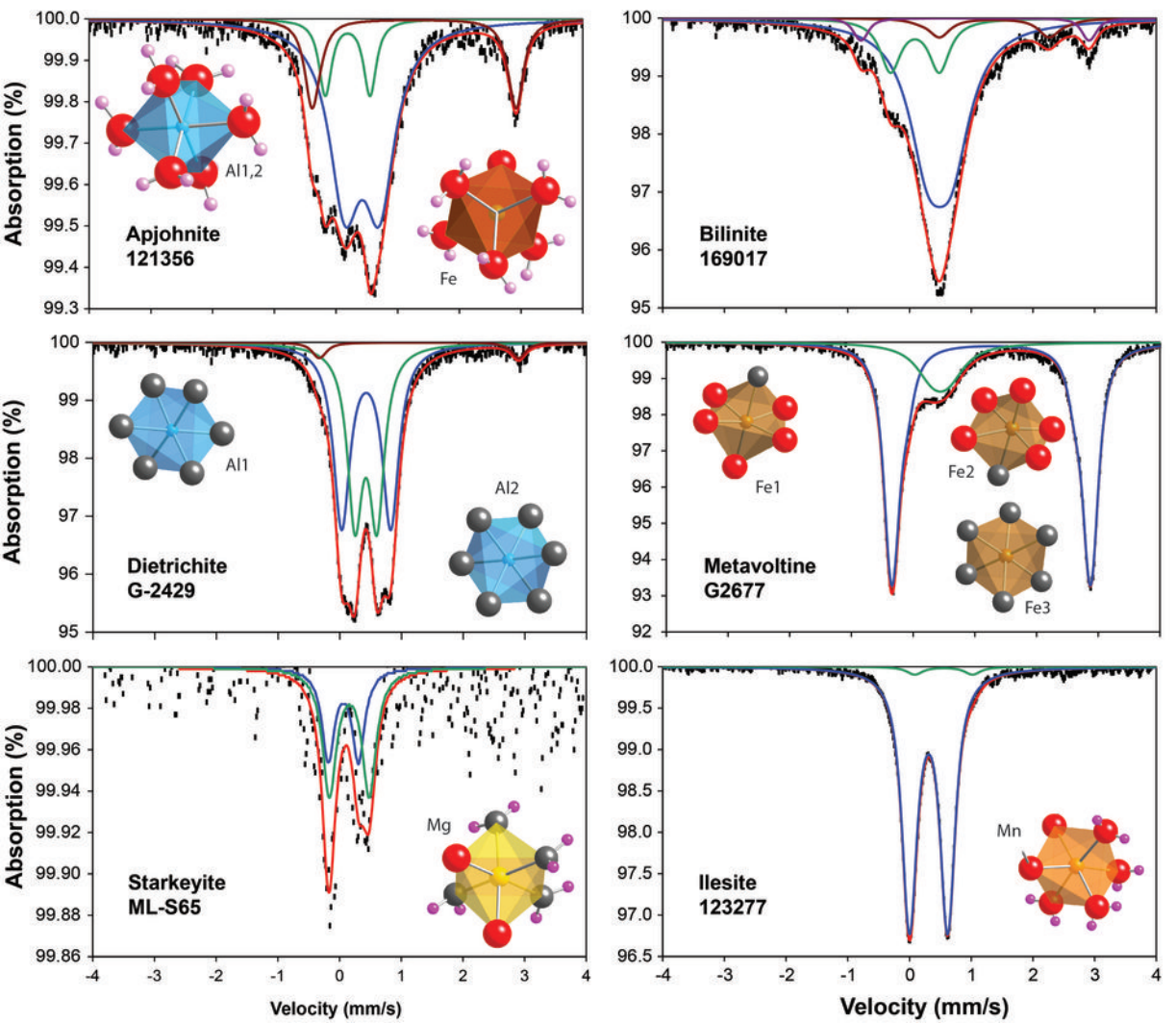
Absorption (%)
Apjohnite
121356
Al1,2
Fe
Bilinite
169017
Dietrichite
G-2429
Al1
Al2
Metavoltine
G2677
Fe1
Fe2
Fe3
Starkeyite
ML-S65
Mg
Ilesite
123277
Mn
Velocity (mm/s)
Velocity (mm/s)

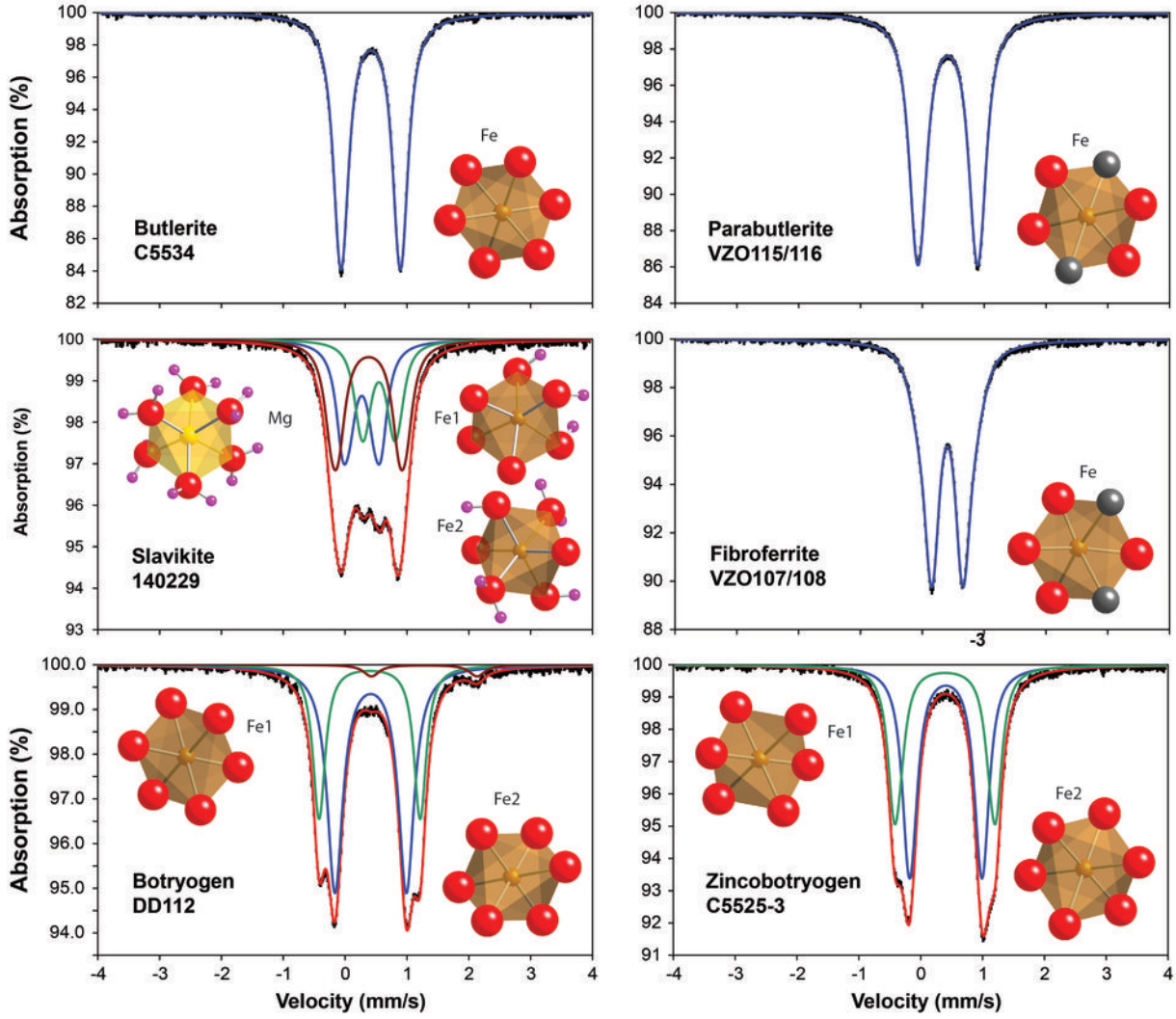
Absorption (%)
Butlerite
C5534
Fe
Parabutlerite
VZO115/116
Fe
Slavikite
140229
Mg
Fe1
Fe2
Fibroferrite
VZO107/108
Fe
Botryogen
DD112
Fe1
Fe2
Zincobotryogen
C5525-3
Fe1
Fe2
Velocity (mm/s)
Velocity (mm/s)

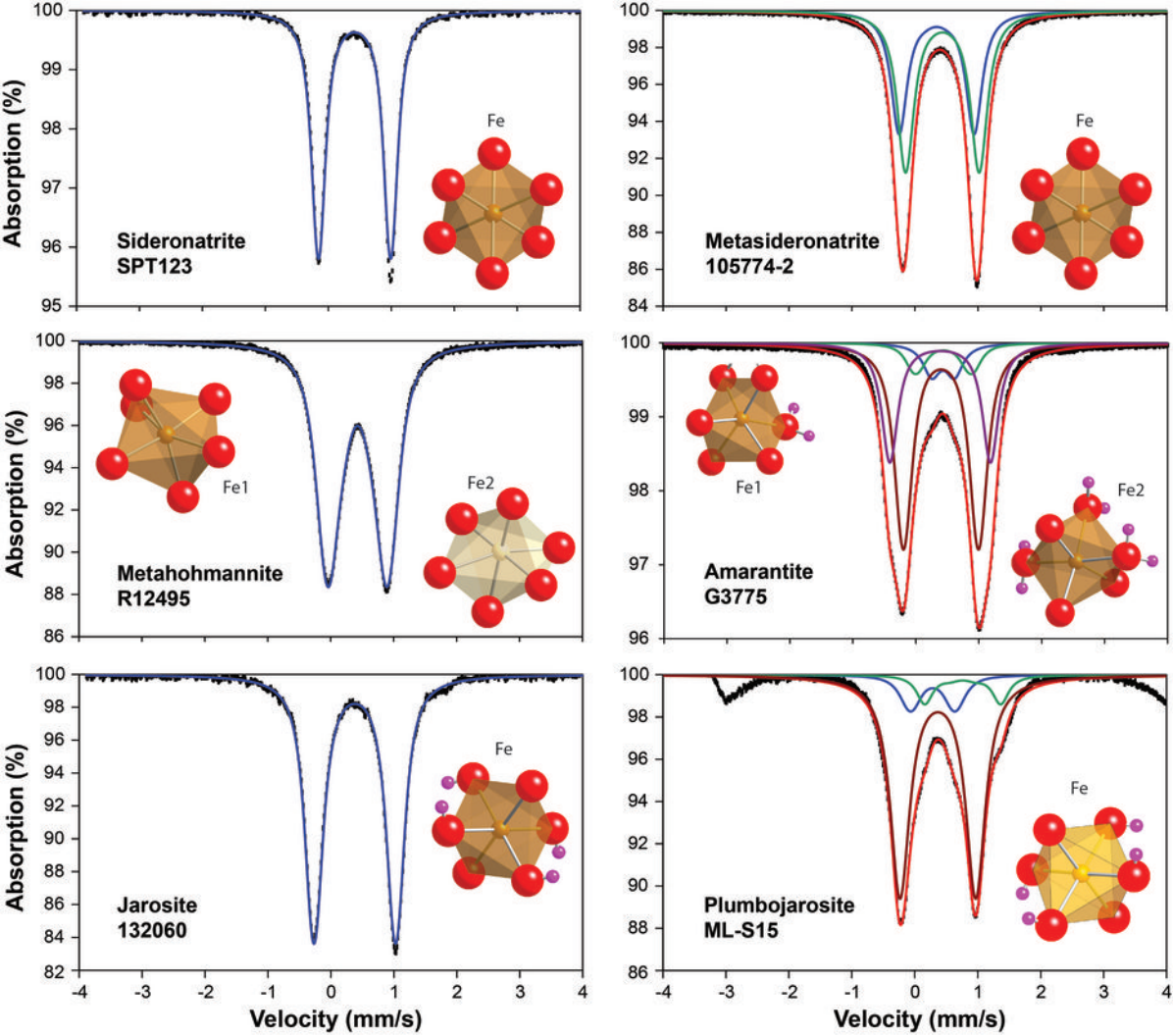
Absorption (%)
Velocity (mm/s)
Sideronatrite
SPT123
Fe
Metasideronatrite
105774-2
Fe
Metahohmannite
R12495
Fe1
Fe2
Amarantite
G3775
Fe1
Fe2
Jarosite
132060
Fe
Plumbojarosite
ML-S15
Fe

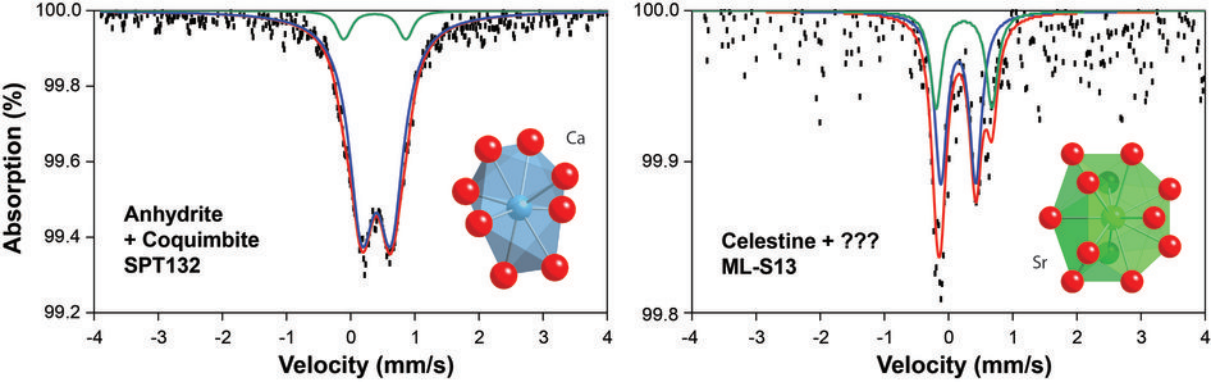
Absorption (%)
100.0
99.8
99.6
99.4
99.2
Anhydrite
+ Coquimbite
SPT132
Ca
-4
-3
-2
-1
0
1
2
3
4
Velocity (mm/s)
100.0
99.9
99.8
Celestine + ???
ML-S13
Sr
-4
-3
-2
-1
0
1
2
3
4
Velocity (mm/s)

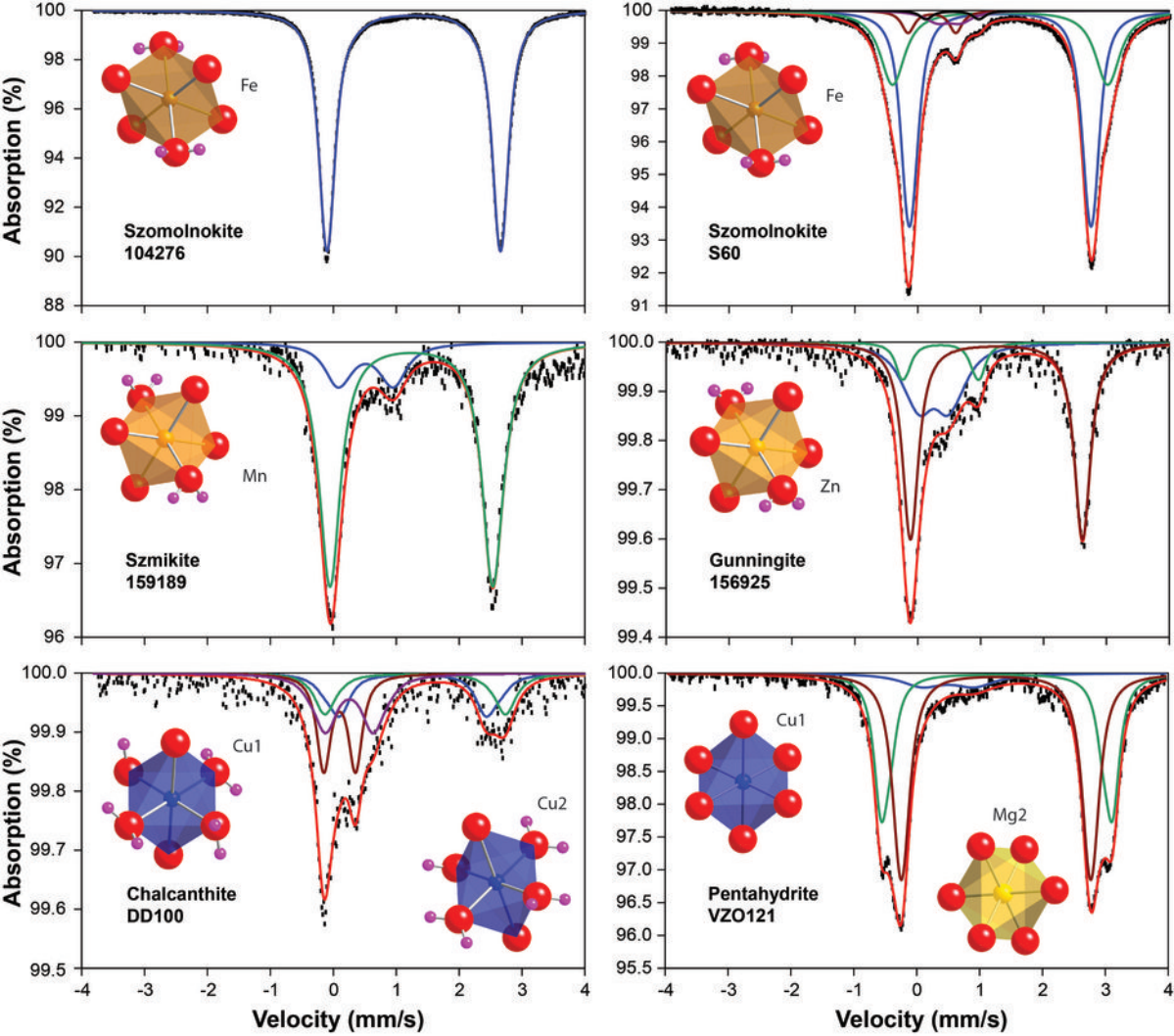
Absorption (%)
Fe
Szomolnokite
104276
Fe
Szomolnokite
S60
Mn
Szmikite
159189
Zn
Gunningite
156925
Cu1
Cu2
Chalcanthite
DD100
Cu1
Mg2
Pentahydrite
VZO121
Velocity (mm/s)
Velocity (mm/s)

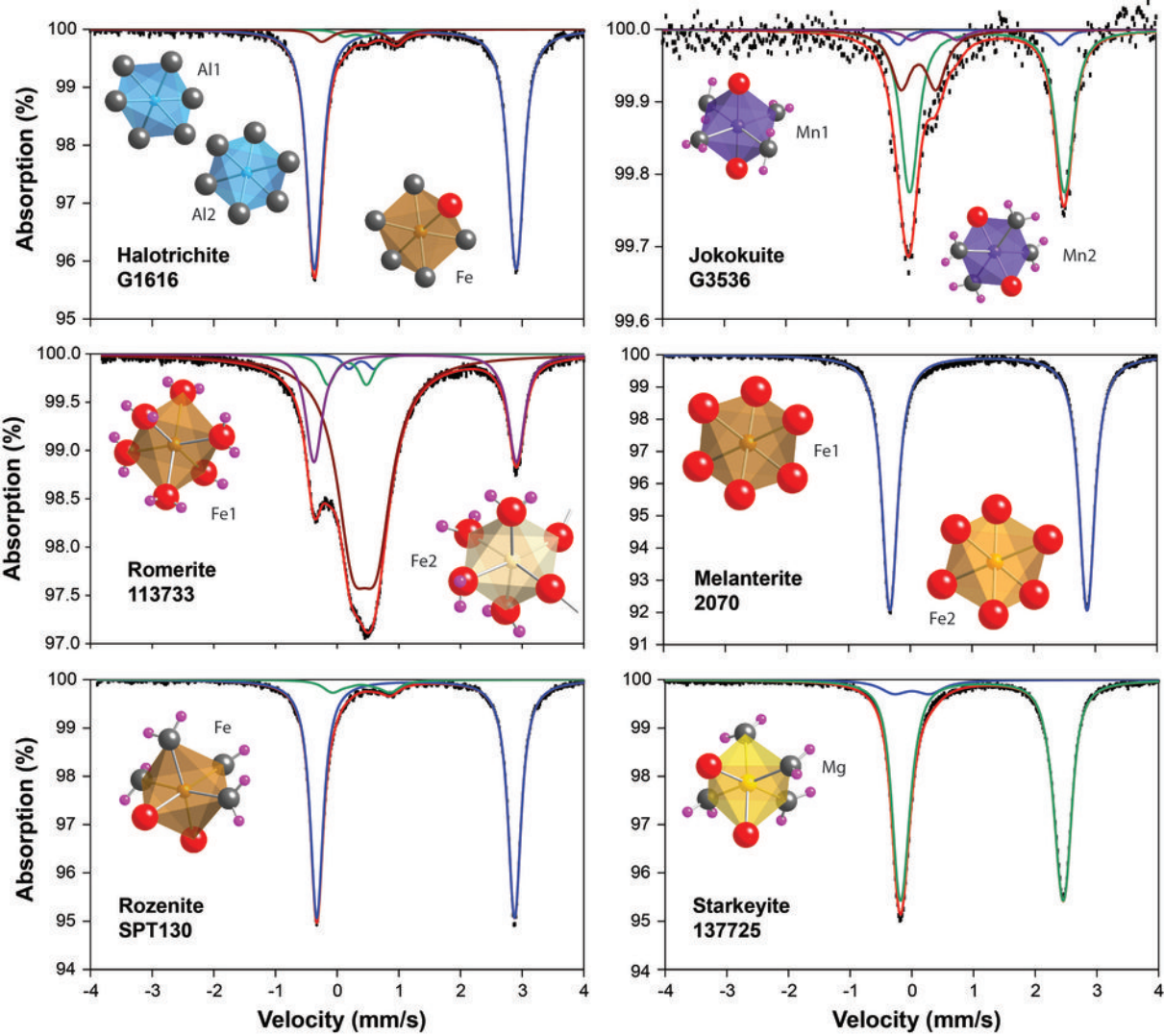
Absorption (%)
Velocity (mm/s)
Halotrichite
G1616
Al1
Al2
Fe
Jokokuite
G3536
Mn1
Mn2
Romerite
113733
Fe1
Fe2
Melanterite
2070
Fe1
Fe2
Rozenite
SPT130
Fe
Starkeyite
137725
Mg

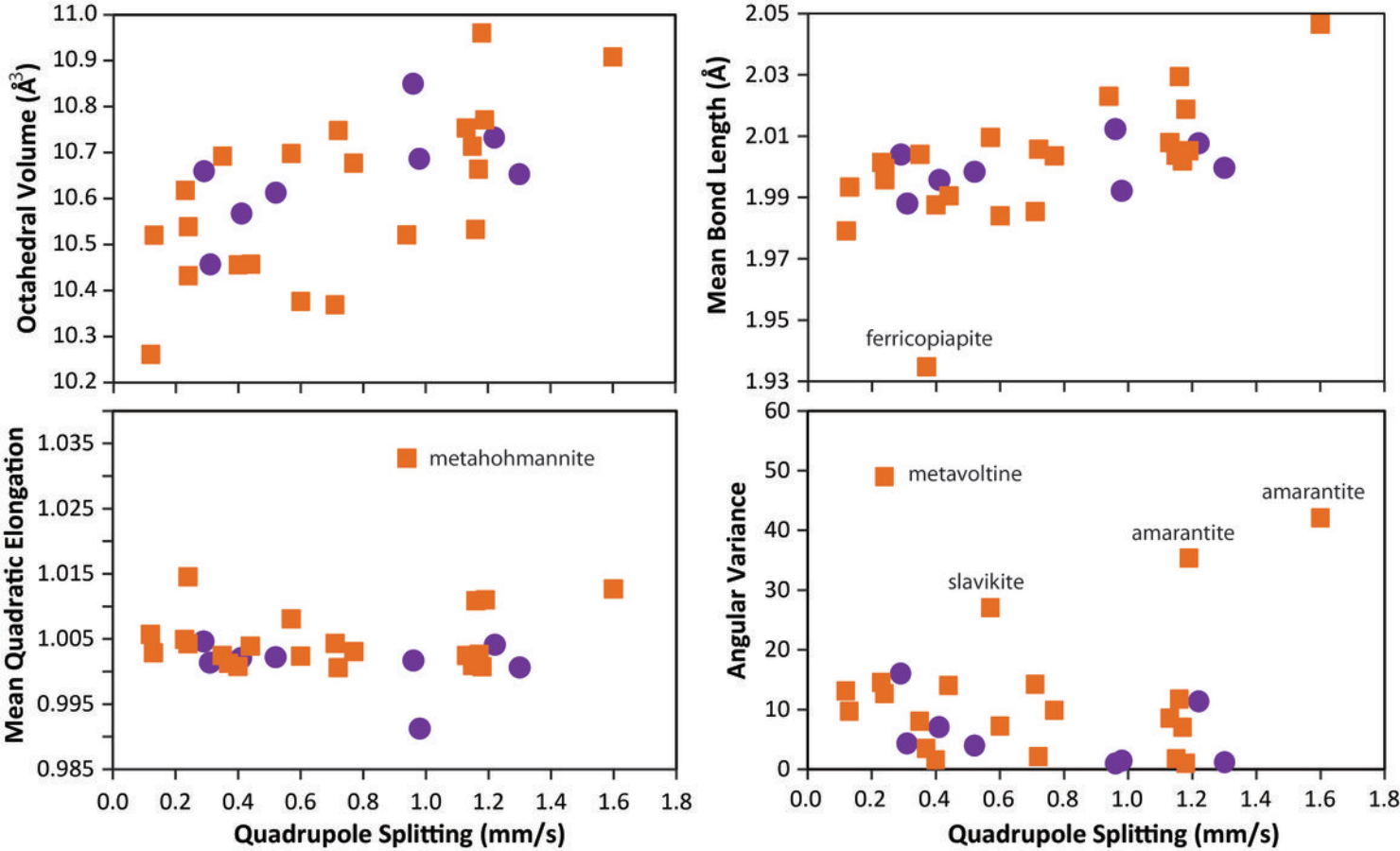
Octahedral Volume (Å3)
11.0
10.9
10.8
10.7
10.6
10.5
10.4
10.3
10.2
Mean Bond Length (Å)
2.05
2.03
2.01
1.99
1.97
1.95
1.93
ferricopiapite
Mean Quadratic Elongation
1.035
1.025
1.015
1.005
0.995
0.985
metahohmannite
Angular Variance
60
50
40
30
20
10
0
metavoltine
amarantite
amarantite
slavikite
0.0
0.2
0.4
0.6
0.8
1.0
1.2
1.4
1.6
1.8
Quadrupole Splitting (mm/s)
Quadrupole Splitting (mm/s)

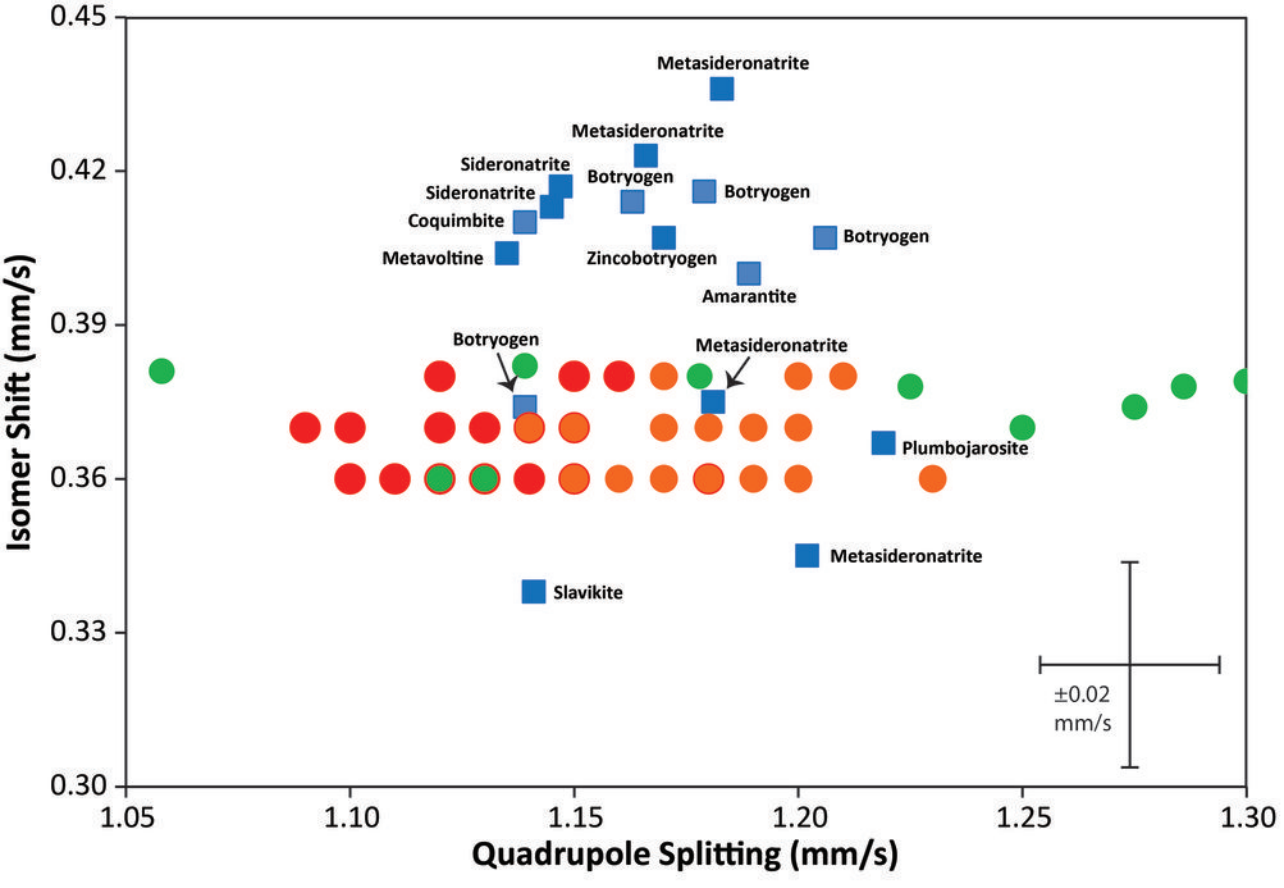
Isomer Shift (mm/s)
Quadrupole Splitting (mm/s)
0.45
0.42
0.39
0.36
0.33
0.30
1.05
1.10
1.15
1.20
1.25
1.30
Metasideronatrite
Metasideronatrite
Sideronatrite
Sideronatrite
Coquimbite
Metavoltine
Botryogen
Botryogen
Botryogen
Botryogen
Zincobotryogen
Amarantite
Botryogen
Metasideronatrite
Plumbojarosite
Metasideronatrite
Slavikite
±0.02
mm/s

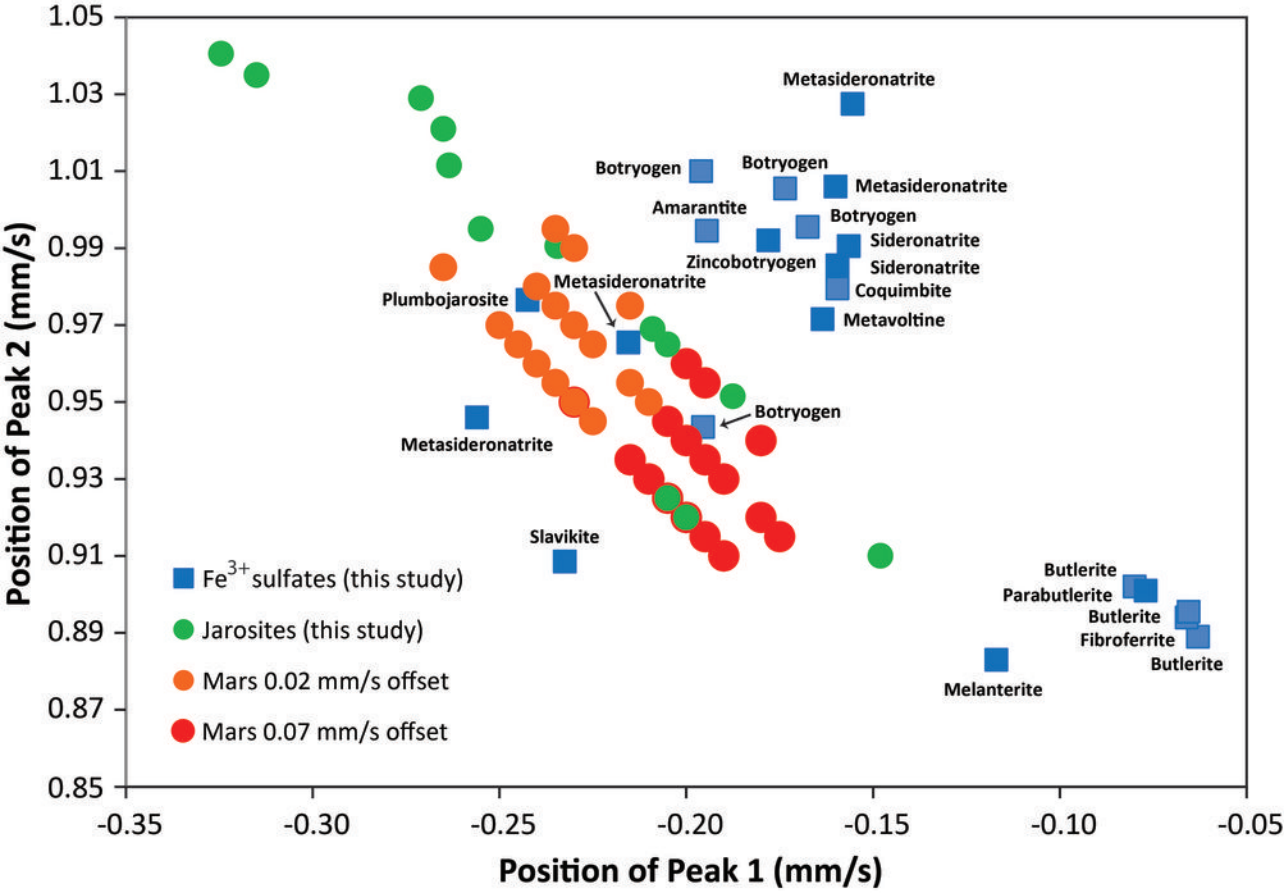
Position of Peak 2 (mm/s)
Position of Peak 1 (mm/s)
1.05
1.03
1.01
0.99
0.97
0.95
0.93
0.91
0.89
0.87
0.85
-0.35
-0.30
-0.25
-0.20
-0.15
-0.10
-0.05
Metasideronatrite
Botryogen
Botryogen
Metasideronatrite
Amarantite
Botryogen
Sideronatrite
Zincobotryogen
Sideronatrite
Coquimbite
Plumbojarosite
Metasideronatrite
Metavoltine
Botryogen
Metasideronatrite
Slavikite
Butlerite
Parabutlerite
Butlerite
Fibroferrite
Butlerite
Melanterite
Fe3+ sulfates (this study)
Jarosites (this study)
Mars 0.02 mm/s offset
Mars 0.07 mm/s offset

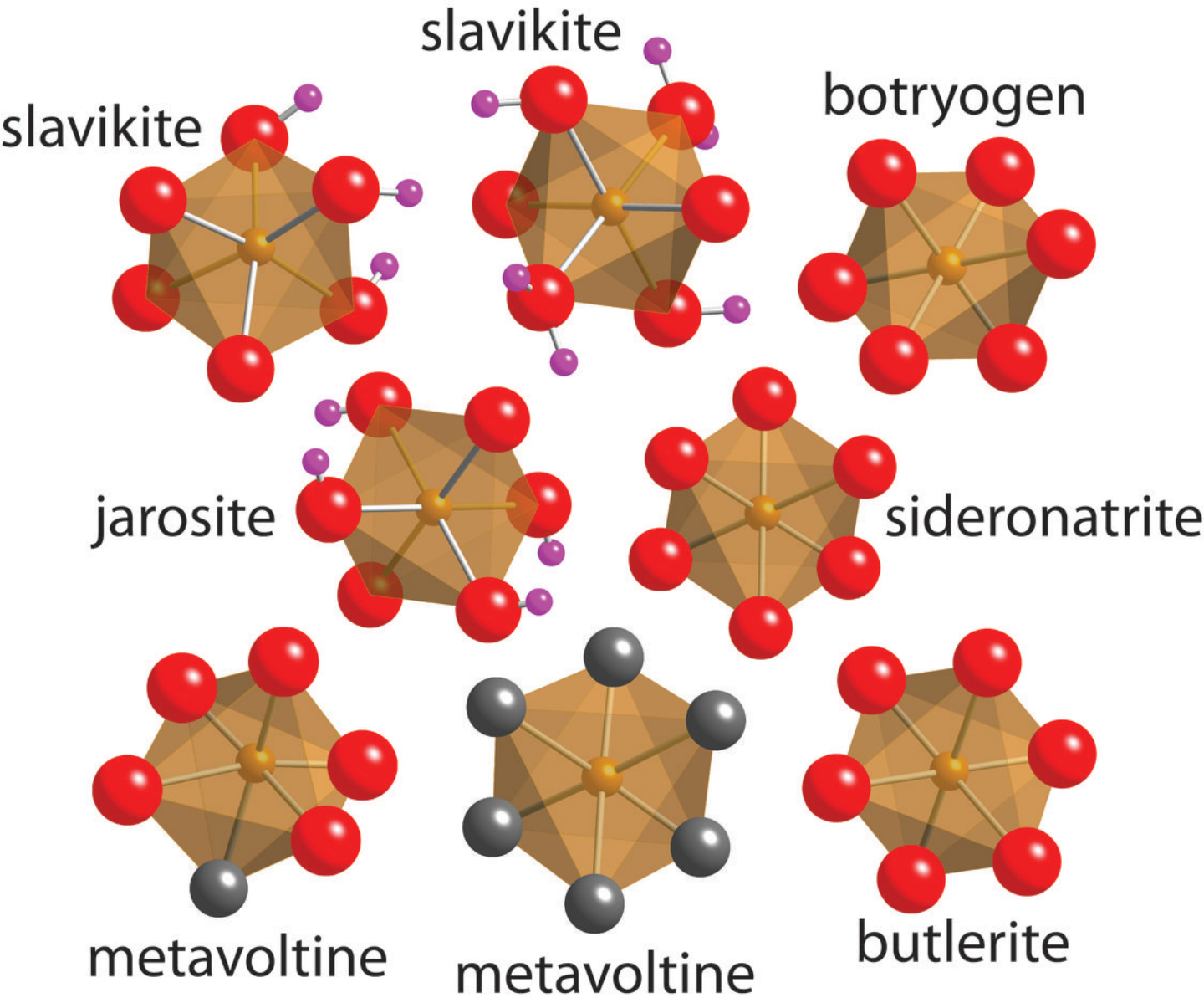
slavikite
slavikite
botryogen
jarosite
sideronatrite
metavoltine
metavoltine
butlerite

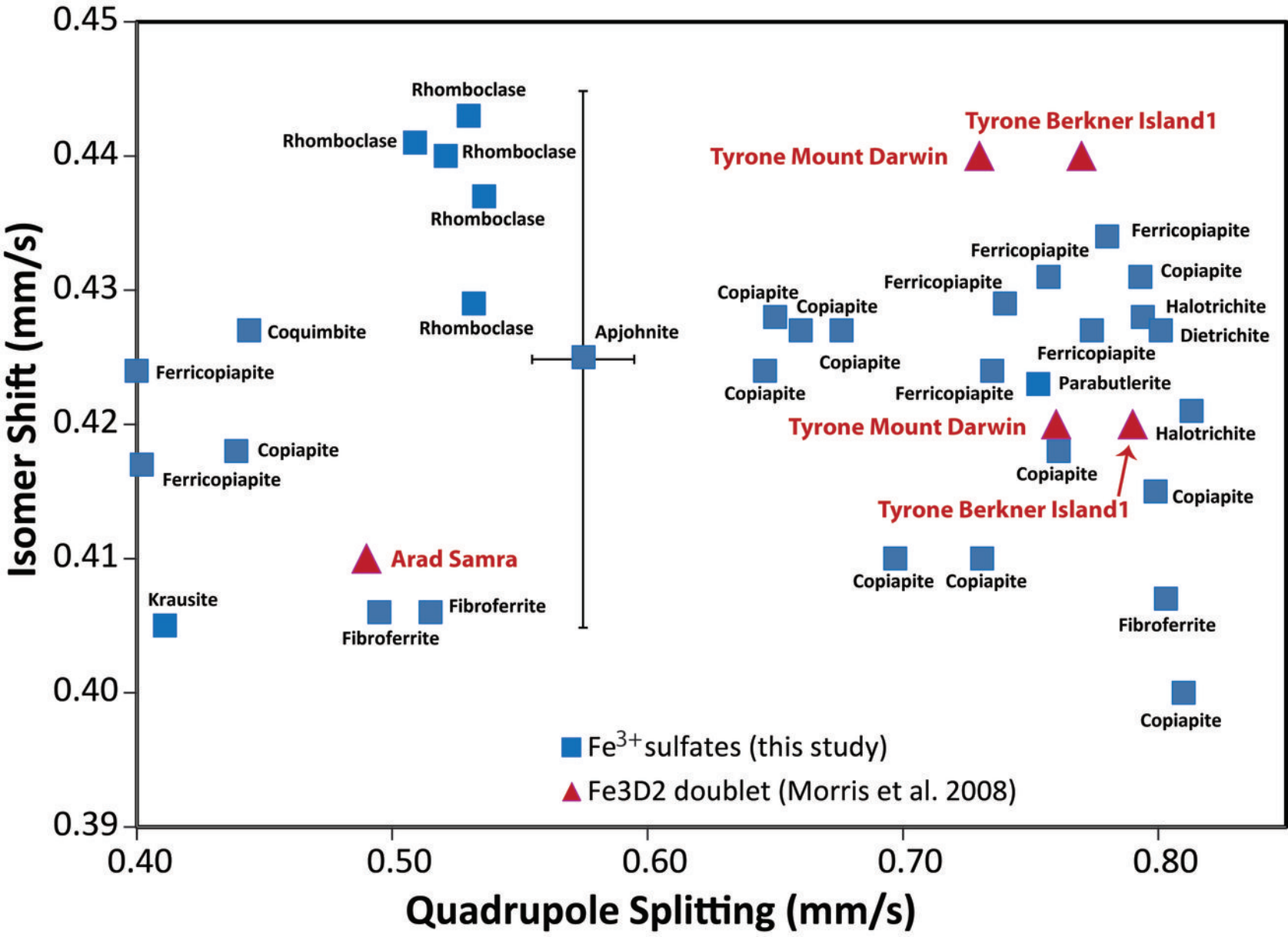
Isomer Shift (mm/s)
Quadrupole Splitting (mm/s)
0.45
0.44
0.43
0.42
0.41
0.40
0.39
0.40
0.50
0.60
0.70
0.80
Rhomboclase
Rhomboclase
Rhomboclase
Rhomboclase
Rhomboclase
Coquimbite
Ferricopiapite
Copiapite
Ferricopiapite
Krausite
Arad Samra
Fibroferrite
Fibroferrite
Apjohnite
Tyrone Berkner Island1
Tyrone Mount Darwin
Ferricopiapite
Ferricopiapite
Copiapite
Ferricopiapite
Copiapite
Copiapite
Halotrichite
Dietrichite
Copiapite
Ferricopiapite
Copiapite
Ferricopiapite
Parabutlerite
Tyrone Mount Darwin
Halotrichite
Copiapite
Tyrone Berkner Island1
Copiapite
Copiapite
Copiapite
Fibroferrite
Copiapite
Fe3+ sulfates (this study)
Fe3D2 doublet (Morris et al. 2008)

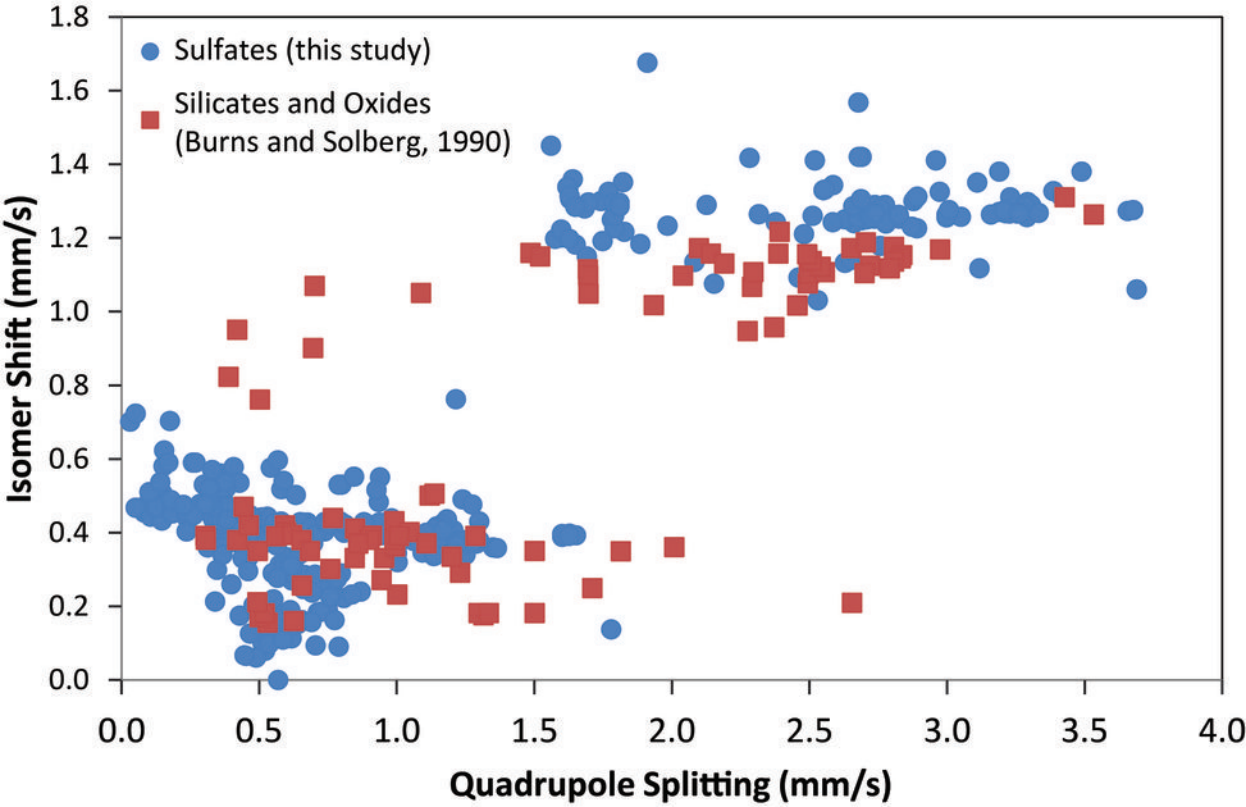
Sulfates (this study)
Silicates and Oxides
(Burns and Solberg, 1990)
Isomer Shift (mm/s)
Quadrupole Splitting (mm/s)
0.0
0.2
0.4
0.6
0.8
1.0
1.2
1.4
1.6
1.8
0.0
0.5
1.0
1.5
2.0
2.5
3.0
3.5
4.0